



LABORATÓRIO NACIONAL
DE ENGENHARIA CIVIL

STRUCTURAL ANALYSIS OF GRAVITY DAMS CONSIDERING NON-LINEAR BEHAVIOR IN THE DAM-FOUNDATION INTERFACE

Development of a 3DFE code using MATLAB: DamSlide3D

Work carried out under the project P2I/LNEC
"Cutting-edge solutions for sustainable assessment
of concrete dam foundations"

Lisbon • April 2019

R&D CONCRETE DAMS

REPORT 150/2019 – **DBB/NMMR**

Title

STRUCTURAL ANALYSIS OF GRAVITY DAMS CONSIDERING NON-LINEAR BEHAVIOR IN THE DAM-FOUNDATION INTERFACE

Development of a 3DFE code using MATLAB: DamSlide3D

Autoria

CONCRETE DAMS DEPARTMENT

Miguel Ângelo da Silva Rodrigues

Doctoral Research Fellow, Modelling and Rock Mechanics Unit

Sérgio Bruno Martins de Oliveira

Assistant Researcher, Modelling and Rock Mechanics Unit

Copyright © LABORATÓRIO NACIONAL DE ENGENHARIA CIVIL, I. P.

AV DO BRASIL 101 • 1700-066 LISBOA

e-mail: lnec@lnec.pt

www.lnec.pt

Report 150/2019

File no. 0403/112/20755, 0402/112/2075501

STRUCTURAL ANALYSIS OF GRAVITY DAMS CONSIDERING NON-LINEAR BEHAVIOR IN THE DAM-FOUNDATION INTERFACE

Development of a 3DFE code using MATLAB: DamSlide3D

Abstract

The main objective of this work is the development and presentation of a three-dimensional finite element program, **DamSlide3D**, to study the behavior of gravity dams for scenarios of sliding through the dam-foundation interface. The **DamSlide3D**, developed using MATLAB, includes cube-type finite elements with 20 nodal points ("serendipity") and finite interface elements with 16 nodal points (joint elements).

Initially, we present the fundamental equations of Solid Mechanics, referring to the main simplified hypotheses considered in the computationally implemented formulation, which is presented mathematically as a problem of boundary values using a displacement formulation. For the structure body and for the foundation, the hypothesis of isotropic materials with linear elastic behavior is assumed and for the interfaces the hypothesis of non-linear behavior is considered using the Mohr-Coulomb criterion.

The **DamSlide3D** input data is provided in an excel file and includes structure geometry data, material properties, support conditions and load parameters. As output, the program graphically displays the stress field (principal stresses) and the displacement field (deformed structure).

The program was verified throughout three numerical tests with known theoretical solutions. In these tests a simple structure was used, composed by a column discretized in 3DFE. At the contact surface between the column and the base (horizontal surface) it was considered an interface discretized using joint finite elements. A plane surface that crosses the column with a given slope is also considered, discretized using the same type of joint finite elements. In the first test, the field of elastic stresses at the base, due to self-weight (SW) and hydrostatic pressure (HP), was compared with the theoretical results. In the second test the nonlinear column response was studied for different values of the friction angle at the inclined interface (in this test the structure is only submitted to SW). In the third test, for the main SW + HP loads, the stability of the column is studied for a variation of the friction angle, and for a variation of the water level. In these three numerical tests the results were always consistent with the theoretical solutions.

Finally, as an example of application, a gravity dam structural behavior was analyzed considering the non-linear behavior in the dam-foundation interface. The dam was subjected to self-weight and hydrostatic pressure. A parametric study was developed in order to study the dam stability for different values of water level and friction angle.

Keywords: Gravity dam / 3D solid finite elements / Joint finite elements / Interface non-linear behavior / Stress-transfer / Mohr-Coulomb failure criterion / Dam-foundation interface friction angle

ANÁLISE ESTRUTURAL DE BARRAGENS GRAVIDADE CONSIDERANDO COMPORTAMENTO NÃO LINEAR NA INTERFACE BARRAGEM-FUNDAÇÃO

Desenvolvimento de um programa de EF3D, em MATLAB: DamSlide3D

Resumo

O principal objetivo deste trabalho é o desenvolvimento e apresentação de um programa de elementos finitos tridimensionais, **DamSlide3D**, para estudar o comportamento de barragens gravidade considerando o efeito de eventuais roturas ao nível da interface barragem-fundação, por tração e corte. Utilizou-se o MATLAB para desenvolver o pretendido programa, tendo-se adotado elementos finitos tridimensionais tipo cubo com 20 pontos nodais (“serendipity”) e elementos finitos de interface com 16 pontos nodais (elementos de junta).

Inicialmente, apresentam-se as equações fundamentais da mecânica dos sólidos, referindo as principais hipóteses simplificativas consideradas na formulação implementada computacionalmente, a qual é apresentada matematicamente como um problema de valores de fronteira usando uma formulação de deslocamento. Para o corpo da estrutura e para a fundação admite-se a hipótese de materiais isotrópicos com comportamento elástico linear e para as interfaces admite-se a hipótese de comportamento não linear considerando o critério de Mohr-Coulomb.

Relativamente ao programa desenvolvido, os dados de *input* são fornecidos num ficheiro de EXCEL e incluem a geometria da estrutura, as propriedades dos materiais, as condições de apoio e os parâmetros de carga. Como *output*, o programa permite visualizar graficamente o campo de tensões e o campo de deslocamento (estrutura deformada).

O programa foi previamente verificado usando três testes numéricos com soluções teóricas conhecidas. Nesses testes foi utilizada uma estrutura simples, composta por um pilar discretizado em EF3D sobre uma base, também discretizada em EF3D, utilizando elementos de interface para discretizar a superfície de contacto entre o pilar e a base (superfície horizontal) e também para discretizar uma superfície plana que atravessa o pilar com uma dada inclinação. No primeiro teste, o campo de tensões elásticas na base, devido ao peso próprio (PP) e à pressão hidrostática (PH), foi comparado com os resultados teóricos. No segundo teste foi estudada a resposta não linear do pilar para diferentes valores do ângulo de atrito na interface inclinada (neste teste a estrutura é apenas submetida ao PP). Finalmente, no terceiro teste, para as cargas principais PP+PH, a estabilidade do pilar é estudada, inicialmente, para uma variação do ângulo de atrito, e, posteriormente, para uma variação do nível da água. Nestes três testes numéricos os resultados foram sempre coerentes com as soluções teóricas.

Finalmente, como exemplo de aplicação, foi estudado o comportamento estrutural de uma barragem gravidade tendo-se analisado, em particular, o comportamento não linear ao nível da interface barragem-fundação para a combinação PP+PH. Foi efetuado um estudo paramétrico para analisar a estabilidade da barragem para diferentes valores do nível de água e do ângulo de atrito.

Palavras-chave: Barragem de gravidade / Elementos finitos sólidos 3D / Elementos finitos de junta com comportamento não-linear / Método de *stress-transfer* / Critério de rotura de Mohr-Coulomb / Ângulo de atrito na interface barragem-fundação

Table of contents

1	Introduction.....	1
2	Solid Mechanics. Fundamental Equations	3
2.1	Introductory considerations	3
2.2	Structural analysis: problem statement.....	4
2.3	The strain-displacement relations	5
2.4	The stress-strain relation. Constitutive equation.....	6
2.5	Equilibrium equation. The relation between stress spatial derivatives and body forces	7
2.6	Navier’s equation	8
2.7	Weak formulation	9
3	Finite Element Method. Solid Finite Elements and correspondent Interface Elements	11
3.1	Introductory considerations	11
3.2	Solid finite element of cubic type with 20 nodal points	14
3.3	Interface finite elements	15
3.3.1	General considerations	15
3.3.2	Interface finite elements with 8 nodes per face	17
3.3.3	Coordinates transformation. From the local coordinates system to the global coordinates system	20
3.3.4	Interface element non-linear behavior	24
4	The DamSlide3D program	28
5	Numerical tests.....	31
5.1	Test structure presentation	31
5.2	Joint behavior. Linear elastic test	31
5.3	Joint behavior. Non-linear tests	34
5.3.1	Inclined joint	34
5.3.2	Analysis of the base joint behavior considering hydrostatic pressure. Parametric study on the influence of friction angle (constant water height H=12 m)	36
5.3.3	Analysis of the base joint behavior considering hydrostatic pressure. Parametric study on the influence of water height (constant friction angle $\phi=30^\circ$)	44
6	Case Study: Gravity Dam.....	50
6.1	Dam presentation.....	50
6.2	Dam sliding scenario. Analysis of dam-foundation interface non-linear behavior	51
6.2.1	Parametric study on the influence of friction angle (full reservoir).....	52
6.2.2	Parametric study on the influence of water level (friction angle $\phi=30^\circ$)	57
7	Conclusions.....	65
	Bibliographic References.....	68

List of figures

Figure 2.1 – Displacement components, state of stress and state of strain in a point inside a solid (adapted from Oliveira, S., 2016)	3
Figure 2.2 – From the Navier equation to the numerical solution using FEM (adapted from Oliveira, S.; 2016)	4
Figure 2.3 – Solid mechanics. Stablishing the problem for the general 3D case.....	5
Figure 2.4 – Normal strain components (on the left) and shear strain components (on the right), adapted from (Oliveira, S.; 2016)	5
Figure 2.5 – Strains-displacements relation (adapted from Oliveira, S.; 2016)	6
Figure 2.6 – Stress-Strain relation. Isotropic material (adapted from Oliveira, S.; 2016).....	7
Figure 2.7 – Normal and shear stresses along axis x_1 , acting on a differential element (adapted from Oliveira, S.; 2016).....	8
Figure 2.8 – Equilibrium equations. The stress-body forces relation (adapted from Oliveira, S.; 2016)	8
Figure 2.9 – Main equations of Solid Mechanics (adapted from Oliveira, S., 2016)	9
Figure 3.1 – Structural analysis using FEM. Introduction of FEM’s fundamental approximation in the integral form of Navier’s equation	13
Figure 3.2 – 3D visualizations of the 20 nodal points isoparametric master element. On the left, are represented the nodal points and the local axes. On the right, are represented the 27 Gauss Points used (red crosses)	14
Figure 3.3 – 2D top view of the 20 node cubic element. The Gauss points location is represented with red crosses.....	14
Figure 3.4 – Interface element. Relationship between stresses and displacement differences (between interface faces). Definition of normal stiffness, K_N , and shear stiffness, K_T , of a joint. (Oliveira, S., 2016)	16
Figure 3.5 – Three dimensional interface element of 2x8 nodes (48 DoF). (a.) 3D view of the interface element. (b.) Top view of the interface element.....	17
Figure 3.6 – 3D interface element with 2x8 nodes (48 degrees of freedom). Representation of the three coordinate systems used: i) global coordinate system (tri-orthogonal); ii) local coordinate system, y_1 and y_2 (possibly curved and not orthogonal axes) towards the interface element surface; and iii) tri-orthogonal coordinate system defined at each point P of the interface elements, in which is established the joint’s constitutive relation through the diagonal elasticity matrix \underline{D}_j (Figure 3.4).....	20
Figure 3.7 – Interface element. (a.) Numbering of nodal points and Gauss points local coordinates (b.) Nodal points local coordinates. Gauss points local coordinates and corresponding influence area (weight) used on the stiffness matrix numerical integration.....	21
Figure 3.8 – Mohr’s circle representation	24
Figure 3.9 – Relation between the strength parameters c , ϕ , f_t and f_c (adapted from S. Oliveira, 1991).....	25
Figure 3.10 – Stress transfer. Schematic representation of a convergent (a) and divergent scenario (b)	26
Figure 4.1 – MATLAB programming script scheme for the element stiffness matrix calculus and subsequent assembly of the global stiffness matrix, considering a cubic “serendipity” element of 20 nodes	29
Figure 4.2 – Stress-transfer MATLAB script. Routine executed after the linear elastic calculus. The red rectangle highlights the unbalanced global forces vector calculation. The green rectangle highlights the global displacements vector calculation. The blue rectangle highlights the convergence verification.....	30
Figure 5.1 – Test structure characterization and loads (Hydrostatic pressure and self-weight $\gamma=24 \text{ kN/m}^3$).....	31

Figure 5.2 – Linear (gray) and non-linear stress distribution (red) in the horizontal joint at the column base.....31

Figure 5.3 – 3D finite element mesh31

Figure 5.4 – Gauss points considered (red crosses) for the analysis of the stress distribution at the interface column-base.....32

Figure 5.5 – Elastic behavior of the test structure. Displacements field and stress distribution at the interface column-base.....33

Figure 5.6 – Schematic representation of the forces equilibrium at the inclined joint.....34

Figure 5.7 – Numerical study of sliding across the inclined joint ($\varphi = 30^\circ$) on a concrete column under the self-weight load. (a.) Results for friction angle $\phi=30.01^\circ$, slightly higher than the joint inclination angle; a convergent solution was obtained: no sliding, as expected. (b.) Results for friction angle $\phi=29.99^\circ$, slightly lower than the joint inclination angle; divergent process, meaning that a sliding occurred35

Figure 5.8 – Column-base structural behavior for $\phi=35^\circ$. On top left, dam’s displacement field; on top right, “stress-transfer” convergence, on the middle, elastic and non-linear, normal and shear, stresses across the center section of the interface column-base; on the bottom, the dam’s principal stresses throughout the interface column-base.....37

Figure 5.9 – Column-base structural behavior for $\phi=30^\circ$. On top left, dam’s displacement field; on top right, “stress-transfer” convergence, on the middle, elastic and non-linear, normal and shear, stresses across the center section of the interface column-base; on the bottom, the dam’s principal stresses throughout the interface column-base.....38

Figure 5.10 – Column-base structural behavior for $\phi=25^\circ$. On top left, dam’s displacement field; on top right, “stress-transfer” convergence, on the middle, elastic and non-linear, normal and shear, stresses across the center section of the interface column-base; on the bottom, the dam’s principal stresses throughout the interface column-base.....39

Figure 5.11 – Column-base structural behavior for $\phi=24^\circ$. On top left, dam’s displacement field; on top right, “stress-transfer” convergence, on the middle, elastic and non-linear, normal and shear, stresses across the center section of the interface column-base; on the bottom, the dam’s principal stresses throughout the interface column-base.....40

Figure 5.12 – Column-base structural behavior for $\phi=23^\circ$. On top left, dam’s displacement field; on top right, “stress-transfer” convergence, on the middle, elastic and non-linear, normal and shear, stresses across the center section of the interface column-base; on the bottom, the dam’s principal stresses throughout the interface column-base.....41

Figure 5.13 – Column-base structural behavior for $\phi=22^\circ$. On top left, dam’s displacement field; on top right, “stress-transfer” convergence, on the middle, elastic and non-linear, normal and shear, stresses across the center section of the interface column-base; on the bottom, the dam’s principal stresses throughout the interface column-base.....42

Figure 5.14 – Column-base structural behavior for $\phi=21^\circ$. On top left, dam’s displacement field; on top right, “stress-transfer” convergence, on the middle, elastic and non-linear, normal and shear, stresses across the center section of the interface column-base; on the bottom, the dam’s principal stresses throughout the interface column-base.....43

Figure 5.15 – Stress-transfer divergence for $\phi=20^\circ$ 44

Figure 5.16 – Column-base structural behavior for $h_{\text{water}} = 12.25$ m. On top left, dam’s displacement field; on top right, “stress-transfer” convergence, on the middle, elastic and non-linear, normal and shear, stresses across the center section of the interface column-base; on the bottom, the dam’s principal stresses throughout the interface column-base45

Figure 5.17 – Column-base structural behavior for $h_{\text{water}}=12.30$ m. On top left, dam’s displacement field; on top right, “stress-transfer” convergence, on the middle, elastic and non-linear, normal and shear, stresses across the center section of the interface column-base; on the bottom, the dam’s principal stresses throughout the interface column-base46

Figure 5.18 – Column-base structural behavior for $h_{\text{water}}=12.35$ m. On top left, dam’s displacement field; on top right, “stress-transfer” convergence, on the middle, elastic and non-linear, normal and shear, stresses across the center section of the interface column-base; on the bottom, the dam’s principal stresses throughout the interface column-base47

Figure 5.19 – Column-base structural behavior for $h_{\text{water}}=12.40$ m. On top left, dam’s displacement field; on top right, “stress-transfer” convergence, on the middle, elastic and non-linear, normal and shear, stresses across the center section of the interface column-base; on the bottom, the dam’s principal stresses throughout the interface column-base48

Figure 5.20 – Stress-transfer divergence for $h_{\text{water}}=12.45$ m.....49

Figure 6.1 – Gravity dam. (a.) Downstream view (photo). (b.) Cross section (block 7, B7). (c.) The site plan. (d.) Downstream view50

Figure 6.2 – Finite element mesh adopted to study the dam sliding along the dam-foundation interface51

Figure 6.3 – Dam structural behavior for $\phi=35^\circ$. On top left, displacement field; on top right, stress-transfer convergence, in the middle, stresses across the center section of the interface dam-foundation; on the bottom, the dam’s principal stresses throughout the interface dam-foundation53

Figure 6.4 – Dam structural behavior for $\phi=30^\circ$. On top left, displacement field; on top right, stress-transfer convergence, in the middle, stresses across the center section of the interface dam-foundation; on the bottom, the dam’s principal stresses throughout the interface dam-foundation54

Figure 6.5 – Dam structural behavior for $\phi=27^\circ$. On top left, displacement field; on top right, stress-transfer convergence, in the middle, stresses across the center section of the interface dam-foundation; on the bottom, the dam’s principal stresses throughout the interface dam-foundation55

Figure 6.6 – Dam structural behavior for $\phi=26.5^\circ$. On top left, displacement field; on top right, stress-transfer convergence, in the middle, stresses across the center section of the interface dam-foundation; on the bottom, the dam’s principal stresses throughout the interface dam-foundation56

Figure 6.7 – Stress-transfer convergence for $\phi=26.0^\circ$ 57

Figure 6.8 – Dam structural behavior for $h_{\text{water}}=77$ m. On top left, displacement field; on top right, stress-transfer convergence, in the middle, stresses across the center section of the interface dam-foundation; on the bottom, the dam’s principal stresses throughout the interface dam-foundation58

Figure 6.9 – Dam structural behavior for $h_{\text{water}}=78$ m. On top left, displacement field; on top right, stress-transfer convergence, in the middle, stresses across the center section of the interface dam-foundation; on the bottom, the dam’s principal stresses throughout the interface dam-foundation59

Figure 6.10 – Dam structural behavior for $h_{\text{water}}=79$ m. On top left, displacement field; on top right, stress-transfer convergence, in the middle, stresses across the center section of the interface dam-foundation; on the bottom, the dam’s principal stresses throughout the interface dam-foundation60

Figure 6.11 – Dam structural behavior for $h_{\text{water}}=80$ m. On top left, displacement field; on top right, stress-transfer convergence, in the middle, stresses across the center section of the interface dam-foundation; on the bottom, the dam’s principal stresses throughout the interface dam-foundation61

Figure 6.12 – Dam structural behavior for $h_{\text{water}}=81$ m. On top left, displacement field; on top right, stress-transfer convergence, in the middle, stresses across the center

section of the interface dam-foundation; on the bottom, the dam's principal stresses throughout the interface dam-foundation62
Figure 6.13 – Dam structural behavior for $h_{\text{water}}=82$ m. On top left, displacement field; on top right, stress-transfer convergence, in the middle, stresses across the center section of the interface dam-foundation; on the bottom, the dam's principal stresses throughout the interface dam-foundation63
Figure 6.14 – Stress-transfer divergence for $h_{\text{water}}=83.00$ m.....64

1 | Introduction

“The complex elasticity problems encountered when intending to determine the stresses in dams and shells rarely can be resolved by rigorous methods from the classic mathematical analysis. However, there are many means to approach the problem. The first is the study in a combined model with experimental stress determination methods (...) The second is the numerical calculus” (Zienkiewicz, O.C., 1961)

Early on, even before the development of the computational power which propelled the Finite Element Method (FEM), Zienkiewicz, in a LNEC memory, was emphasizing the importance of numerical methods in the process of ascertaining a dam behavior. Likewise, Arantes e Oliveira, a reference in numerical methods (Oliveira, E.R.A. 1964), also in a LNEC memory about structural calculus automation, said the following:

“The difficulty in the manual resolution of these systems (from the force and displacement methods) from a certain order always been a tremendous obstacle, so strong it was not possible to practically accomplish the theoretical calculus schemes.” (Oliveira, E.R.A., 1964)

Therefore, the importance of having a powerful calculation tool to aid in the simulation of structural behavior through numerical methods was something identified a long time ago. With that thought in mind, this report main goal is to present a 3DFE program named **DamSlide3D**, developed in MATLAB, for the structural analysis of gravity dams considering the non-linear behavior of the dam-foundation interface, using joint elements. A gravity dam is adopted as a case study to show the potential and main capabilities of the **DamSlide3D**.

DamSlide3D requires the use of 3DFE meshes with cubic elements of 20 nodes (for the structure and foundation) and joint elements, with 16 nodes, for the interface. The linear elastic behavior hypothesis is assumed for dam body and foundation, and for the interface is assumed a non-linear behavior: opening and sliding can occur at the joint elements used in the interface discretization.

This program is intended to receive as inputs: the structure geometry, material properties, the support conditions and the loading state to which the structure is subjected. As outputs, the program allows the visualization of the stress field, displacement field and deformed shape using 2D and 3D interactive graphics.

In this report, firstly, the fundamental equations of solid mechanics are described for the general case of 3D equilibria. The displacements formulation is presented and the strong form of the Navier equation is derived. Then, the FEM fundamentals are presented, referring the conversion of the strong form to the weak form used in the FEM formulation. The formulation and numerical implementation details of the cubic finite element of 20 nodes and correspondent joint element of 16 nodes (used in the **DamSlide3D**) are presented. The implementation, in **DamSlide3D**, of the stress-transfer

technique used to simulate the non-linear behavior at the interface elements, considering the Mohr-Coulomb criterion, is also described.

The **DamSlide3D** was verified using three numerical tests with known theoretical solutions. In these tests a simple structure was used, composed by a column discretized in 3DFE. At the contact surface between the column and the base (horizontal surface) it was considered an interface discretized using joint finite elements. A plane surface that crosses the column with a given slope is also considered, discretized using the same type of joint finite elements. In the first test, the field of elastic stresses at the base, due to self-weight (SW) and hydrostatic pressure (HP), was compared with the theoretical results. In the second test, the nonlinear column behavior was studied for different values of the friction angle at the inclined interface (in this test the structure is only submitted to SW). Finally, in the third test, for the main SW + HP loads, the column stability is studied for a variation of the friction angle ϕ at the base joint, and for a water level variation.

Finally, as an example of application, the structural behavior of a gravity dam is analyzed considering the non-linear behavior at the dam-foundation interface. The dam was subjected to the self-weight and hydrostatic pressure. A parametric study was developed in order to study the dam stability for different values of water level and for different values of the interface friction angle.

Finally, the main conclusions and perspectives for future studies are presented.

2 | Solid Mechanics. Fundamental Equations

2.1 Introductory considerations

The main objective of structural analysis is to obtain an approximation of the strain and stress fields of a given structure, knowing its geometry, support conditions, material properties and applied loads. In this chapter there will be a brief presentation of solid mechanics basic equations: the equilibrium equations, the strain-displacements equations and the constitutive equations will be addressed as well as the Navier's equation expressing the relationship between body forces and displacement derivatives.

To describe the state of stress at a given point P in the interior of a solid (as well as the state of strain) is necessary the resource to the concept of tensor (DoITPoMS; 2000).

Scalar fields, like temperature, are represented, in each point P, by a number. A displacement field is a vector field that is represented, in each point, by a vector, with three components in a 3D space. A stress field is a tensor field that is represented in each point P by a second order tensor, which, for a given orthogonal coordinate system x_1 , x_2 and x_3 , is represented by a 3x3 matrix, $\underline{\sigma}$, the stress matrix. Similarly, the state of strain is also mathematically characterized, in each point, by a second order tensor represented by a 3x3 matrix in a 3D space. In Figure 2.1 these main solid mechanics variables (DoITPoMS; 2000) are schematically represented.

The state of stress at a point P is well defined if we can know the stress vector at any plane surface passing by P. In practice, it is only necessary to know the stress vectors in three mutually orthogonal cutting surfaces and, consequently, the state of stress at P is perfectly defined through a matrix which, at each line, holds the components of the three referred stress vectors. Correspondingly, at any point, the state of strain is perfectly defined by 3 vectors associated with 3 orthogonal fibers. Figure 2.1 presents graphically the abovementioned concepts (DoITPoMS; 2000).

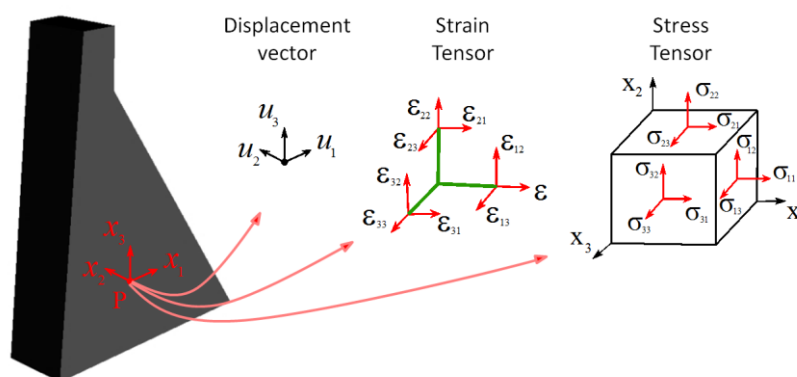


Figure 2.1 – Displacement components, state of stress and state of strain in a point inside a solid (adapted from Oliveira, S., 2016)

2.2 Structural analysis: problem statement

In structural analysis, considering the linear elastic hypothesis and static loads, a computational solution can be achieved throughout the equilibrium equation $\underline{k}\underline{u} = \underline{f}$, where $\underline{k}\underline{u}$ represents the internal forces (e.g. elastic restitution forces) and \underline{f} the external forces. In this equation, the displacements (\underline{u}) are proportional to the applied forces (\underline{f}). The matrix \underline{k} represents the structure stiffness, and is usually computed using the linear elasticity hypothesis. Figure 2.2 presents a scheme showing that the equation $\underline{k}\underline{u} = \underline{f}$ arises from the use of Finite Element Method (FEM) to solve the Navier's equation, a fundamental equation of solid mechanics.

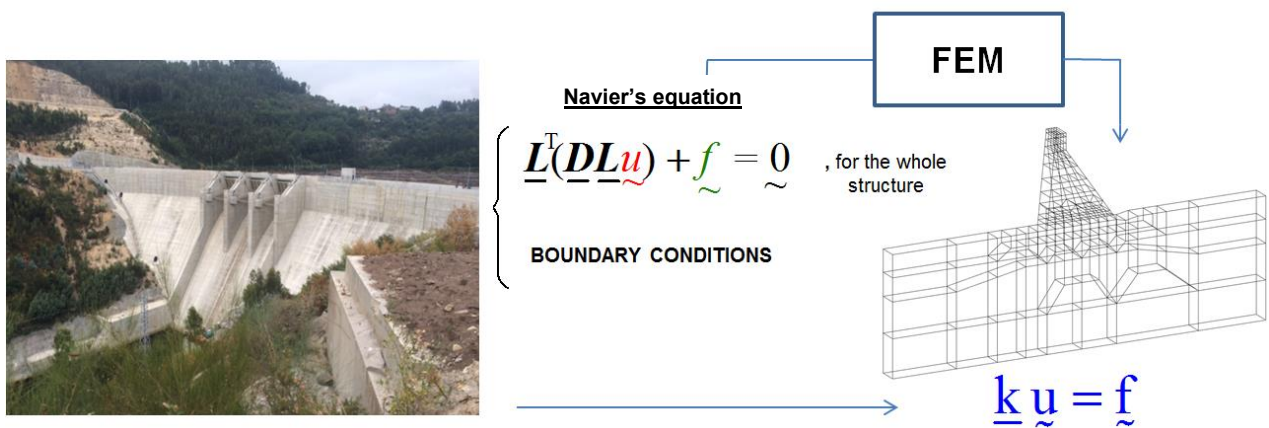


Figure 2.2 – From the Navier equation to the numerical solution using FEM (adapted from Oliveira, S.; 2016)

In structural computational analysis, the main goal is to determine the displacement, strain and stress fields which result from the action of external forces. Figure 2.3 schematically presents which variables are involved in a solid mechanics problem.

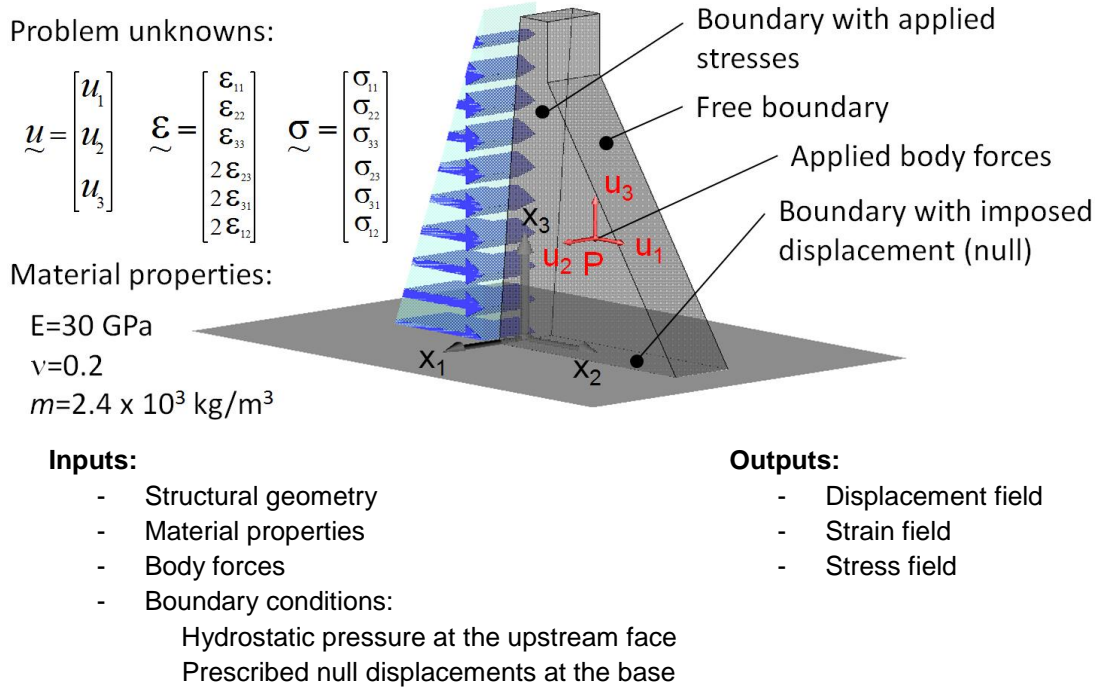


Figure 2.3 – Solid mechanics. Stablishing the problem for the general 3D case

2.3 The strain-displacement relations

The normal strain is the measure of how the displacement changes through space, which can be seen as a displacement gradient. Physically, a normal strain component is the unit change in length of a line element (fiber). Figure 2.4 illustrates, for 2D case, the concept of normal strain components and shear strain components (for small deformations we also have small angular variations so it can be assumed $\alpha = \tan(\alpha)$ and $\beta = \tan(\beta)$, and we can write $\alpha = \partial u_1 / \partial x_2$, and $\beta = \partial u_2 / \partial x_1$) (DES-UA; 2008).

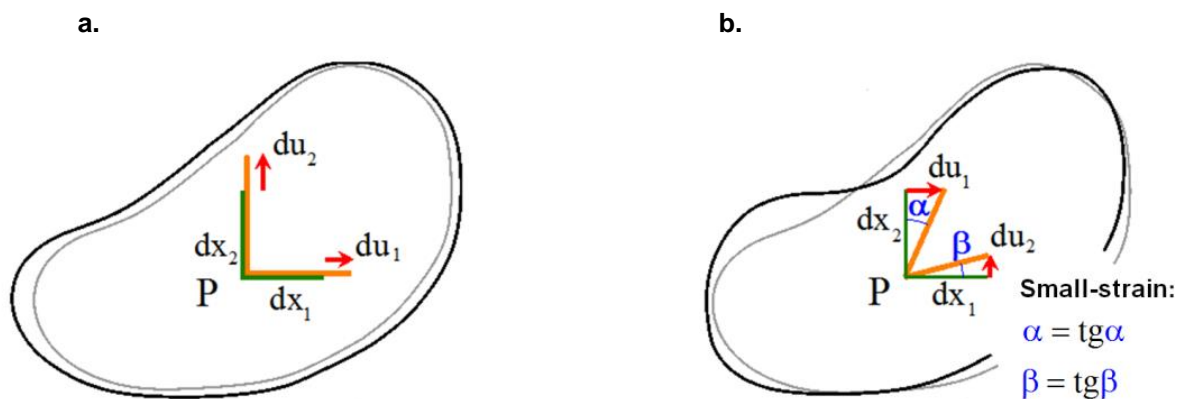


Figure 2.4 – Normal strain components (on the left) and shear strain components (on the right), adapted from (Oliveira, S.; 2016)

Figure 2.4a. represents schematically the concept of normal strain components at a point P, only with fiber length variation, where $\epsilon_{11} = \frac{\partial u_1}{\partial x_1}$ and $\epsilon_{22} = \frac{\partial u_2}{\partial x_2}$.

Figure 2.4b. represents schematically the concept of shear strain components at P, that is related with the angle variation of perpendicular material lines, being $\epsilon_{12} = \epsilon_{21} = \frac{1}{2}(\alpha + \beta) = \frac{1}{2}\left(\frac{\partial u_1}{\partial x_2} + \frac{\partial u_2}{\partial x_1}\right)$.

For the 3D case, the strain-displacement relationships are displayed in Figure 2.5.

$$\begin{cases} \epsilon_{11} = \frac{\partial u_1}{\partial x_1} \\ \epsilon_{22} = \frac{\partial u_2}{\partial x_2} \\ \epsilon_{33} = \frac{\partial u_3}{\partial x_3} \\ \epsilon_{23} = \frac{1}{2}\left(\frac{\partial u_2}{\partial x_3} + \frac{\partial u_3}{\partial x_2}\right) \\ \epsilon_{31} = \frac{1}{2}\left(\frac{\partial u_3}{\partial x_1} + \frac{\partial u_1}{\partial x_3}\right) \\ \epsilon_{12} = \frac{1}{2}\left(\frac{\partial u_1}{\partial x_2} + \frac{\partial u_2}{\partial x_1}\right) \end{cases} \quad \begin{bmatrix} \epsilon_{11} \\ \epsilon_{22} \\ \epsilon_{33} \\ 2\epsilon_{23} \\ 2\epsilon_{31} \\ 2\epsilon_{12} \end{bmatrix} = \underbrace{\begin{bmatrix} \frac{\partial}{\partial x_1} & 0 & 0 \\ 0 & \frac{\partial}{\partial x_2} & 0 \\ 0 & 0 & \frac{\partial}{\partial x_3} \\ 0 & \frac{\partial}{\partial x_3} & \frac{\partial}{\partial x_2} \\ \frac{\partial}{\partial x_3} & 0 & \frac{\partial}{\partial x_1} \\ \frac{\partial}{\partial x_2} & \frac{\partial}{\partial x_1} & 0 \end{bmatrix}}_{\substack{\underline{L} \\ (6 \times 3) \text{ Differential} \\ \text{operator}}} \begin{bmatrix} u_1 \\ u_2 \\ u_3 \end{bmatrix} \quad \begin{matrix} \underline{\epsilon} = \underline{L} \underline{u} \\ (6 \times 1) \quad \quad (3 \times 1) \end{matrix}$$

Figure 2.5 – Strains-displacements relation (adapted from Oliveira, S.; 2016)

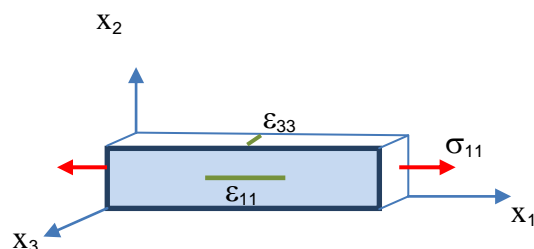
In Figure 2.5, the components of the strain tensor are arranged into a vector (the strain tensor is symmetric). Therefore, the strain displacement relation, for the 3D case, is given by the expression $\underline{\epsilon} = \underline{L} \underline{u}$, where \underline{L} is a linear differential operator (Zienkiewicz, O. C. et al., 2005).

2.4 The stress-strain relation. Constitutive equation

Considering an isotropic and homogeneous material subjected to uniaxial tensile stress, one can expect it to extend towards the axis direction and to contract transversally. In linear elasticity, stresses are proportional to strains, being the Young's Modulus (E) the proportionality constant. The proportion of contraction relative to the normal extension is given by the Poisson ratio (ν). (DES-UA, 2015)

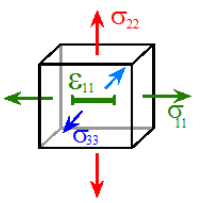
The abovementioned relation, also known as elasticity equation or Hooke's law, can be written as follows

$$\epsilon_{11} = \frac{1}{E} \sigma_{11}, \quad \epsilon_{22} = \epsilon_{33} = -\frac{\nu}{E} \sigma_{11} \quad (1)$$



For a 3D equilibrium the constitutive equations are presented in Figure 2.6, where the elasticity matrix \underline{D} , for isotropic materials, is expressed in terms of E and ν , and, also, in terms of the bulk modulus

$$K_v = \frac{E}{3(1-2\nu)} \text{ and the shear modulus } G = \frac{E}{2(1+\nu)}.$$

$$\begin{cases} \varepsilon_{11} = \frac{\sigma_{11}}{E} - \nu \frac{\sigma_{22}}{E} - \nu \frac{\sigma_{33}}{E} \\ \varepsilon_{22} = \frac{\sigma_{22}}{E} - \nu \frac{\sigma_{11}}{E} - \nu \frac{\sigma_{33}}{E} \\ \varepsilon_{33} = \frac{\sigma_{33}}{E} - \nu \frac{\sigma_{11}}{E} - \nu \frac{\sigma_{22}}{E} \\ 2\varepsilon_{23} = \frac{\sigma_{23}}{G} \\ 2\varepsilon_{31} = \frac{\sigma_{31}}{G} \\ 2\varepsilon_{12} = \frac{\sigma_{12}}{G} \end{cases} \quad \underline{\varepsilon} = \underline{D}^{-1} \underline{\sigma}$$


$$\underline{\varepsilon} = \underline{D}^{-1} \underline{\sigma} = \begin{bmatrix} \frac{1}{E} & -\frac{\nu}{E} & -\frac{\nu}{E} & 0 & 0 & 0 \\ -\frac{\nu}{E} & \frac{1}{E} & -\frac{\nu}{E} & 0 & 0 & 0 \\ -\frac{\nu}{E} & -\frac{\nu}{E} & \frac{1}{E} & 0 & 0 & 0 \\ 0 & 0 & 0 & \frac{1}{G} & 0 & 0 \\ 0 & 0 & 0 & 0 & \frac{1}{G} & 0 \\ 0 & 0 & 0 & 0 & 0 & \frac{1}{G} \end{bmatrix} \begin{bmatrix} \sigma_{11} \\ \sigma_{22} \\ \sigma_{33} \\ \sigma_{23} \\ \sigma_{31} \\ \sigma_{12} \end{bmatrix}$$

$$\underline{\sigma} = \underline{D} \underline{\varepsilon}$$

(6×1) (6×1)

$$\underline{D} = \begin{bmatrix} \frac{E(1-\nu)}{(1+\nu)(1-2\nu)} & \frac{E\nu}{(1+\nu)(1-2\nu)} & \frac{E\nu}{(1+\nu)(1-2\nu)} & 0 & 0 & 0 \\ & \frac{E(1-\nu)}{(1+\nu)(1-2\nu)} & \frac{E\nu}{(1+\nu)(1-2\nu)} & 0 & 0 & 0 \\ & \text{sym.} & \frac{E(1-\nu)}{(1+\nu)(1-2\nu)} & 0 & 0 & 0 \\ \hline 0 & 0 & 0 & G & 0 & 0 \\ 0 & 0 & 0 & 0 & G & 0 \\ 0 & 0 & 0 & 0 & 0 & G \end{bmatrix} \quad \underline{D} = \begin{bmatrix} K_v + \frac{4}{3}G & K_v - \frac{2}{3}G & K_v - \frac{2}{3}G & 0 & 0 & 0 \\ & K_v + \frac{4}{3}G & K_v - \frac{2}{3}G & 0 & 0 & 0 \\ & \text{sym.} & K_v + \frac{4}{3}G & 0 & 0 & 0 \\ \hline 0 & 0 & 0 & G & 0 & 0 \\ 0 & 0 & 0 & 0 & G & 0 \\ 0 & 0 & 0 & 0 & 0 & G \end{bmatrix}$$

(6×6) (6×6)

Figure 2.6 – Stress-Strain relation. Isotropic material (adapted from Oliveira, S.; 2016)

2.5 Equilibrium equation. The relation between stress spatial derivatives and body forces

In Figure 2.7 is shown the equilibrium, in x_1 direction, of a 3D infinitesimal material element (cubic element of volume $dx_1 dx_2 dx_3$) considering the stress spatial variation and the resultant forces at the infinitesimal cube faces. In the figure, f_1 represents the body force in x_1 direction. It is relevant to note that f_1 could represent gravitational forces as well as inertial and damping forces.

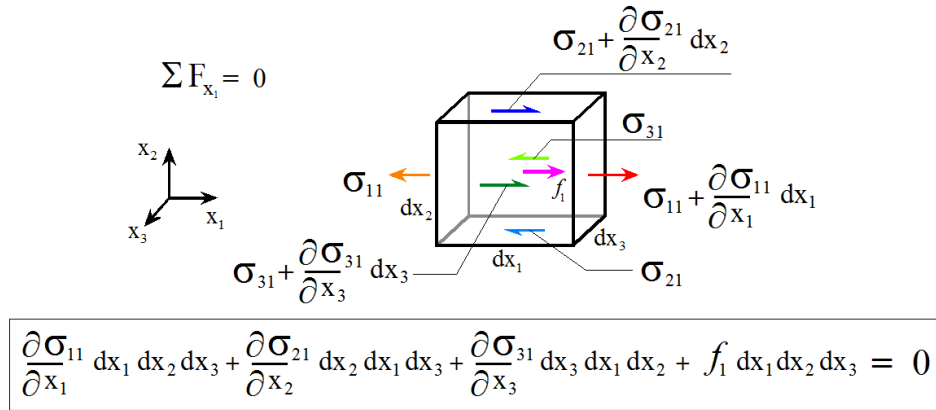


Figure 2.7 – Normal and shear stresses along axis x_1 , acting on a differential element (adapted from Oliveira, S.; 2016).

The equilibrium equation for 3D case is represented in Figure 2.8.

$$\begin{aligned} \Sigma F_{x_1} = 0 &\rightarrow \left\{ \begin{aligned} \frac{\partial \sigma_{11}}{\partial x_1} + \frac{\partial \sigma_{21}}{\partial x_2} + \frac{\partial \sigma_{31}}{\partial x_3} + f_1 &= 0 \\ \frac{\partial \sigma_{12}}{\partial x_1} + \frac{\partial \sigma_{22}}{\partial x_2} + \frac{\partial \sigma_{32}}{\partial x_3} + f_2 &= 0 \\ \frac{\partial \sigma_{13}}{\partial x_1} + \frac{\partial \sigma_{23}}{\partial x_2} + \frac{\partial \sigma_{33}}{\partial x_3} + f_3 &= 0 \end{aligned} \right. \\ &\Downarrow \\ \begin{bmatrix} \frac{\partial}{\partial x_1} & 0 & 0 & 0 & \frac{\partial}{\partial x_3} & \frac{\partial}{\partial x_2} \\ 0 & \frac{\partial}{\partial x_2} & 0 & \frac{\partial}{\partial x_3} & 0 & \frac{\partial}{\partial x_1} \\ 0 & 0 & \frac{\partial}{\partial x_3} & \frac{\partial}{\partial x_2} & \frac{\partial}{\partial x_1} & 0 \end{bmatrix} \begin{bmatrix} \sigma_{11} \\ \sigma_{22} \\ \sigma_{33} \\ \sigma_{23} \\ \sigma_{31} \\ \sigma_{12} \end{bmatrix} + \begin{bmatrix} f_1 \\ f_2 \\ f_3 \end{bmatrix} &= \begin{bmatrix} 0 \\ 0 \\ 0 \end{bmatrix} \\ &\Downarrow \\ \underline{\mathbf{L}}^T \underline{\boldsymbol{\sigma}} + \underline{\mathbf{f}} &= \underline{\mathbf{0}} \\ \text{(3x6)} \quad \text{(6x1)} \quad \text{(3x1)} \quad \text{(3x1)} & \end{aligned}$$

Figure 2.8 – Equilibrium equations. The stress-body forces relation (adapted from Oliveira, S.; 2016)

2.6 Navier's equation

In Figure 2.9 it can be noticed that it is possible to replace $\boldsymbol{\varepsilon}$ by $\underline{\mathbf{L}}\underline{\mathbf{u}}$ in the elasticity equation and that $\underline{\mathbf{D}}\underline{\mathbf{L}}\underline{\mathbf{u}}$ can replace $\boldsymbol{\sigma}$ in the equilibrium equation. So it results the Navier's equation, which is a

fundamental equation of solid mechanics (displacement formulation)¹. The Navier's equation establishes a relation between body forces and displacement derivatives.

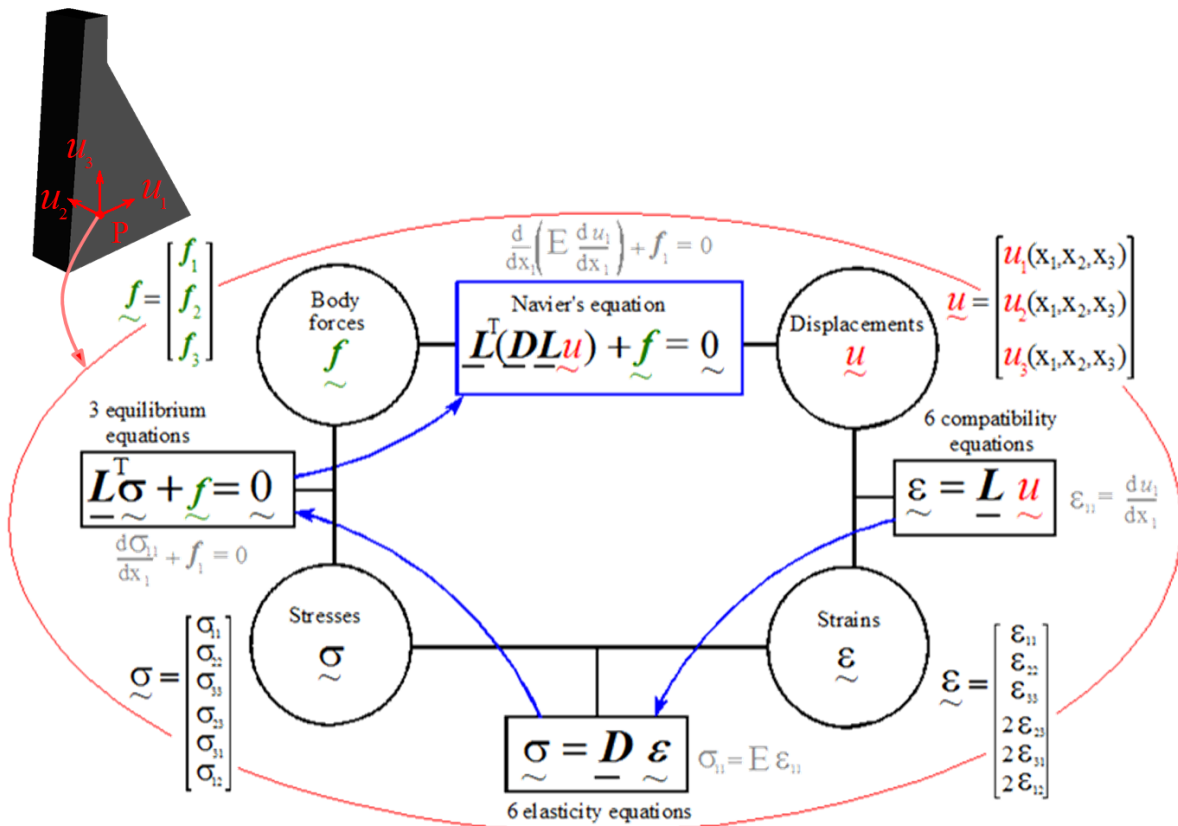


Figure 2.9 – Main equations of Solid Mechanics (adapted from Oliveira, S., 2016)

For engineering structures it is not possible to solve analytically the correspondent boundary values problem involving the Navier equation (differential equation with second order partial derivatives), consequently, it is necessary the use of numerical methods like the FEM.

The next section briefly explains how the Navier's equation (differential equation, or strong form) can be transformed into an integral equation, known as the weak form, used for obtaining the numerical solution by FEM.

2.7 Weak formulation

As referred above, in order to achieve numerical solutions for Navier's differential equation using the FEM, it is convenient to find an integral form (weak form) of the equation $\underline{\tilde{L}}^T (\underline{\tilde{D}} \underline{\tilde{L}} \underline{\tilde{u}}) + \underline{\tilde{f}} = \underline{\tilde{0}}$, which is a differential equation, of the general form $F(x)=0$, that should be verified in the domain (structure's

¹ For a stress formulation the fundamental equation would be Beltrami-Mitchell's equation.

volume) for some predefined boundary conditions. Through the application of the Fundamental Lemma of Calculus of Variations (FLCV), which is the basis of the weighted residual method, function $F(x)$ is zero in its domain if the integral of $F(x)$ multiplied by any trial function $v = v(x)$ is equal to zero (eq.3)

$$F(x) = 0, x \in V \Leftrightarrow \int_V F(x) v dx = 0, \text{ for any trial function } v = v(x) \in C_V^\infty \quad (3)$$

Consequently,

$$\left\{ \begin{array}{l} \int_V \underline{v}^T \cdot [\underline{L}^T(\underline{D}\underline{L}\underline{u}) + \underline{f}] dV = 0, \forall \underline{v} \in C_V^\infty \\ \text{Boundary Conditions} \end{array} \right. \quad (4)$$

Using the Green-Gauss theorem, equation 4 becomes,

$$\int_V (\underline{L}\underline{v})^T \underline{D}\underline{L}\underline{u} dV = \int_V \underline{v}^T \underline{f} dV, \forall \underline{v} \in C_V^\infty \quad (5)$$

There are three last notes which deserve mentioning. Firstly, it is noticeable that equation 5 is free of second order derivatives. There are only first order partial derivatives from the unknown function \underline{u} . Secondly, it is important to remind that one can directly deduce the integral form of Navier's Equation by applying the Principle of Virtual Works (PVW). Finally, the trial functions (\underline{v}) correspond to the concept of virtual displacement field used when the PVW is evoked.

3 | Finite Element Method. Solid Finite Elements and correspondent Interface Elements

3.1 Introductory considerations

In structural analysis, the numerical solution of the boundary value problem involving the Navier's equation is usually performed using a discretization into finite elements (FE). The structure is divided into elements of finite volume (FE), connected with each other by nodal points. The goal is to compute the displacement vectors at the nodal points considered.

The FEM's main idea is to consider that the displacement field $\underline{u} = \underline{u}(x_1, x_2, x_3)$ may be achieved through a linear combination of interpolation functions or shape functions \underline{N} . At a given point P within a finite element, the displacement vector \underline{u}_p can be obtained using the values \underline{N}_p of the interpolation functions in P, and the values of the element nodal displacements (\underline{u}^e): $\underline{u}_p = \underline{N}_p \underline{u}^e$. It should be noticed that \underline{u}^e is a column vector with the displacement values at the element nodal points.

For the 3D cubic element of 20 nodes, \underline{u}_p becomes:

$$\underline{u}_p = \underline{N}_p \underline{u}^e \Leftrightarrow \begin{bmatrix} u_1 \\ u_2 \\ u_3 \end{bmatrix}_p = \begin{bmatrix} N_1 & 0 & 0 & N_2 & 0 & 0 & \dots & N_{20} & 0 & 0 \\ 0 & N_1 & 0 & 0 & N_2 & 0 & \dots & 0 & N_{20} & 0 \\ 0 & 0 & N_1 & 0 & 0 & N_2 & \dots & 0 & 0 & N_{20} \end{bmatrix}_p \begin{bmatrix} \underline{u}_1^{e,1} \\ \underline{u}_2^{e,1} \\ \underline{u}_3^{e,1} \\ \underline{u}_1^{e,2} \\ \underline{u}_2^{e,2} \\ \underline{u}_3^{e,2} \\ \vdots \\ \underline{u}_1^{e,20} \\ \underline{u}_2^{e,20} \\ \underline{u}_3^{e,20} \end{bmatrix} \quad (6)$$

Considering that the virtual displacement field within a finite element can also be reached by an expression identical to 6, it results

$$\underline{v} = \underline{N} \underline{v}^e \quad (7)$$

Hence, the weak form of Navier's equation can be written as follows, for a finite element of volume V_e , considering expressions 5, 6 and 7

$$\int_{V_e} [\underline{L}(\underline{N} \underline{v}^e)]^T \underline{D} \underline{L}(\underline{N} \underline{u}^e) dV = \int_{V_e} (\underline{N} \underline{v}^e)^T \underline{f} dV, \quad \forall \underline{v} = \underline{N} \underline{v}^e \quad (8)$$

Simplifying, by elimination of \underline{v}^e , we obtain

$$\int_{V_e} (\underline{\underline{LN}})^T \underline{\underline{D}}(\underline{\underline{LN}}) dV \underline{\underline{u}}^e = \int_{V_e} \underline{\underline{N}}^T \underline{\underline{f}} dV \quad (9)$$

Using the notation $\underline{\underline{B}} = \underline{\underline{L}}\underline{\underline{N}}$ for the derivatives of the interpolation functions (Zienkiewicz et al., 2005), we can write

$$\int_{V_e} \underline{\underline{B}}^T \underline{\underline{D}}\underline{\underline{B}} dV \underline{\underline{u}}^e = \int_{V_e} \underline{\underline{N}}^T \underline{\underline{f}} dV \quad (10)$$

or,

$$\underline{\underline{K}}^e \underline{\underline{u}}^e = \underline{\underline{F}}^e \quad (11)$$

that is known as the equilibrium equation of a finite element, in the algebraic form, where,

$$\underline{\underline{K}}^e = \int_{V_e} \underline{\underline{B}}^T \underline{\underline{D}}\underline{\underline{B}} dV \text{ - Stiffness matrix of a finite element}$$

$$\underline{\underline{F}}^e = \int_{V_e} \underline{\underline{N}}^T \underline{\underline{f}} dV \text{ - Vector of nodal forces (equivalent to the body forces } \underline{\underline{f}} \text{) of a finite element}$$

$$\underline{\underline{u}}^e \text{ - Vector of nodal displacements}$$

Figure 3.1 schematically presents the use of FEM: a structure discretization in finite elements and the introduction of the FEM's fundamental approximation into the weak form of Navier's equation to obtain the equilibrium equations in the algebraic form.

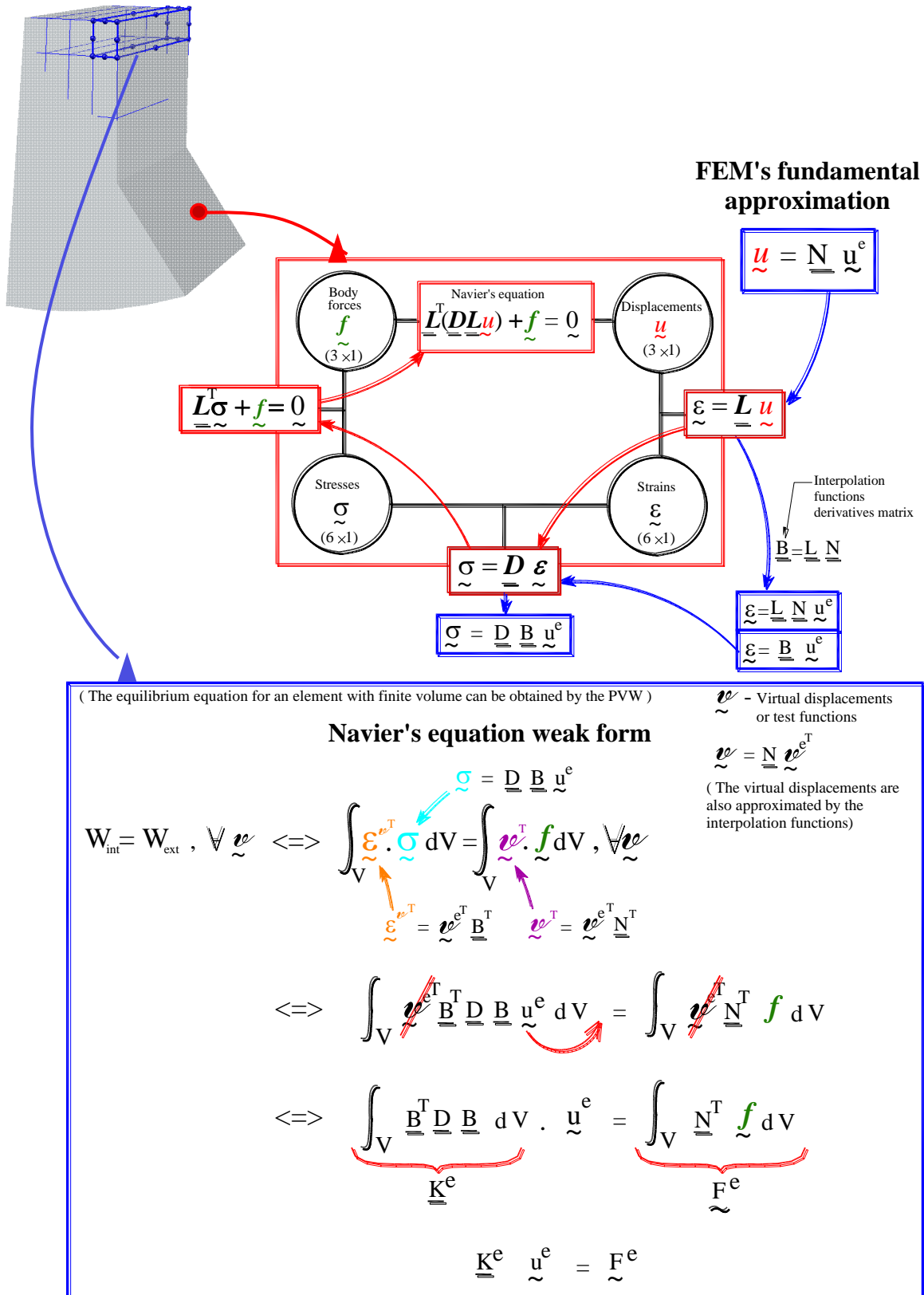


Figure 3.1 – Structural analysis using FEM. Introduction of FEM's fundamental approximation in the integral form of Navier's equation

3.2 Solid finite element of cubic type with 20 nodal points

For this study, considering a 3D equilibrium analysis, it was decided the use of a 20 nodal points cubic element (isoparametric) from the “serendipity” series. Figure 3.2 displays a 3D view of the master element used to build the FE models studied in this work.

Figure 3.2a. presents the local axes and the position of nodal points. On the other hand, Figure 3.2b. shows the location of Gauss points.

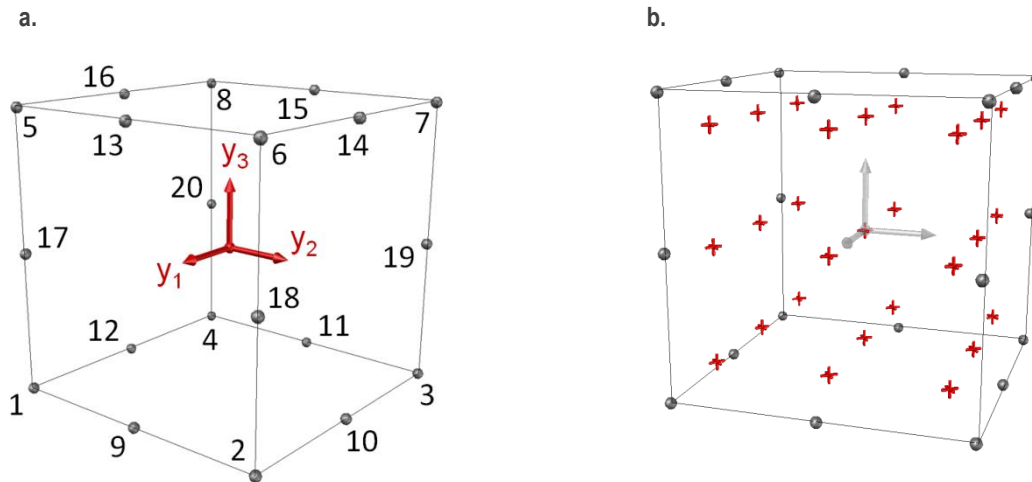


Figure 3.2 – 3D visualizations of the 20 nodal points isoparametric master element. On the left, are represented the nodal points and the local axes. On the right, are represented the 27 Gauss Points used (red crosses)

Figure 3.3 displays a 2D top visualization of the master element. This figure illustrates the cube dimensions, the location of the GP's (red in the figure) and their respective influence area (for calculate the Gauss weights).

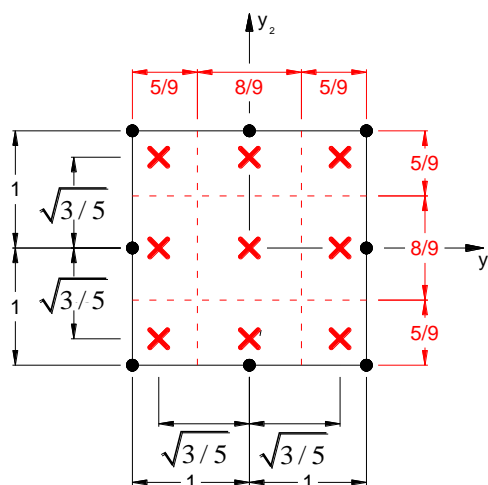


Figure 3.3 – 2D top view of the 20 node cubic element. The Gauss points location is represented with red crosses

The interpolation function N_i (associated to node i) is equal to 1 at node i and is zero in all other nodes. Equation 12 presents the interpolation functions of the cubic element of 20 nodes.

$$\left\{ \begin{array}{ll} N_i = \frac{1}{8}(1 + y_1^{(i)}y_1)(1 + y_3^{(i)}y_3)(y_1^{(i)}y_1 + y_2^{(i)}y_2 + y_3^{(i)}y_3 - 2) & (i = 1, 2, \dots, 8) \\ N_i = \frac{1}{4}(1 - y_1^2)(1 + y_2^{(i)}y_2)(1 + y_3^{(i)}y_3) & (i = 10, 12, 14, 16) \\ N_i = \frac{1}{4}(1 - y_2^2)(1 + y_3^{(i)}y_3)(1 + y_1^{(i)}y_1) & (i = 9, 11, 13, 15) \\ N_i = \frac{1}{4}(1 - y_3^2)(1 + y_1^{(i)}y_1)(1 + y_2^{(i)}y_2) & (i = 17, 18, 19, 20) \end{array} \right. \quad (12)$$

Where,

i – Nodal point index.

$y_1^{(i)}$, $y_2^{(i)}$ and $y_3^{(i)}$ – Local coordinates of node i

y_1 , y_2 and y_3 – Local coordinates of a general point inside the element

3.3 Interface finite elements

3.3.1 General considerations

The elastic properties of the interfaces (Figure 3.4) are the normal stiffness K_N and shear stiffness K_T , which are defined per unit area of the joint. Joints are defined by two faces: a lower face (face 1) and an upper face (face 2). In the finite elements discretization the faces are initially coincident and, due to the loads, there may be relative displacements between the faces: tangential displacements u_T and normal displacements u_N .

To estimate the values of K_N and K_T it can be assumed that there is a joint filling material with a given modulus of elasticity E and a distortion modulus G and that the joint has a given thickness e_f (denoted as fictitious thickness because in numerical models is not represented - the faces of the joint are coincident). With this hypothesis one can estimate the normal stiffness of the joint (13) based on the formula for calculating the axial stiffness of a column of length L , which is EA / L . In this case of the joint, L is replaced by the fictitious thickness of the joint (e_f) and the unit area ($A = 1$, stiffness per unit area) is considered and thus the normal stiffness of the joint per unit area becomes:

$$K_N = E/e_f \quad (13)$$

For the shear stiffness, is the same, using now the shear modulus G , being

$$K_T = G/e_f \quad (14)$$

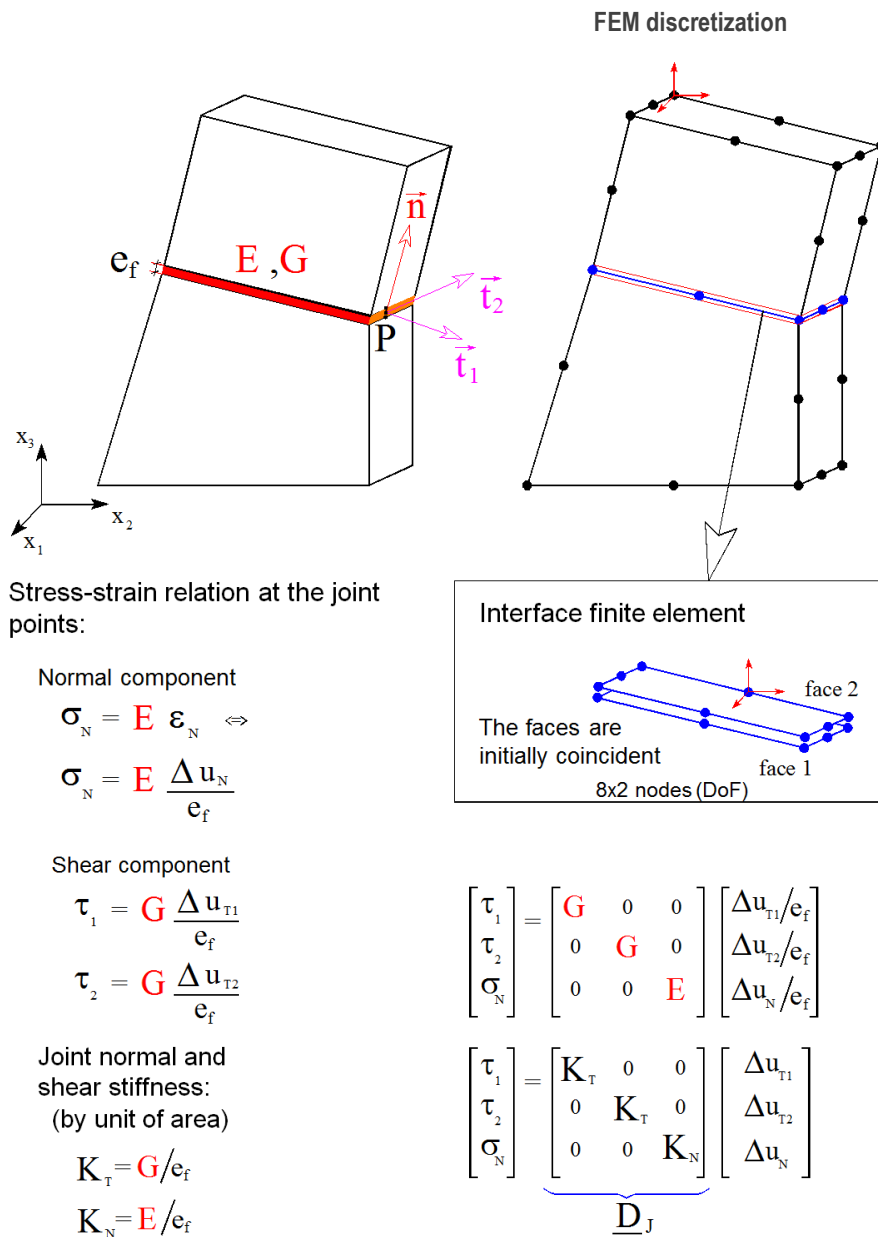


Figure 3.4 – Interface element. Relationship between stresses and displacement differences (between interface faces). Definition of normal stiffness, K_N , and shear stiffness, K_T , of a joint. (Oliveira, S., 2016)

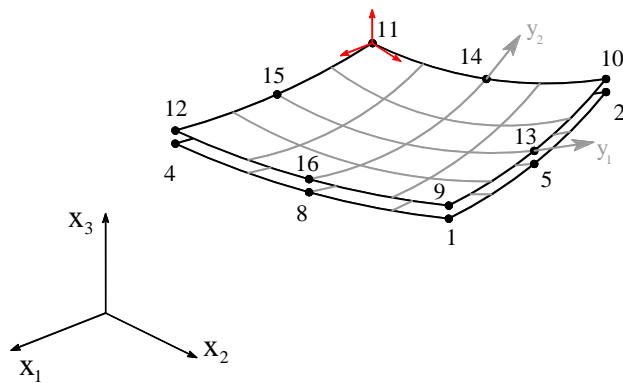
3.3.2 Interface finite elements with 8 nodes per face

The interface elements are used to simulate the behavior of discontinuities that represent the contact surface between two materials in diaclases, cracks, construction joints in dams, etc.

The 16 nodes interface finite elements (8 nodes per face) are used to simulate the interaction between the two faces of two 20 nodes finite elements that possess two adjacent faces. The interface element establishes the “connection” between both faces (8 nodes per face). This kind of interface finite element is named “2x8 interface element” (Genésio, M.L.V.P., 1993).

Figure 3.5 presents a 3D interface finite element with 2x8 nodal points and 3 Degrees of Freedom (DoF) per node (48 DoF). The interpolation functions are identical to those used in the 8 nodes 2D quadratic finite elements (Equations 15).

a. 3D 8x2 nodes interface element



b. Interface element top view

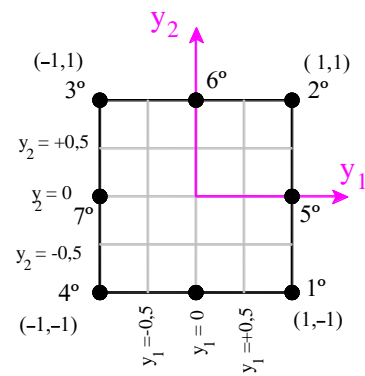


Figure 3.5 – Three dimensional interface element of 2x8 nodes (48 DoF). (a.) 3D view of the interface element. (b.) Top view of the interface element

$$\left\{ \begin{array}{l} N_i = \frac{1}{4}(1 + y_1^{(i)} y_1)(1 + y_2^{(i)} y_2)(y_1^{(i)} y_1 + y_2^{(i)} y_2 - 1) \quad (i=1,2,3,4) \\ N_i = \frac{1}{2}(1 - y_1^2)(1 + y_2^{(i)} y_2) \quad (y_1^{(i)} = 0) \quad (i = 6, 8) \\ N_i = \frac{1}{2}(1 + y_1^{(i)} y_1)(1 - y_2^2) \quad (y_2^{(i)} = 0) \quad (i = 5, 7) \end{array} \right. \quad (15)$$

For every point of the interface element, named P, the constitutive relation between stresses (one normal and two shear components in relation to the joint plane) and strains (one normal and two shear strain components) can be written according to expression 16, considering a local tri-orthogonal coordinates system $(\vec{n}, \vec{t}_1, \vec{t}_2)$, Figure 3.4), where one of the axes is perpendicular to the joint, and the remaining are contained in the tangential plane to the joint, at point P.

$$\begin{bmatrix} \tau_1 \\ \tau_2 \\ \sigma_N \end{bmatrix} = \underbrace{\begin{bmatrix} G & 0 & 0 \\ 0 & G & 0 \\ 0 & 0 & E \end{bmatrix}}_{\underline{D}'} \underbrace{\begin{bmatrix} \gamma_1 \\ \gamma_2 \\ \varepsilon_N \end{bmatrix}}_{\underline{\varepsilon}'} \Leftrightarrow \begin{bmatrix} \tau_1 \\ \tau_2 \\ \sigma_N \end{bmatrix} = \begin{bmatrix} G & 0 & 0 \\ 0 & G & 0 \\ 0 & 0 & E \end{bmatrix} \begin{bmatrix} \Delta u_{T1}/e_i \\ \Delta u_{T2}/e_i \\ \Delta u_N/e_i \end{bmatrix} \quad (16)$$

Therefore,

$$\begin{bmatrix} \tau_1 \\ \tau_2 \\ \sigma_N \end{bmatrix} = \underbrace{\begin{bmatrix} K_{T1} & 0 & 0 \\ 0 & K_{T2} & 0 \\ 0 & 0 & K_N \end{bmatrix}}_{\underline{D}'_J} \underbrace{\begin{bmatrix} \Delta u_{T1} \\ \Delta u_{T2} \\ \Delta u_N \end{bmatrix}}_{\underline{\Delta u}'}, \quad K_T = G/e_i, \quad K_N = E/e_i \quad (17)$$

Where,

K_{T1} - Shear stiffness towards direction t_1 , which is contained in the joint's tangent plane, at point P (joint's stiffness per area unit).

K_{T2} - Shear stiffness towards direction t_2 , perpendicular to t_1 and contained in the joint's tangent plane, at point P (joint's stiffness per area unit).

K_N - Normal stiffness towards the perpendicular direction of the joint's tangent plane, at point P.

Generally, $K_{T1}=K_{T2}=K_T$ (this hypothesis is valid for an isotropic joint filling material).

Consequently, for every point P of the joint, the relation between stresses and displacement differences (between faces), can be expressed as follows

$$\underline{\sigma}'_P = \underline{D}'_J \underline{\Delta u}'_P \quad (18)$$

Where the symbol " ' " is used to distinguish the coordinate system at use, which, in this case, is the tri-orthogonal t_1 , t_2 and t_3 (the t_3 direction coincides with the direction of vector n , Figure 3.4).

Using the interpolation method, vector $\underline{\Delta u}'_P$ can be written in order to the terms of the displacement differences at each interface element node. The bidimensional 8 nodes quadratic shape functions are used and the result is the following

$$\Delta \underline{u}' = \begin{bmatrix} \Delta u_{T1} \\ \Delta u_{T2} \\ \Delta u_N \end{bmatrix}_P = \begin{bmatrix} N_1 & 0 & 0 & \dots & N_8 & 0 & 0 \\ 0 & N_1 & 0 & \dots & 0 & N_8 & 0 \\ 0 & 0 & N_1 & \dots & 0 & 0 & N_8 \end{bmatrix}_P \begin{bmatrix} u_{T1}^{e9} - u_{T1}^{e1} \\ u_{T2}^{e9} - u_{T2}^{e1} \\ u_N^{e9} - u_N^{e1} \\ \vdots \\ u_{T1}^{e16} - u_{T1}^{e8} \\ u_{T2}^{e16} - u_{T2}^{e8} \\ u_N^{e16} - u_N^{e8} \end{bmatrix} \quad (19)$$

Equivalently, the equation can be written in the following form.

$$\Delta \underline{u}' = \begin{bmatrix} \Delta u_{T1} \\ \Delta u_{T2} \\ \Delta u_N \end{bmatrix}_{3 \times 1} = \begin{bmatrix} -N_1 & 0 & 0 & \dots & -N_8 & 0 & 0 & N_1 & 0 & 0 & \dots & N_8 & 0 & 0 \\ 0 & -N_1 & 0 & \dots & 0 & -N_8 & 0 & 0 & N_1 & 0 & \dots & 0 & N_8 & 0 \\ 0 & 0 & -N_1 & \dots & 0 & 0 & -N_8 & 0 & 0 & N_1 & \dots & 0 & 0 & N_8 \end{bmatrix}_P \begin{bmatrix} u_1^{e1} \\ u_2^{e1} \\ u_3^{e1} \\ \vdots \\ u_1^{e8} \\ u_2^{e8} \\ u_3^{e8} \\ \hline u_1^{e9} \\ u_2^{e9} \\ u_3^{e9} \\ \vdots \\ u_1^{e16} \\ u_2^{e16} \\ u_3^{e16} \end{bmatrix}_{48 \times 1} \quad (20)$$

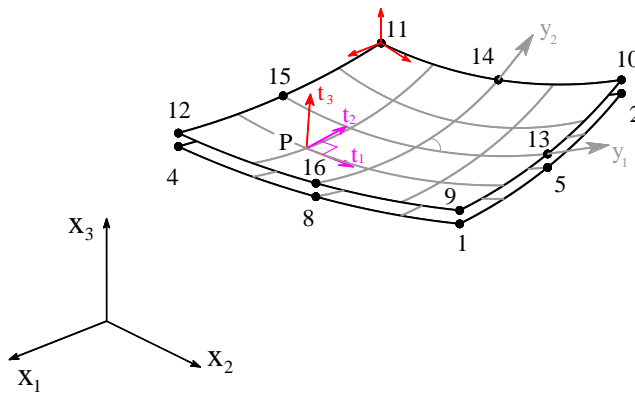
$\underbrace{\hspace{15em}}_{\substack{N_P \\ 3 \times 48}}$

or

$$\Delta \underline{u}'_P = \underline{N}_P \underline{u}'^e \quad (21)$$

3.3.3 Coordinates transformation. From the local coordinates system to the global coordinates system

To obtain the interface element stiffness matrix, referred to the global axes, it should be used a transformation matrix (\underline{T}), in each of the Gauss points. This transformation matrix is composed by the local axes direction cosines relatively to the global axes (x_1, x_2 and x_3). The axes t_1 and t_2 are coplanar with the plane tangent to the joint's plane and t_3 is perpendicular to t_1 and t_2 , at each Gauss point (Figure 3.6).



Vectors \vec{t}_1, \vec{t}_2 and \vec{t}_3 calculation:

\vec{t}_1 - unit vector tangent to y_1 (jacobian matrix first column at point P);

\vec{t}_3 - normal unit vector (the jacobian matrix two columns vector product);

\vec{t}_2 - unit vector perpendicular to both, \vec{t}_1 and \vec{t}_3 (vector product $\vec{t}_1 \times \vec{t}_3$). This vector might not be coincident with y_2 .

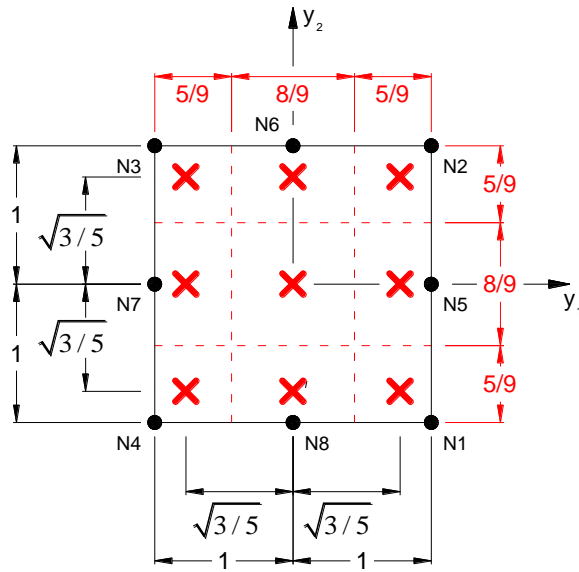
Figure 3.6 – 3D interface element with 2x8 nodes (48 degrees of freedom). Representation of the three coordinate systems used: i) global coordinate system (tri-orthogonal); ii) local coordinate system, y_1 and y_2 (possibly curved and not orthogonal axes) towards the interface element surface; and iii) tri-orthogonal coordinate system defined at each point P of the interface elements, in which is established the joint's constitutive relation through the diagonal elasticity matrix \underline{D}_j (Figure 3.4)

The transformation matrix \underline{T} should be determined for each Gauss point of the interface element. This process starts with the calculation of the Jacobian matrix (for each Gauss point). The Jacobian matrix contains the directions of the local axes (y_1 and y_2) of the tangent plane to the joint, at each Gauss point. The result is the following 3x2 matrix

$$\underline{J}_{GP} = \begin{bmatrix} J_{11} & J_{12} \\ J_{21} & J_{22} \\ J_{31} & J_{32} \end{bmatrix}_{GP} = \begin{matrix} \text{Global coordinates for} \\ \text{the joint's nodal points.} \\ \begin{bmatrix} x_1^{e1} & \dots & x_1^{e8} \\ x_2^{e1} & \dots & x_2^{e8} \\ x_3^{e1} & \dots & x_3^{e8} \end{bmatrix} \end{matrix} \begin{matrix} \begin{bmatrix} \frac{\partial N_1}{\partial y_1} & \frac{\partial N_1}{\partial y_2} \\ \vdots & \vdots \\ \frac{\partial N_8}{\partial y_1} & \frac{\partial N_8}{\partial y_2} \end{bmatrix}_{GP} \end{matrix} \quad (22)$$

The interpolation functions N_i and the corresponding derivatives $\partial N_i / \partial y_j$, are equal to those used in the 8 nodes quadratic 2D elements. An interface element is formed by two faces of the 3D elements (with 8 nodes each). Figure 3.7 displays the local coordinates of nodal points and Gauss points of the presented interface element, as well as the Gauss weights.

a.



b.

Local nodal coordinates

Node (i)	$y_1^{(i)}$	$y_2^{(i)}$
1	1	-1
2	1	1
3	-1	1
4	-1	-1
5	1	0
6	0	1
7	-1	0
8	0	-1

c. Gauss points local coordinates and Gauss weights

$W_1=5/9$					$W_2=8/9$					$a = \sqrt{3/5}$				
GP	Type	y_1	y_2	A_{GP}	GP	Type	y_1	y_2	A_{GP}	GP	Type	y_1	y_2	A_{GP}
1	Corner	a	$-a$	W_1^2	5	Side	a	0	$W_1.W_2$	9	Center	0	0	W_2^2
2		a	a		6		0	a						
3		$-a$	a		7		$-a$	0						
4		$-a$	$-a$		8		0	$-a$						

Figure 3.7 – Interface element. (a.) Numbering of nodal points and Gauss points local coordinates (b.) Nodal points local coordinates. Gauss points local coordinates and corresponding influence area (weight) used on the stiffness matrix numerical integration

This way, the Jacobian matrix, for a given Gauss point, is displayed in equation 23

$$\underline{J}_{PG} = \begin{bmatrix} J_{11} & J_{12} \\ J_{21} & J_{22} \\ J_{31} & J_{32} \end{bmatrix} \quad (23)$$

Considering the above Jacobian matrix, one can determine a tri-orthogonal coordinate system, with versors \vec{T}_1 , \vec{T}_2 and \vec{T}_3 (unit vectors), using the following three equations.

$$\vec{T}_1 = \frac{(J_{11}, J_{21}, J_{31})}{\sqrt{J_{11}^2 + J_{21}^2 + J_{31}^2}} \quad (24)$$

$$\vec{T}_3 = \frac{\vec{t}_3}{\|\vec{t}_3\|}, \quad \vec{t}_3 = (J_{11}, J_{21}, J_{31}) \times (J_{12}, J_{22}, J_{32}) \quad (25)$$

$$\vec{T}_2 = \vec{T}_3 \times \vec{T}_1 \quad (26)$$

Therefore, the transformation matrix \underline{T} can be assembled for each Gauss point, being

$$\underline{T}_{GP} = \begin{bmatrix} \overline{T}_1 \\ \overline{T}_2 \\ \overline{T}_3 \end{bmatrix}_{GP} = \begin{bmatrix} T_{11} & T_{12} & T_{13} \\ T_{21} & T_{22} & T_{23} \\ T_{31} & T_{32} & T_{33} \end{bmatrix}_{GP} \quad (27)$$

So, at any P_k point of the joint (P_1 's belonging to face $k=1$, P_2 's belonging to face $k=2$, ...), the relation between displacement components in axes, t_1 , t_2 and t_3 , and in global axes, x_1 , x_2 and x_3 , is given by the following equation

$$\begin{bmatrix} u_{T1} \\ u_{T2} \\ u_N \end{bmatrix}_{\substack{P \\ \text{face } k \\ (t_1, t_2, t_3)}} = \begin{bmatrix} T_{11} & T_{12} & T_{13} \\ T_{21} & T_{22} & T_{23} \\ T_{31} & T_{32} & T_{33} \end{bmatrix}_P \cdot \begin{bmatrix} u_1 \\ u_2 \\ u_3 \end{bmatrix}_{\substack{P \\ \text{face } k \\ (x_1, x_2, x_3)}} \quad (28)$$

In a more abbreviated notation, the abovementioned equation, takes the following form

$$\underline{u}'_P = \underline{T}_P \underline{u}_P \quad (29)$$

Thus, in local axes t_1 , t_2 and t_3 , the displacement differences at any P joint section (being P a point belonging to the mean surface and P_1 and P_2 points belonging to each face) can be related with the nodal displacements associated with the global axes through the following interpolation formula

$$\begin{bmatrix} \Delta u_{T1} \\ \Delta u_{T2} \\ \Delta u_N \end{bmatrix}_{3 \times 1}^P = \begin{bmatrix} T_{11} & T_{12} & T_{13} \\ T_{21} & T_{22} & T_{23} \\ T_{31} & T_{32} & T_{33} \end{bmatrix}_P \begin{bmatrix} -N_1 & 0 & 0 & -N_8 & 0 & 0 & N_1 & 0 & 0 & N_8 & 0 & 0 \\ 0 & -N_1 & 0 & \dots & 0 & -N_8 & 0 & 0 & N_1 & 0 & \dots & 0 & N_8 & 0 \\ 0 & 0 & -N_1 & 0 & 0 & -N_8 & 0 & 0 & N_1 & 0 & 0 & 0 & N_8 & 0 \end{bmatrix}_{(3 \times 48)} \begin{bmatrix} u_1^{e1} \\ u_2^{e1} \\ u_3^{e1} \\ \vdots \\ u_1^{e8} \\ u_2^{e8} \\ u_3^{e8} \\ u_1^{e9} \\ u_2^{e9} \\ u_3^{e9} \\ \vdots \\ u_1^{e16} \\ u_2^{e16} \\ u_3^{e16} \end{bmatrix}_{(48 \times 1)} \quad (30)$$

In an abbreviated notation, the abovementioned equation, takes the following form

$$\Delta \underline{u}'_P = \underline{T}_P \underline{N}_P \underline{u}^e \quad (31)$$

The joint's elasticity equation in its local coordinate system is represented by the following equation

$$\underline{\underline{\sigma}}' = \underline{\underline{D}}_J \underline{\underline{\Delta}} \underline{\underline{u}}' \quad (32)$$

$\begin{matrix} (3 \times 1) & (3 \times 3) & (3 \times 1) \end{matrix}$

Taking the last two equations into account, it is possible to reach the following equation for global axes

$$\underline{\underline{\sigma}}' = \underline{\underline{D}}_J \underline{\underline{T}} \underline{\underline{N}} \underline{\underline{u}}^e \quad (33)$$

$\begin{matrix} (3 \times 1) & (3 \times 3) & (3 \times 3) & (3 \times 48) & (48 \times 1) \end{matrix}$

Finally, the integral expression corresponding to the stiffness matrix of the joint element can be obtained by introducing the above interpolation formulas into the weak (or integral) form of the Navier equation which, as is known, can be obtained by applying the PVW to the joint finite element. Thus, taking into account that the work of the internal forces associated with the virtual deformations $\underline{\underline{\varepsilon}}_u'$ is given by

$$W_{int} = \int_{V_J} \underline{\underline{\varepsilon}}_u'^T \underline{\underline{\sigma}}' dV = e_f \int_{A_J} \underline{\underline{\varepsilon}}_u'^T \underline{\underline{\sigma}}' dA \quad (34)$$

and that $\underline{\underline{\varepsilon}}_u' = \underline{\underline{\Delta}} \underline{\underline{u}}_u' / e_f$, then, by introducing in this integral expression the above interpolation formulas of the FEM, we obtain the expression (35) for the stiffness matrix of the joint element

$$\underline{\underline{k}}_J^e = \int_{A_J} \underline{\underline{N}}^T \underline{\underline{T}}^T \underline{\underline{D}}_J \underline{\underline{T}} \underline{\underline{N}} dA \quad (35)$$

$\begin{matrix} (48 \times 48) & A_J & (48 \times 3) & (3 \times 3) & (3 \times 48) \end{matrix}$

In the aforementioned equation is noticeable that the joint thickness is not present anymore explicitly. By integrating into the local axes y_1, y_2 we obtain

$$\underline{\underline{k}}_J^e = \int_{A_J} \underline{\underline{N}}^T \underline{\underline{T}}^T \underline{\underline{D}}_J \underline{\underline{T}} \underline{\underline{N}} \phi_J dy_1 dy_2 \quad (36)$$

$\begin{matrix} (48 \times 48) & A_J & (48 \times 3) & (3 \times 3) & (3 \times 48) \end{matrix}$

where $\phi_J = \|\underline{\underline{J}}_{i1} \times \underline{\underline{J}}_{i2}\|$ (area of the parallelogram defined by the vectors corresponding to the two columns of the Jacobian matrix).

Using the Gauss method to perform the integration numerically, it is obtained the usual summation (37) extended to the 9 Gauss points of the joint element, which is currently used in the structural FEM programs

$$\underline{\underline{k}}_J^e = \sum_{i=1}^{N_{gp}=9} \underline{\underline{N}}_i^T \underline{\underline{T}}_i^T \underline{\underline{D}} \underline{\underline{T}}_i \underline{\underline{N}}_i \phi_{Ji} A_i \quad (37)$$

$\begin{matrix} (48 \times 48) \end{matrix}$

Finally, it should be noted that in most structural analysis programs available on the market, the elastic properties of the joint elements that users are required to enter are only K_N and K_T ($K_N = E/e_f$, $K_T = G/e_f$), and it is not required to specify the value of the joint thickness e_f , hence the usual designation of fictitious thickness.

3.3.4 Interface element non-linear behavior

The non-linear behavior of the joint's materials is characterized not only by its elastic properties, which are the normal and shear stiffness, K_N and K_T , respectively, but also by its strength properties, which are the cohesion c , and the friction angle ϕ . With this strength parameters we are able to evaluate the admissibility of the state of stress installed in the interface elements

$$\underline{\sigma}_{GP,J} = \underline{D}_J \underline{T} \underline{N}_p \underline{u}_e = \begin{bmatrix} \tau_{t1} \\ \tau_{t2} \\ \sigma_n \end{bmatrix} \quad (38)$$

To study the admissibility of a state of stress at a given point is useful its representation by a Mohr's circle (Figure 3.8).

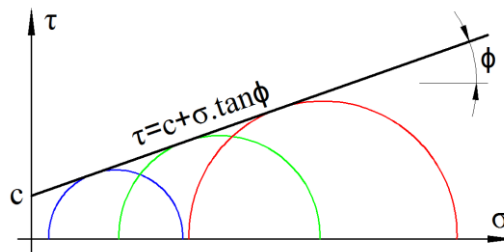


Figure 3.8 – Mohr's circle representation

If it is found that at a given Gauss point of the joint element the normal stress exceeds the uniaxial tensile strength, f_t , (if $c=0$ we will have $f_t=0$) or the shear stress exceeds the shear strength, τ_r , a joint local failure will occur, and it will be necessary to redistribute the unbalanced stresses

$$\tau = \sqrt{\tau_{t1}^2 + \tau_{t2}^2} \quad (39)$$

$$f_t = c \times \frac{2 \cos(\phi)}{1 + \sin(\phi)} \quad (40)$$

$$\tau_r = c + \sigma_n \times \tan(\phi) \quad (41)$$

In the developed program **DamSlide3D**, criteria were established for the determination of the maximum uniaxial compression strength (f_c) and for the maximum uniaxial tension strength (f_t). This values can be related with cohesion c and friction angle ϕ (Figure 3.9).

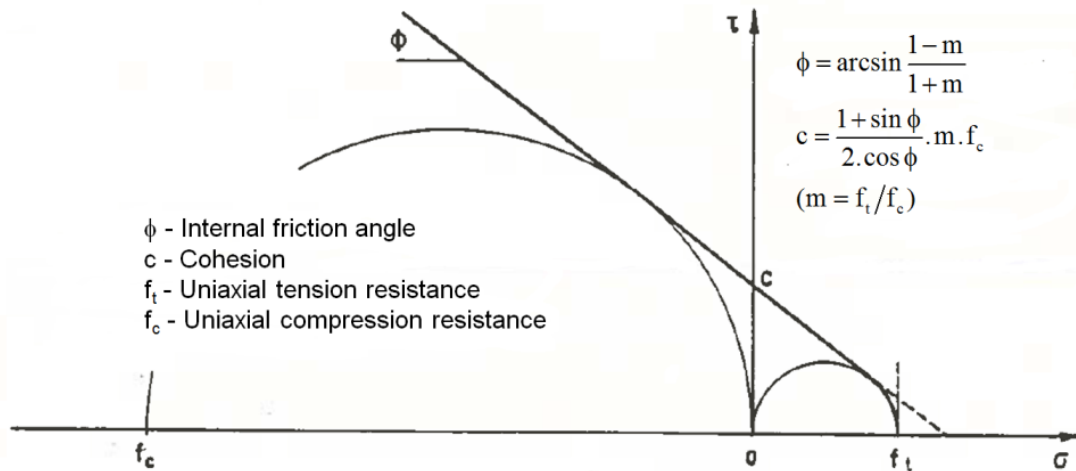


Figure 3.9 – Relation between the strength parameters c , ϕ , f_t and f_c (adapted from S. Oliveira, 1991)

In nonlinear structural analysis with joint elements, the redistribution of stresses higher than the admissible (verification to be performed at the Gauss points of the joint elements) is achieved by a process that transforms the non-admissible stresses into forces to be applied in the nodes of the joint element. In this way, a vector of unbalanced forces is built for every joint element (42)

$$\underline{F}_{\text{Unb}} = \sum_1^9 \underline{N}_p^T \underline{T}^T \underline{\sigma}_{\text{unb}} \phi_J \underline{W}_{\text{GP},J} \quad (42)$$

The vectors of unbalanced forces in a joint element are then assembled into the global vector of unbalanced forces $\underline{\psi}$. The unbalanced forces are re-applied iteratively. This non-linear calculus methodology is named stress-transfer. The following equation summarizes the process

$$\underline{K}_0 \underline{u} = \underline{F}_{\text{ap}} + \underline{\psi} \quad (43)$$

With the internal forces redistribution, two scenarios can occur:

- The applied loads are compatible with the global strength of the structure. In this scenario, the stress-transfer process converges.
- The applied loads are not compatible with the global strength of the structure. In this scenario, the stress-transfer process diverges.

Figure 3.10 shows, graphically, the iterative stress-transfer process whether it reaches a solution (3.10a), and whether it is not able to reach a solution (3.10b), which is the case of a divergent stress-transfer process.

$$\underline{K}_0 \underline{u} = \underline{F}_{ap} + \underline{\psi}$$

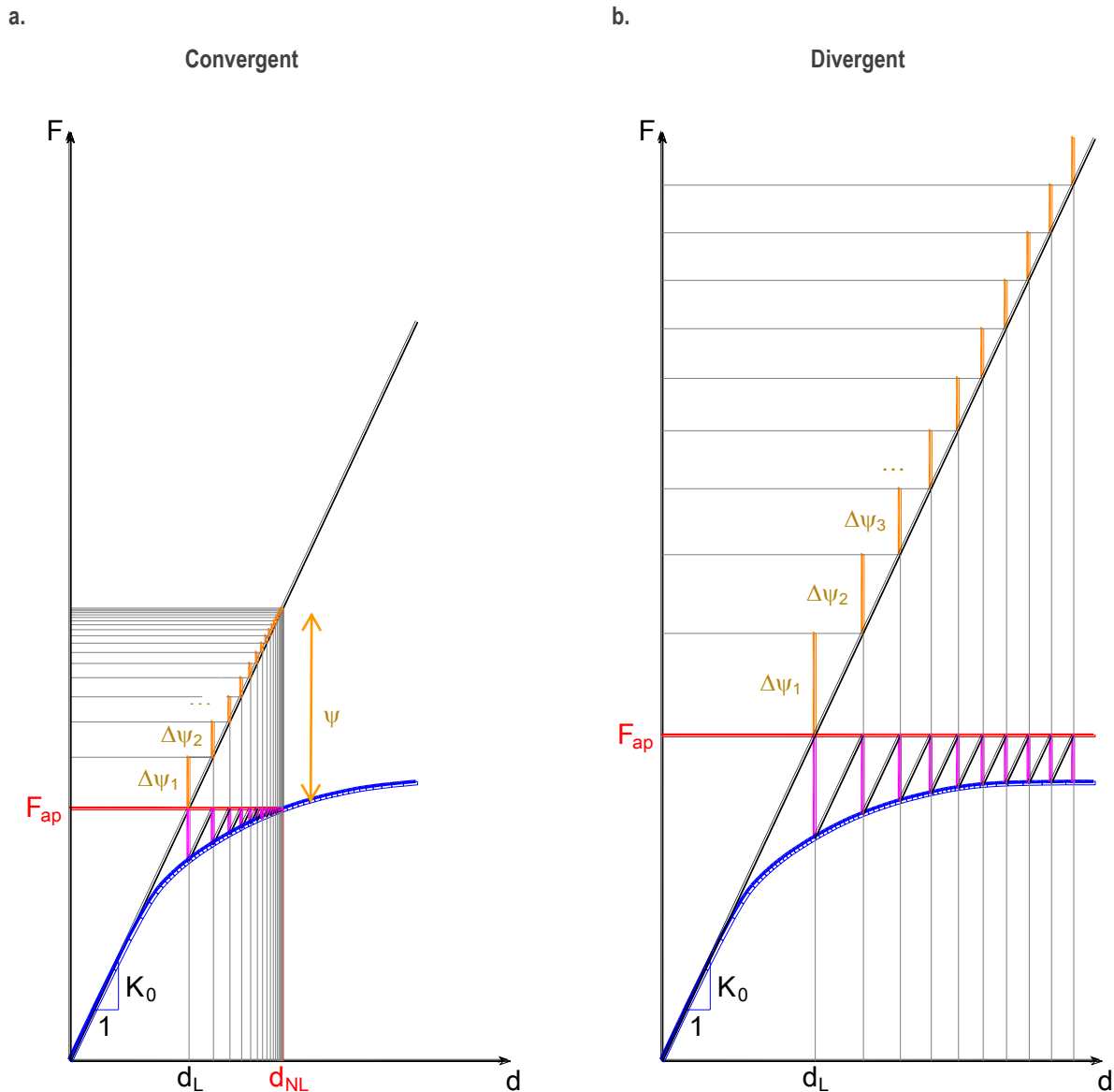


Figure 3.10 – Stress transfer. Schematic representation of a convergent (a) and divergent scenario (b)

As it is depicted in Figure 3.10a, when the stress transfer method converges to the solution, it does so with a resulting decreasing difference between displacements, between two consecutive iterations. This difference, when approaching the solution, tends to zero. It is necessary to establish a convergence criteria which stops the iterative process when the obtained displacement values are sufficiently close to the solution. The following two equations display the criteria adopted to interrupt the iteration process. When the difference between the results from the first iteration displacements (\underline{u}_1) and the elastic displacements (\underline{u}_{el}) is equal to zero, $Norm_i$ will be equal to zero and, therefore,

lesser than a predefined tolerance (Tol), hence, the iteration process finishes. When the difference $\underline{u}_1 - \underline{u}_{el}$ is not zero and the difference $\underline{u}_i - \underline{u}_{i-1}$ decreases between consecutive iterations, the process will stop when

$\frac{|\underline{u}_i - \underline{u}_{i-1}|}{|\underline{u}_1 - \underline{u}_{el}|} \times 100$ is below the admitted tolerance

$$Norm_i = \begin{cases} \frac{|\underline{u}_i - \underline{u}_{i-1}|}{|\underline{u}_1 - \underline{u}_{el}|} \times 100, & |\underline{u}_1 - \underline{u}_{el}| > 0 \\ 0, & |\underline{u}_1 - \underline{u}_{el}| = 0 \end{cases} \quad (44)$$

$$Norm_i < Tol \quad (45)$$

For a divergent process, the difference $\underline{u}_i - \underline{u}_{i-1}$ does not decrease in consecutive iterations and, consequently $Norm_i$ is always higher than Tol . In this case, it is necessary to define a limit value for the number of iterations in order, once again, to stop the process.

4 | The DamSlide3D program

To achieve the objectives of this work, it was developed a computational FEM program, using MATLAB, named **DamSlide3D**. As explained in chapter 3, this program uses the 20 nodal point's cubic element and the correspondent 16 nodal point's joint elements.

The input data for **DamSlide3D** include the structure geometry (its FE mesh: nodal coordinates and elements definition), the material properties, the support conditions and the loads. As outputs we can obtain information about the convergence method and 3D and 2D graphics with stress field and displacement field detailed information.

Figure 4.1 summarily addresses how the element and global stiffness matrix are computed and the script for the stress transfer iterative process is presented in Figure 4.2. In this figure it can be seen that the stress-transfer algorithm recalculate the global displacements vector, through a redistribution of unbalanced stresses (considering that they exist, if not, the non-linear threshold was not met and the stress-transfer routine is not executed). This unbalanced stresses come from the linear elastic calculus and corresponds to the difference between the acting and strength stresses at the interface elements (which is the non-linear domain for this model). Consequently, with known unbalanced stresses is possible to determine the unbalanced nodal forces vector (Figure 4.2 red code section), which, added to the global nodal forces vector determines the global displacements vector of the structure² (Figure 4.2 green code section). If the difference from the norm of two consecutive displacement vectors is infinitesimal (Figure 4.2 blue code section), then, the iterative process stops (Figure 3.10 convergence), if not, the calculation cycle restarts. Additionally, if the unbalanced stresses are too high and do not redistribute themselves across the joint, then the iterative process is unable to converge and the cycle will continue until the predefined maximum iterations number is achieved (Figure 3.10 divergence).

It is important to mention that, in Figure 4.1 scheme, the restrained DoF's (at the supports) were not removed from the element and global stiffness matrices; therefore, after the global stiffness matrix assembly, in the diagonal elements of that matrix, associated with those restrained DoF's, an extremely high stiffness value was added. That value is equal to $1e^{15}$ for each DoF restrained.

² Is important to highlight the fact that the global displacement vector is recalculated without the need to recalculate the stiffness matrix, which is exactly the advantage of this method.

For each finite element (**for n=1:NE**)

Calculate $\underline{x} = \begin{bmatrix} x_1^{e_1} & x_1^{e_2} & \dots & x_1^{e_{20}} \\ x_2^{e_1} & x_2^{e_2} & \dots & x_2^{e_{20}} \\ x_3^{e_1} & x_3^{e_2} & \dots & x_3^{e_{20}} \end{bmatrix}$, element n , nodes coordinates matrix

For each Gauss Point (**for iPG = 1: 27**) with the local coordinates presented in Table 3.1

Calculate the Interpolation Function (IF) values (equation 12) and corresponding partial derivatives in respect to the local coordinates (in GP iPG):

$$N_1, N_2, \dots, N_{27} \quad \frac{\partial N_1}{\partial y_1}, \frac{\partial N_2}{\partial y_1}, \dots, \frac{\partial N_{27}}{\partial y_1} \quad \frac{\partial N_1}{\partial y_2}, \frac{\partial N_2}{\partial y_2}, \dots, \frac{\partial N_{27}}{\partial y_2} \quad \frac{\partial N_1}{\partial y_3}, \frac{\partial N_2}{\partial y_3}, \dots, \frac{\partial N_{27}}{\partial y_3}$$

Calculate the Jacobian matrix:

$$\underline{J} = \begin{bmatrix} J_{11} & J_{12} & J_{13} \\ J_{21} & J_{22} & J_{23} \\ J_{31} & J_{32} & J_{33} \end{bmatrix} \Leftrightarrow$$

$$\Leftrightarrow \underline{J} = \begin{bmatrix} x_1^{e_1} & x_1^{e_2} & \dots & x_1^{e_{20}} \\ x_2^{e_1} & x_2^{e_2} & \dots & x_2^{e_{20}} \\ x_3^{e_1} & x_3^{e_2} & \dots & x_3^{e_{20}} \end{bmatrix} \begin{bmatrix} \frac{\partial N_1}{\partial y_1} & \frac{\partial N_1}{\partial y_2} & \frac{\partial N_1}{\partial y_3} \\ \frac{\partial N_2}{\partial y_1} & \frac{\partial N_2}{\partial y_2} & \frac{\partial N_2}{\partial y_3} \\ \vdots & \vdots & \vdots \\ \frac{\partial N_{27}}{\partial y_1} & \frac{\partial N_{27}}{\partial y_2} & \frac{\partial N_{27}}{\partial y_3} \end{bmatrix}$$

Calculate the IF partial derivatives in respect to the global coordinates:

$$\begin{bmatrix} \frac{\partial N_1}{\partial x_1} & \frac{\partial N_1}{\partial x_2} & \frac{\partial N_1}{\partial x_3} \\ \frac{\partial N_2}{\partial x_1} & \frac{\partial N_2}{\partial x_2} & \frac{\partial N_2}{\partial x_3} \\ \vdots & \vdots & \vdots \\ \frac{\partial N_{27}}{\partial x_1} & \frac{\partial N_{27}}{\partial x_2} & \frac{\partial N_{27}}{\partial x_3} \end{bmatrix} = \begin{bmatrix} \frac{\partial N_1}{\partial y_1} & \frac{\partial N_1}{\partial y_2} & \frac{\partial N_1}{\partial y_3} \\ \frac{\partial N_2}{\partial y_1} & \frac{\partial N_2}{\partial y_2} & \frac{\partial N_2}{\partial y_3} \\ \vdots & \vdots & \vdots \\ \frac{\partial N_{27}}{\partial y_1} & \frac{\partial N_{27}}{\partial y_2} & \frac{\partial N_{27}}{\partial y_3} \end{bmatrix}_{GP} \cdot \underline{J}_{PG}^{-1}$$

Assemble matrix \underline{B} ($\underline{B} = \underline{L} \underline{N}$, $\underline{\varepsilon} = \underline{B} \underline{u}^e$)

$$\underline{B} = \begin{bmatrix} \frac{\partial N_1}{\partial x_1} & 0 & 0 & \frac{\partial N_1}{\partial x_1} & 0 & 0 & \dots & \frac{\partial N_{27}}{\partial x_1} & 0 & 0 \\ 0 & \frac{\partial N_1}{\partial x_2} & 0 & 0 & \frac{\partial N_1}{\partial x_2} & 0 & \dots & 0 & \frac{\partial N_{27}}{\partial x_2} & 0 \\ 0 & 0 & \frac{\partial N_1}{\partial x_3} & 0 & 0 & \frac{\partial N_1}{\partial x_3} & \dots & 0 & 0 & \frac{\partial N_{27}}{\partial x_3} \\ 0 & \frac{\partial N_1}{\partial x_3} & \frac{\partial N_1}{\partial x_2} & 0 & \frac{\partial N_1}{\partial x_3} & \frac{\partial N_1}{\partial x_2} & \dots & 0 & \frac{\partial N_{27}}{\partial x_3} & \frac{\partial N_{27}}{\partial x_2} \\ \frac{\partial N_1}{\partial x_3} & 0 & \frac{\partial N_1}{\partial x_1} & \frac{\partial N_1}{\partial x_3} & 0 & \frac{\partial N_1}{\partial x_1} & \dots & \frac{\partial N_{27}}{\partial x_3} & 0 & \frac{\partial N_{27}}{\partial x_1} \\ \frac{\partial N_1}{\partial x_2} & \frac{\partial N_1}{\partial x_1} & 0 & \frac{\partial N_1}{\partial x_2} & \frac{\partial N_1}{\partial x_1} & 0 & \dots & \frac{\partial N_{27}}{\partial x_2} & \frac{\partial N_{27}}{\partial x_1} & 0 \end{bmatrix}$$

Calculate the matrix corresponding to the following matrix product:

$$\underline{B}^T \underline{D} \underline{B}$$

The numerical integration through the Gauss method for matrix $\underline{B}^T \underline{D} \underline{B}$ over the finite element volume (split in 27 cubes associated to the Gauss Points) is equal to the sum of matrix $\underline{B}^T \underline{D} \underline{B} |\underline{J}| A_{PG}^{master}$ computed each Gauss Point (Gauss sum to obtain \underline{K}^e)

$$\underline{K}^e = \left(\underline{B}^T \underline{D} \underline{B} |\underline{J}| A_{PG}^{master} \right)_{PG1} + \left(\underline{B}^T \underline{D} \underline{B} |\underline{J}| A_{PG}^{master} \right)_{PG2} + \dots + \left(\underline{B}^T \underline{D} \underline{B} |\underline{J}| A_{PG}^{master} \right)_{PG27}$$

end

“Spreading” of the element matrices \underline{K}^e into the global stiffness matrix \underline{K} (assembly)

end

Figure 4.1 – MATLAB programming script scheme for the element stiffness matrix calculus and subsequent assembly of the global stiffness matrix, considering a cubic “serendipity” element of 20 nodes

```

% (LINEAR ELASTIC CALCULUS)
% ...
%%% ----- Stress-Transfer Beginning ----- %%%
% 'while' cycle to the iteration number of interface elements
while (Norm > Tol) && (niter < MNITER)
    niter=niter+1; FDes(1:NGL,1)=0;

    % ----- Vector FDes calculus -----
    for nj=1:NEJ % Cycle to the interface elements
        knormal=KN(imatJ(nj)); ktangencial=KT(imatJ(nj));
        DJ=[ktangencial 0 0; 0 ktangencial 0; 0 0 knormal];
        Coesao=Coesaov(imatJ(nj)); Phi=Phiv(imatJ(nj));
        % Interface element n x1 x2 and x3 nodal coordinates matrix
        for in=1:2*NPFJ; for ik=1:NGLNO
            ue((in-1)*NGLNO+ik,1)=u((elemJ(nj,in)-1)*NGLNO+ik,1); end; end;
        for i=1:3; for j=1:NPFJ; cej(i,j)=coord(elemJ(nj,j),i); end; end
        FDesJ=zeros(2*NPFJ*NGLNO,1);
        for iPG=1:NPGJunta % Cycle to the GP of each interface element
            y1=YGJ(iPG,1); y2=YGJ(iPG,2); % Local coordinates of PGauss iPG
            dNdy = DerivY2D(y1,y2); % IF's derivatives in order to the local axes
            N= N2D(y1,y2); NN=[-N N]; % IF's values
            % Jacobian matrix (3x2) calculus at GP iPG of interface element n
            J=cej*dNdy; DETT=norm(J(:,1))*norm(J(:,2));
            T1=J(:,1)/norm(J(:,1));
            t3=[J(2,1)*J(3,2)-J(3,1)*J(2,2); -(J(1,1)*J(3,2)-J(3,1)*J(1,2));...
                J(1,1)*J(2,2)-J(2,1)*J(1,2)];
            T3=t3/norm(t3);
            T2=[T3(2)*T1(3)-T3(3)*T1(2); -(T3(1)*T1(3)-T3(3)*T1(1));...
                T3(1)*T1(2)-T3(2)*T1(1)];
            T=[T1'; T2'; T3'];
            sPGJ=DJ*T*NN*ue; % "sigma = D.B.ue" interface referential stresses
            SigmaT=sqrt(sPGJ(1)^2+sPGJ(2)^2); % Shear stress (absolute value)
            SigmaN=sPGJ(3);
            % Interface element uniaxial tension resistance calculus
            ft=Coesao*(2*cos(Phi*pi/180))/(1+sin(Phi*pi/180));
            if SigmaN > ft % Erases normal tension stresses
                SigmaN_Des=SigmaN-ft; SigmaN=ft; else SigmaN_Des=0;
            end % End of if SigmaN > ft
            tau_resist=Coesao+abs(SigmaN)*tan(Phi*pi/180);
            if SigmaT > tau_resist % Mohr-Coulomb shear verification
                % Difference between acting and resistant shear stresses
                SigmaT_Des=(SigmaT-tau_resist*sign(SigmaT));
                SigmaT1_Des=SigmaT_Des*cos(atan2(sPGJ(2),sPGJ(1)));
                SigmaT2_Des=SigmaT_Des*cos(atan2(sPGJ(1),sPGJ(2)));
            else SigmaT1_Des=0; SigmaT2_Des=0; end % end of if SigmaT > tau_resist
            % Unbalanced stresses vector at the interface referential
            S_Des=[SigmaT1_Des; SigmaT2_Des; SigmaN_Des];
            FDesiPGJ=NN'*T'*S_Des*DETT*WPGJ(iPG); % Unbalanced stresses integration
            FDesJ=FDesJ+FDesiPGJ; % Nodal forces vector equivalent to the
            % unbalanced stresses at the interface element i (FDesJ is 48x1)
        end; % Cycle for i=1:NPGJunta end
        % Nodal forces 'Spreading' at the interface
        % Unbalance forces global vector assembly (FDes is NGLx1)
        for i=1:2*NPFJ; for ik=1:NGLNO % 2 cycles to scan K(i,j) lines [i=1:NGL,j=1:NGL]
            noGi=elemJ(nj,i); % Global node (lines,i): nj element , i_th node
            GLGi=(noGi - 1)*NGLNO + ik; % Global DoF (lines,i) - varies from 1 to NGL
            GLEi=(i-1)*NGLNO+ik; % Interface Element DoF (lines,i) - varies from 1 to 48
            FDes(GLGi,1) = FDes(GLGi,1)+ FDesJ(GLEi); end; end
        end; % Cycle for nj=1:NEJ end
    % ----- End of vector FDes calculus -----

    u=Kinv*(F+FDes); % [m] (if the inputs are in meters)

    if niter==1; Norm0=norm(u_bak-u); end;
    if Norm0 >0; Norm=norm(u_bak-u)/Norm0*100; else Norm=0; end % End of if Norm0 >0
    u_bak=u; ITER(niter)=niter; VALNORMA(niter)=Norm;
    end % Cycle while (Norm > Tol) && (niter < 500) end

clear Kinv;
%%% ----- Stress-Transfer End ----- %%%

```

Figure 4.2 – Stress-transfer MATLAB script. Routine executed after the linear elastic calculus. The red rectangle highlights the unbalanced global forces vector calculation. The green rectangle highlights the global displacements vector calculation. The blue rectangle highlights the convergence verification

5 | Numerical tests

5.1 Test structure presentation

In order to verify and validate the program **DamSlide3D**, three tests were carried out. These tests involved the simulation of the behavior of a simple structural system. It was considered a column, and its base, subjected to the self-weight and to the hydrostatic pressure (Figure 5.1). Horizontal joint elements are considered at the contact between the base and the column and inclined joint elements are also considered in the column as indicated in figure 5.1.

In Figure 5.2 it is shown the diagram correspondent to the equilibrium of forces at the base of the column and in Figure 5.3 is shown the adopted FE mesh.

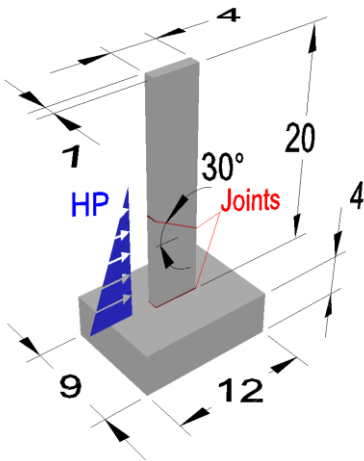


Figure 5.1 – Test structure characterization and loads (Hydrostatic pressure and self-weight $\gamma=24 \text{ kN/m}^3$)

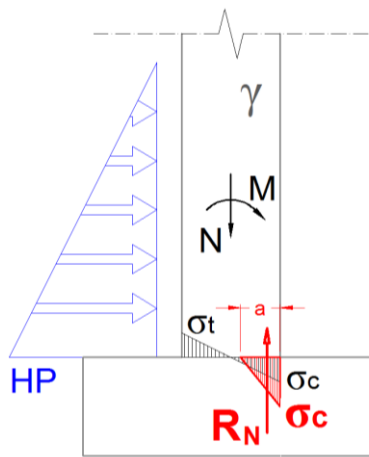


Figure 5.2 – Linear (gray) and non-linear stress distribution (red) in the horizontal joint at the column base

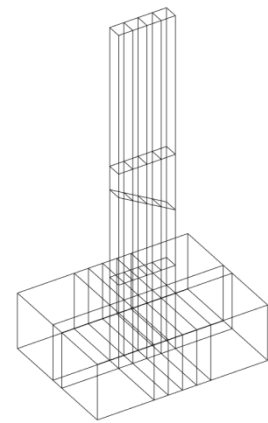


Figure 5.3 – 3D finite element mesh

5.2 Joint behavior. Linear elastic test

In Figure 5.2 is represented, in black, the resulting linear distribution of stresses across the interface column-base (46) as well as the resultant bending moment M and axial force N , being

$$\sigma = \frac{N}{A} \pm \frac{M.y}{I} \Leftrightarrow \begin{cases} \sigma_t = \frac{N}{A} + \frac{M.y}{I} \\ \sigma_c = \frac{N}{A} - \frac{M.y}{I} \end{cases} \quad (46)$$

This analytical result can be used to the verification of the **DamSlide3D**.

Considering the structure geometry and loading (HP and SW), for a water height of 12 m, through equation (46), the resulting maximum compression stress and maximum tension stress are $\sigma_c=1560$ kPa and $\sigma_t=600$ kPa, respectively.

Figure 5.4 displays the Gauss points considered in the computation. Figure 5.5 presents the program outputs for the stress distribution across the interface column-base.

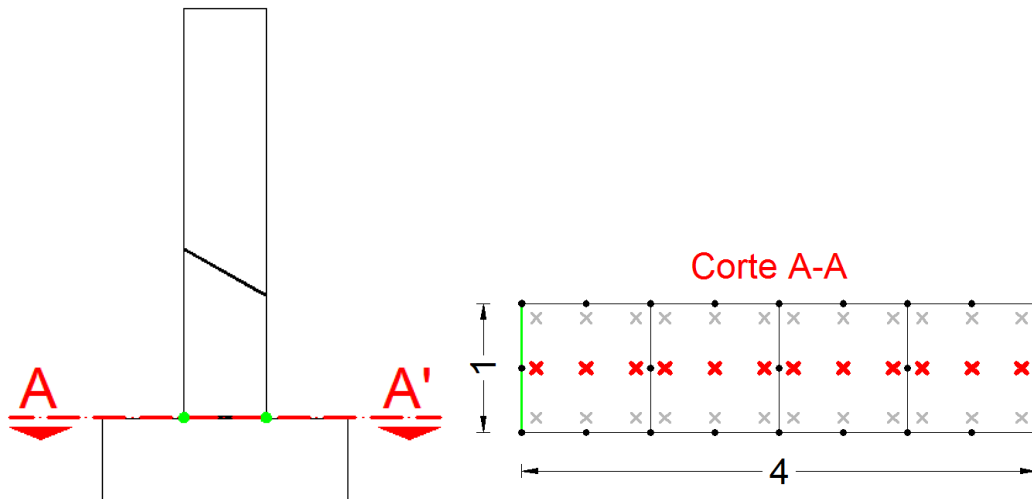
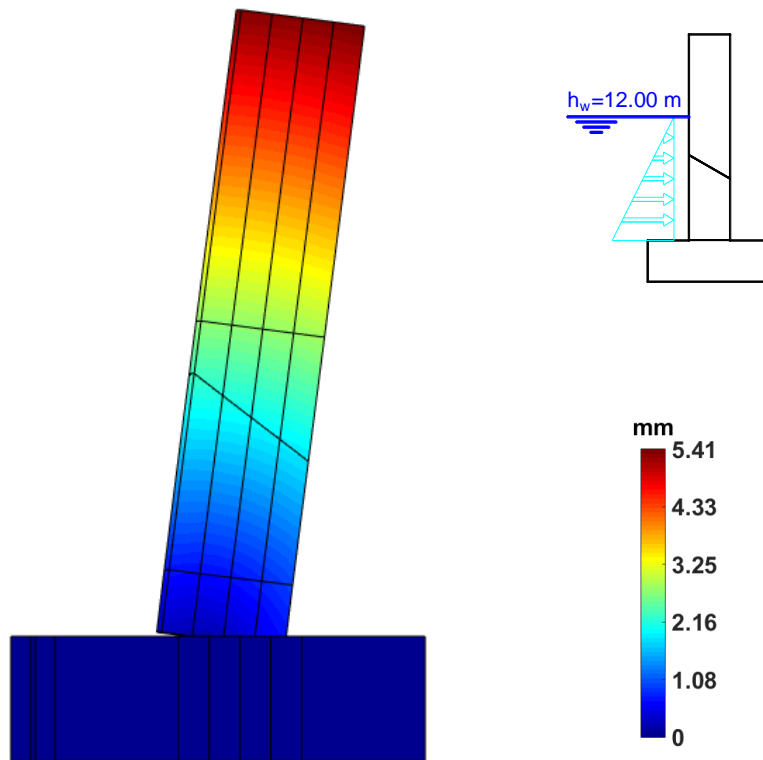


Figure 5.4 – Gauss points considered (red crosses) for the analysis of the stress distribution at the interface column-base

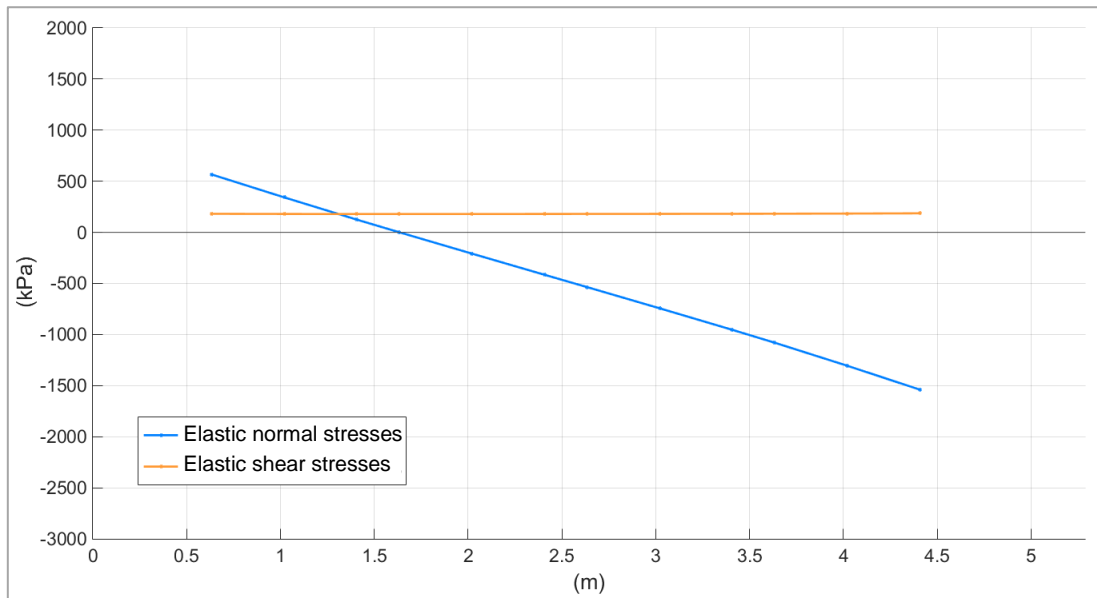
Figure 5.5 presents the elastic stresses variation across the interface dam-foundation and, as expected, the shear elastic stresses are constant and the normal elastic stresses vary linearly.

The maximum stress values computed numerically are, from Figure 5.5, $\sigma_c= 1602.6$ kPa and $\sigma_t= 629.6$ kPa and the analytical values (eq.46) are, respectively, $\sigma_c=1560$ kPa and $\sigma_t=600$ kPa, showing a good agreement between numerical and analytical results.

Displacements



Stresses at the column base (interface elements)



Column and base:

$E_c = E_b = 50$ GPa
 $\nu_c = \nu_b = 0.2$

Interface column-base:

$K_N = 2.5 \times 10^6$ kNm⁻¹
 $K_T = 1.0 \times 10^6$ kNm⁻¹

Loads:

Self-weight ($\gamma_c = 24$ kN/m³)
 Hydrostatic pressure ($\gamma_w = 10$ kN/m³)

Figure 5.5 – Elastic behavior of the test structure. Displacements field and stress distribution at the interface column-base

5.3 Joint behavior. Non-linear tests

5.3.1 Inclined joint

In this section is studied the non-linear behavior of the 30° inclined joint (see Figure 5.1 and Figure 5.6), for self-weight loading, considering different values for the friction angle. If the friction angle of the inclined joint is equal or greater than the inclination of the joint no sliding is expected (the shear resistant force in Figure 5.6 is greater than the acting shear component τ of the weight).

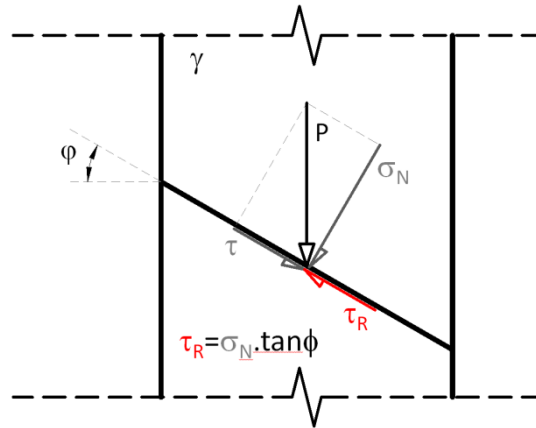


Figure 5.6 – Schematic representation of the forces equilibrium at the inclined joint

The shear resistant stress τ_R , which depends on the normal stress σ_N and on the friction angle ϕ can be evaluated as follows

$$\tau_R = \sigma_N \cdot \tan \phi \quad (47)$$

On the other hand, from the balance of forces displayed on Figure 5.6 we can determine the acting shear stress τ

$$\begin{cases} \tau = P \cdot \sin \phi \\ \sigma_N = P \cdot \cos \phi \end{cases} \Rightarrow \begin{cases} \tau = P \cdot \sin \phi \\ P = \frac{\sigma_N}{\cos \phi} \end{cases} \Rightarrow \tau = \frac{\sigma_N}{\cos \phi} \sin \phi \Rightarrow \tau = \sigma_N \tan \phi \quad (48)$$

Sliding will occur when $\tau > \tau_R$. So, for values of the friction angle ϕ greater or equal to those of the joint inclination angle $\varphi=30^\circ$, there is no sliding.

Figure 5.7 shows the numerical results of **DamSlide3D** for two different scenarios:

- i) the test structure with a $\varphi=30^\circ$ inclined joint is submitted to its self-weight and the friction angle is $\phi=30.01^\circ$ (slightly higher than the joint inclination angle $\varphi=30^\circ$); and
- ii) the friction angle is $\phi=29.99^\circ$ (slightly lower than the joint inclination angle $\varphi=30^\circ$);

a. Friction angle at the inclined joint: $\phi=30.01^\circ$

b. Friction angle at the inclined joint: $\phi=29.99^\circ$

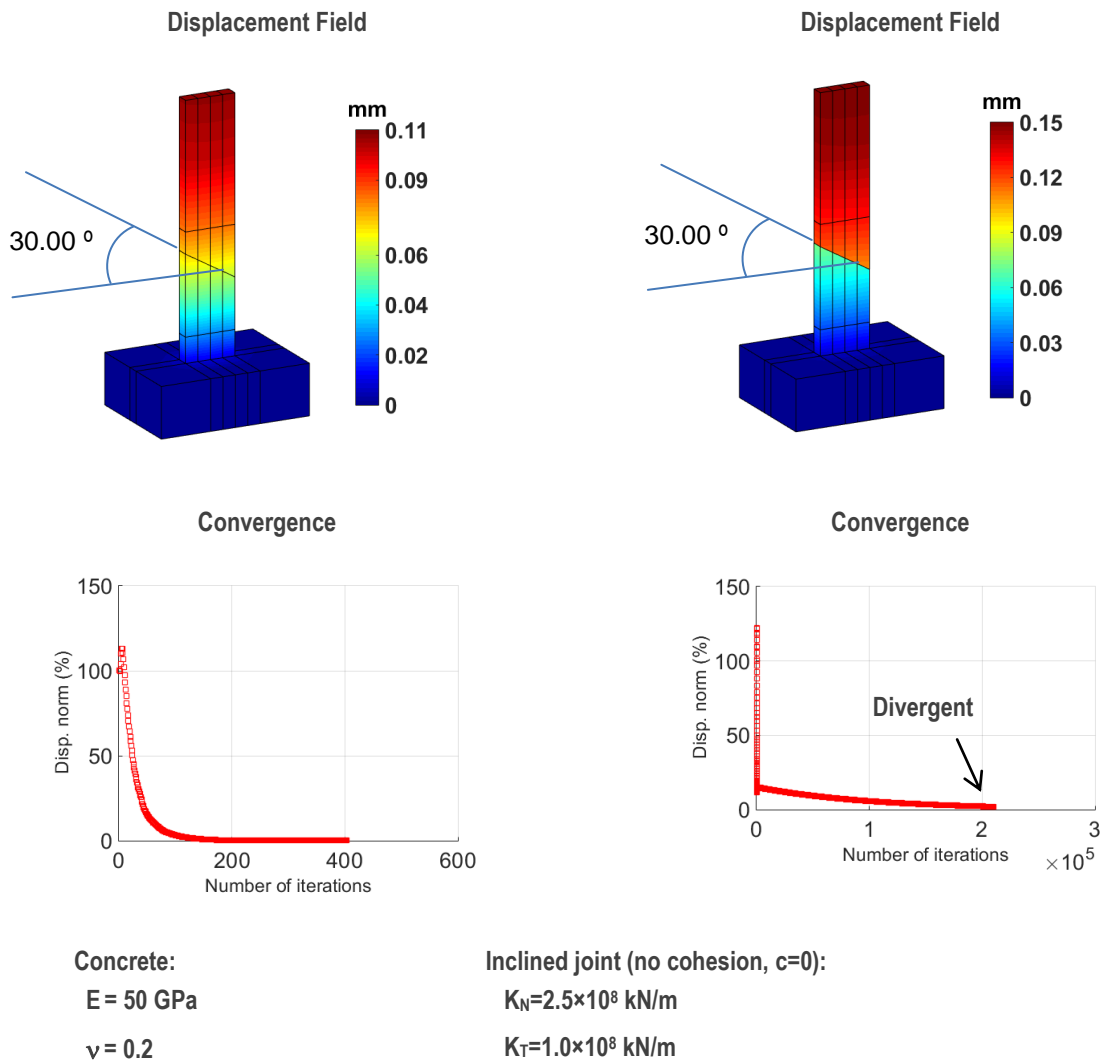


Figure 5.7 – Numerical study of sliding across the inclined joint ($\varphi = 30^\circ$) on a concrete column under the self-weight load. (a.) Results for friction angle $\phi=30.01^\circ$, slightly higher than the joint inclination angle; a convergent solution was obtained: no sliding, as expected. (b.) Results for friction angle $\phi=29.99^\circ$, slightly lower than the joint inclination angle; divergent process, meaning that a sliding occurred

As expected, it is possible to verify numerically with **DamSlide3D** that for $\phi=30.01^\circ$, higher than the joint inclination angle ($\varphi=30^\circ$), no slide occur. For $\phi=29.99^\circ$, lower than the joint inclination angle, sliding is numerically identified. Actually, from the convergence process analysis displayed in the graphics, for $\phi=30.01^\circ$, the iteration process converged (stopped around the 400th iteration for the given tolerance). For $\phi=29.99^\circ$, the iterative process diverges (structural collapse by sliding).

5.3.2 Analysis of the base joint behavior considering hydrostatic pressure. Parametric study on the influence of friction angle (constant water height H=12 m)

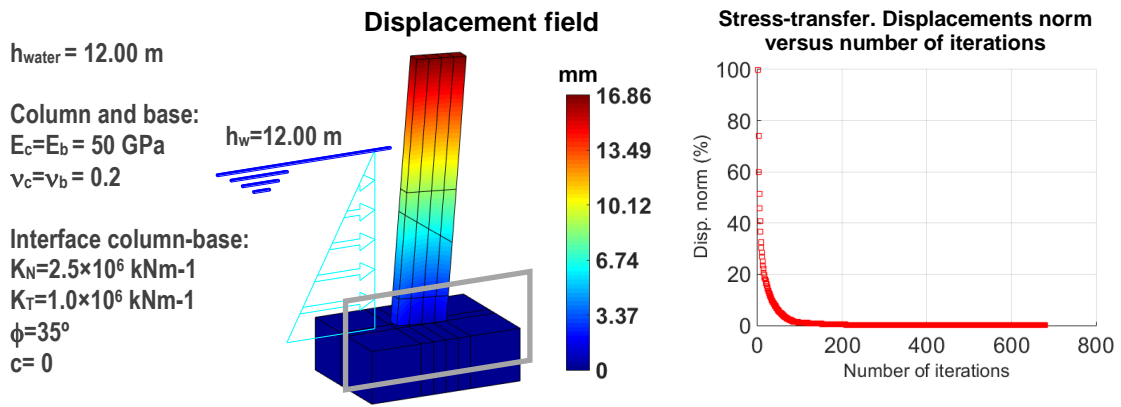
In this section, is considered the non-linear behavior of the horizontal joint at the column base. For the inclined joint it was assumed a linear behavior with high stiffness and strength. In what concern the loads, is assumed that the structure is subjected to the combination SW + HP (water height H=12 m). Is assumed null cohesion for the base joint, meaning that no tension stresses are supported.

In Figure 5.2, is represented, in red, the non-linear distribution of the compression normal stresses in the horizontal joint at the column base, for a bending moment M and for a normal force N. Assuming that no tensile stresses can be supported by the joint (null cohesion), the equilibrium is obtained with high compression normal stresses σ_c , that can be calculated analytically as follows

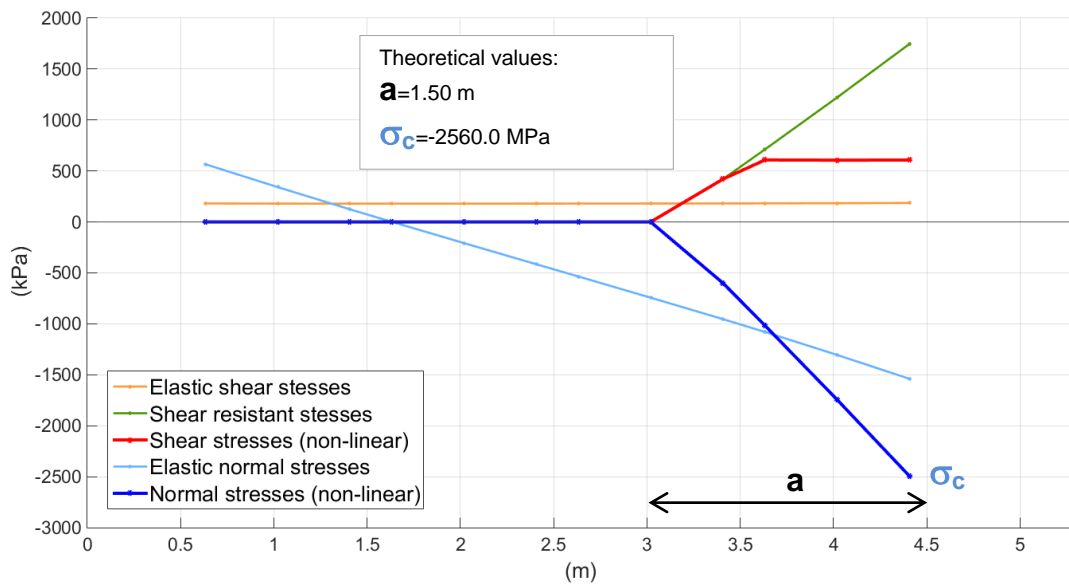
$$\left\{ \begin{array}{l} N = \frac{\sigma_c \cdot a}{2} \\ M = N \cdot \left(\frac{h}{2} - \frac{a}{3} \right) \end{array} \right. \Rightarrow \left\{ \begin{array}{l} \sigma_c = \frac{2N^2}{3 \left(\frac{N \cdot h}{2} - M \right)} \\ a = \frac{3}{N} \left(\frac{N \cdot h}{2} - M \right) \end{array} \right. \quad (49)$$

being h the section height at the column base and a the length under compression.

In this sub-section the joint behavior is studied for different values of the friction angle: the numerical results are presented from Figure 5.8 to Figure 5.15, being, respectively, for $\phi = 35^\circ, 30^\circ, 25^\circ, 24^\circ, 23^\circ, 22^\circ, 21^\circ, 20^\circ$. The analytical values of σ_c and a (from eq.49) will be compared with the correspondent numerical values from **DamSlide3D**.



Stresses across the interface column-base



Interface column-base. Principal stresses

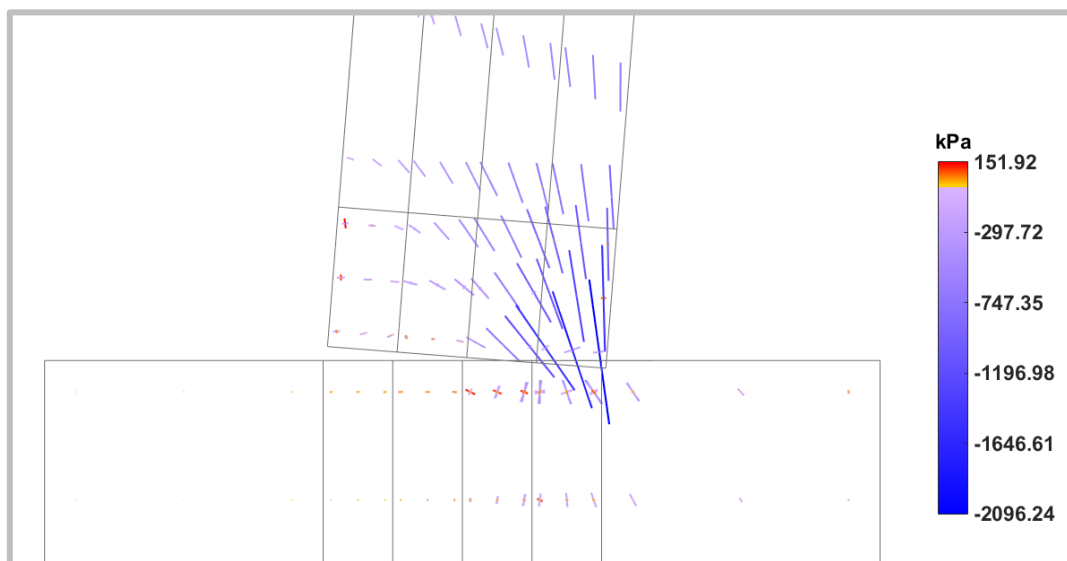


Figure 5.8 – Column-base structural behavior for $\phi=35^\circ$. On top left, dam’s displacement field; on top right, “stress-transfer” convergence, on the middle, elastic and non-linear, normal and shear, stresses across the center section of the interface column-base; on the bottom, the dam’s principal stresses throughout the interface column-base

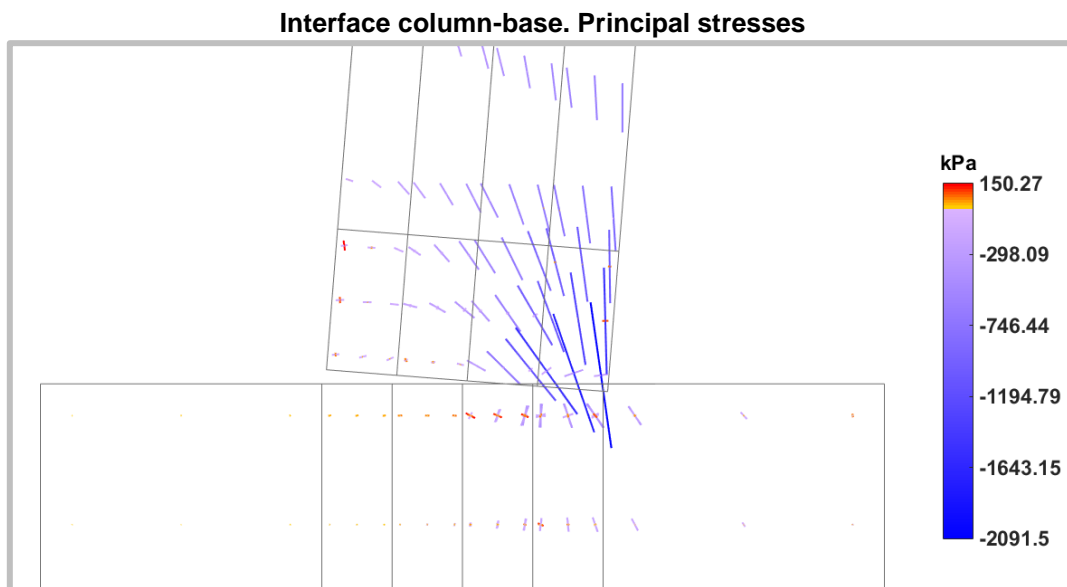
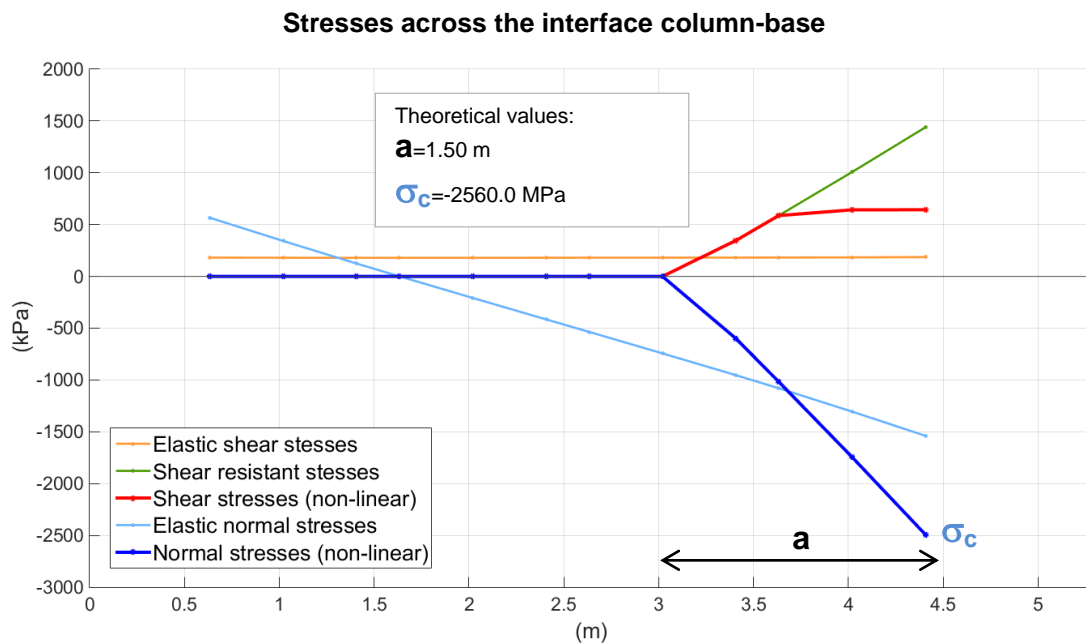
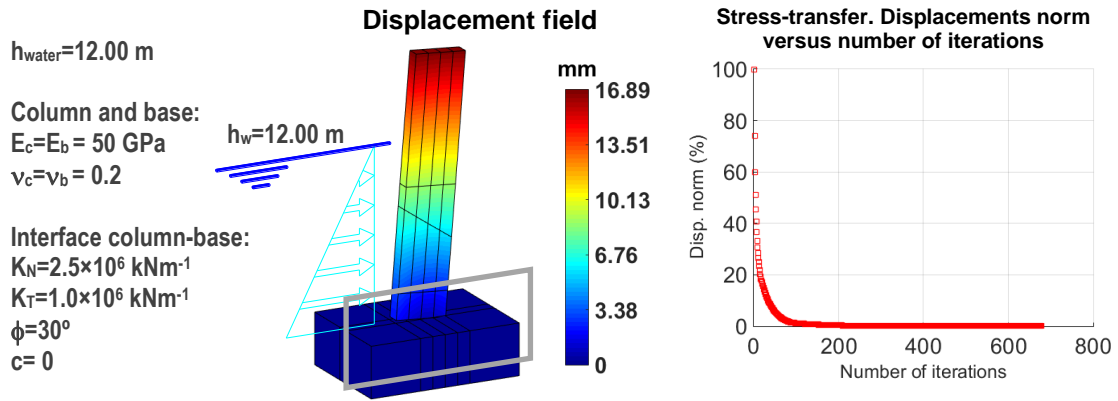


Figure 5.9 – Column-base structural behavior for $\phi=30^\circ$. On top left, dam’s displacement field; on top right, “stress-transfer” convergence, on the middle, elastic and non-linear, normal and shear, stresses across the center section of the interface column-base; on the bottom, the dam’s principal stresses throughout the interface column-base

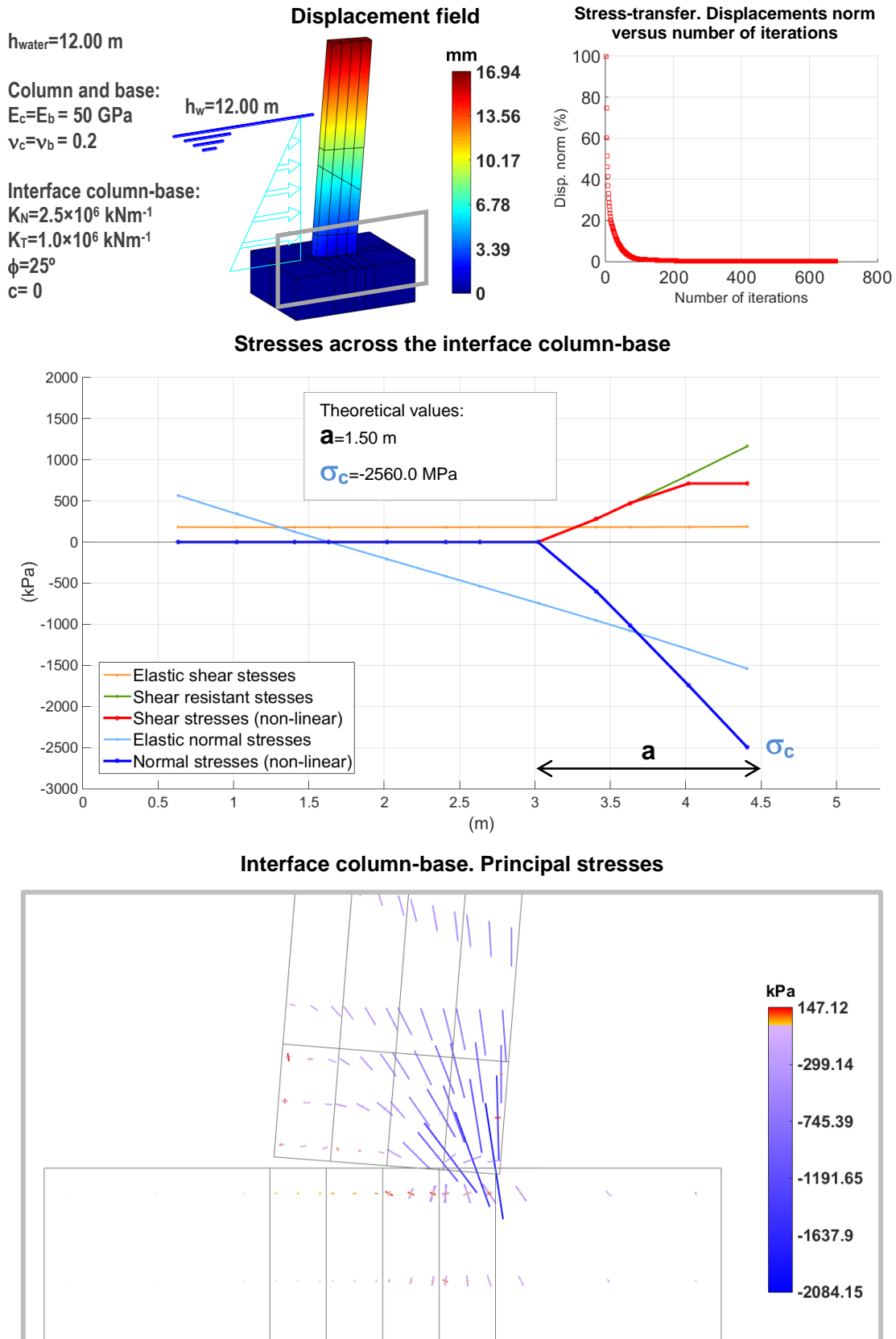


Figure 5.10 – Column-base structural behavior for $\phi=25^\circ$. On top left, dam’s displacement field; on top right, “stress-transfer” convergence, on the middle, elastic and non-linear, normal and shear, stresses across the center section of the interface column-base; on the bottom, the dam’s principal stresses throughout the interface column-base

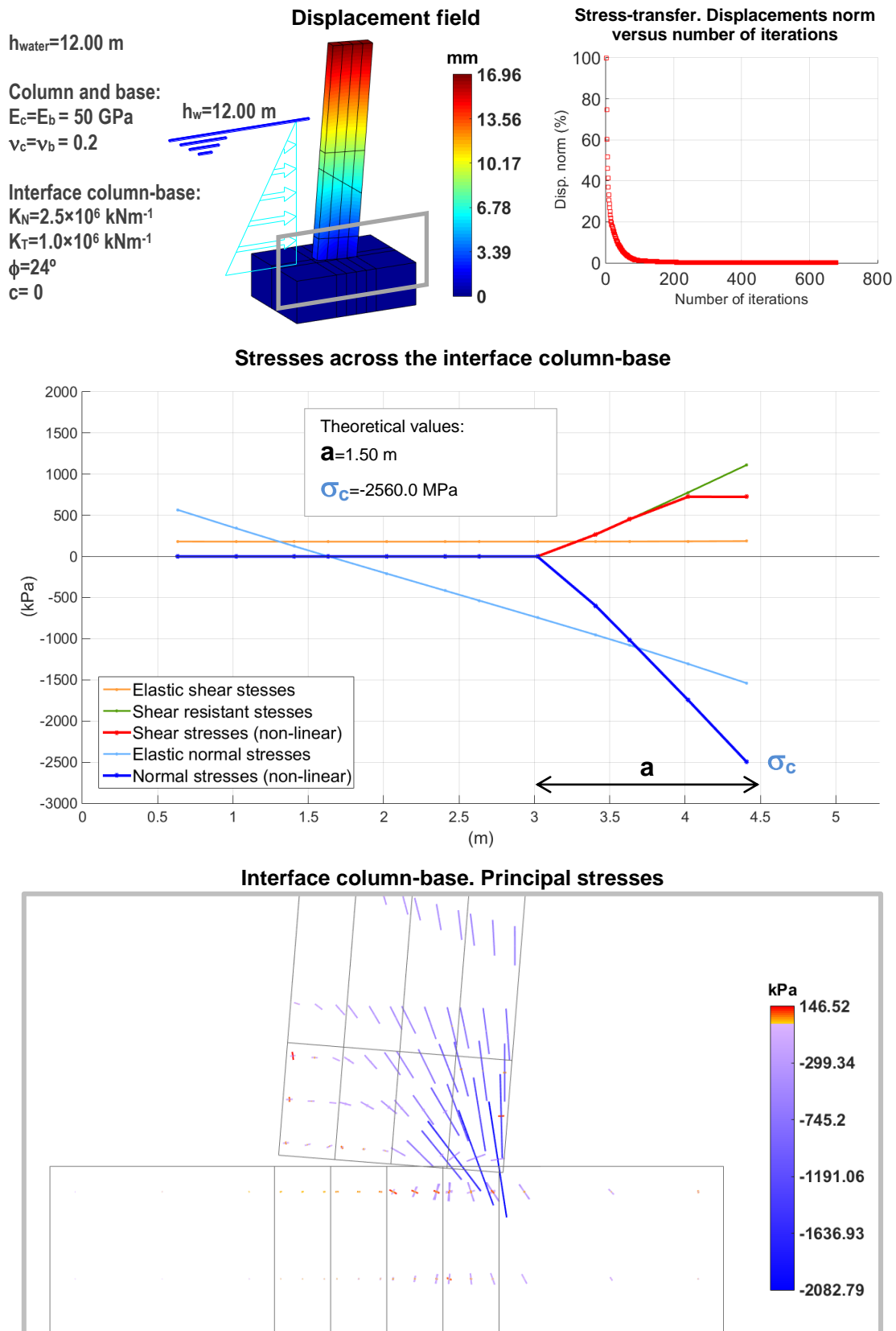


Figure 5.11 – Column-base structural behavior for $\phi=24^\circ$. On top left, dam’s displacement field; on top right, “stress-transfer” convergence, on the middle, elastic and non-linear, normal and shear, stresses across the center section of the interface column-base; on the bottom, the dam’s principal stresses throughout the interface column-base

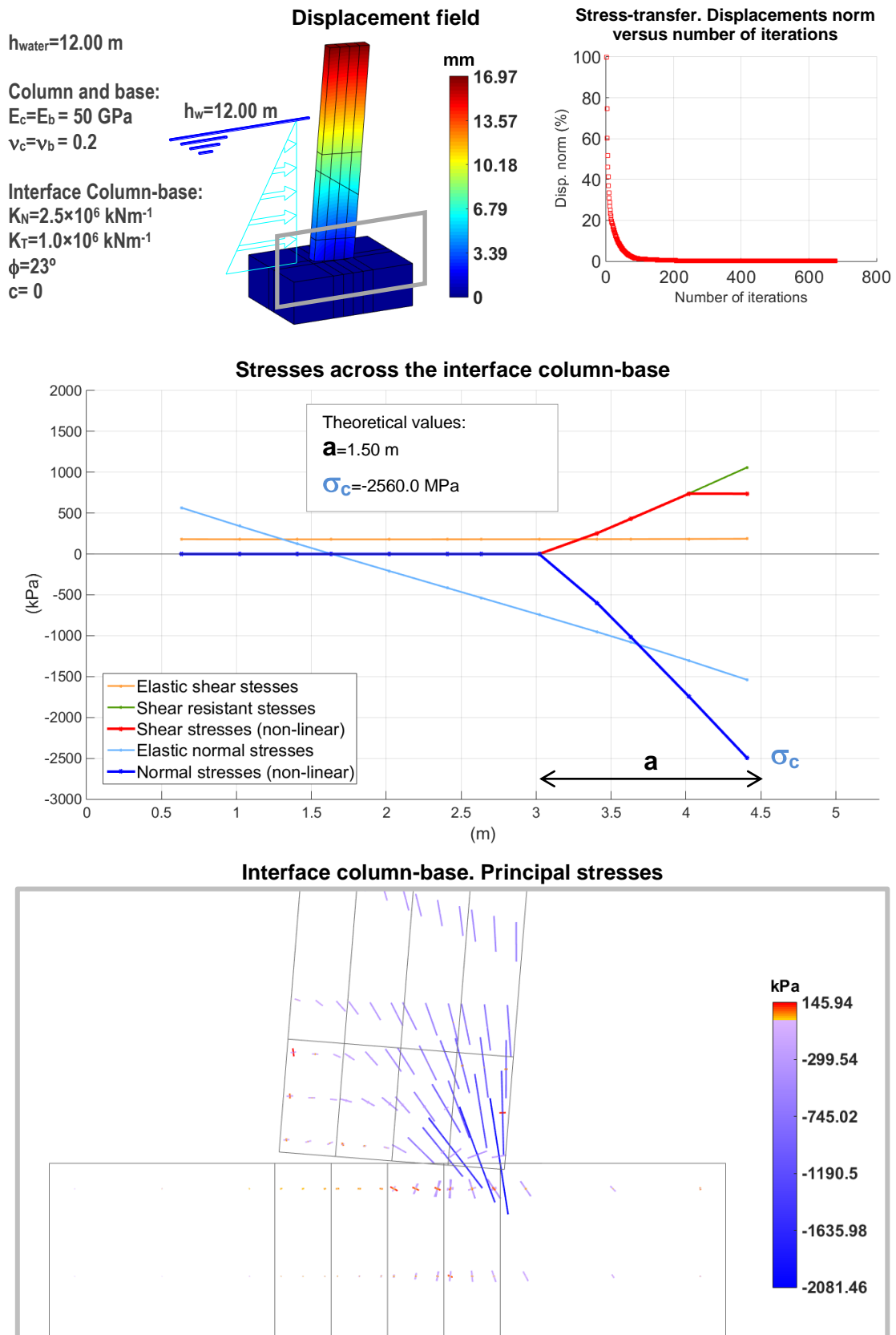


Figure 5.12 – Column-base structural behavior for $\phi=23^\circ$. On top left, dam’s displacement field; on top right, “stress-transfer” convergence, on the middle, elastic and non-linear, normal and shear, stresses across the center section of the interface column-base; on the bottom, the dam’s principal stresses throughout the interface column-base

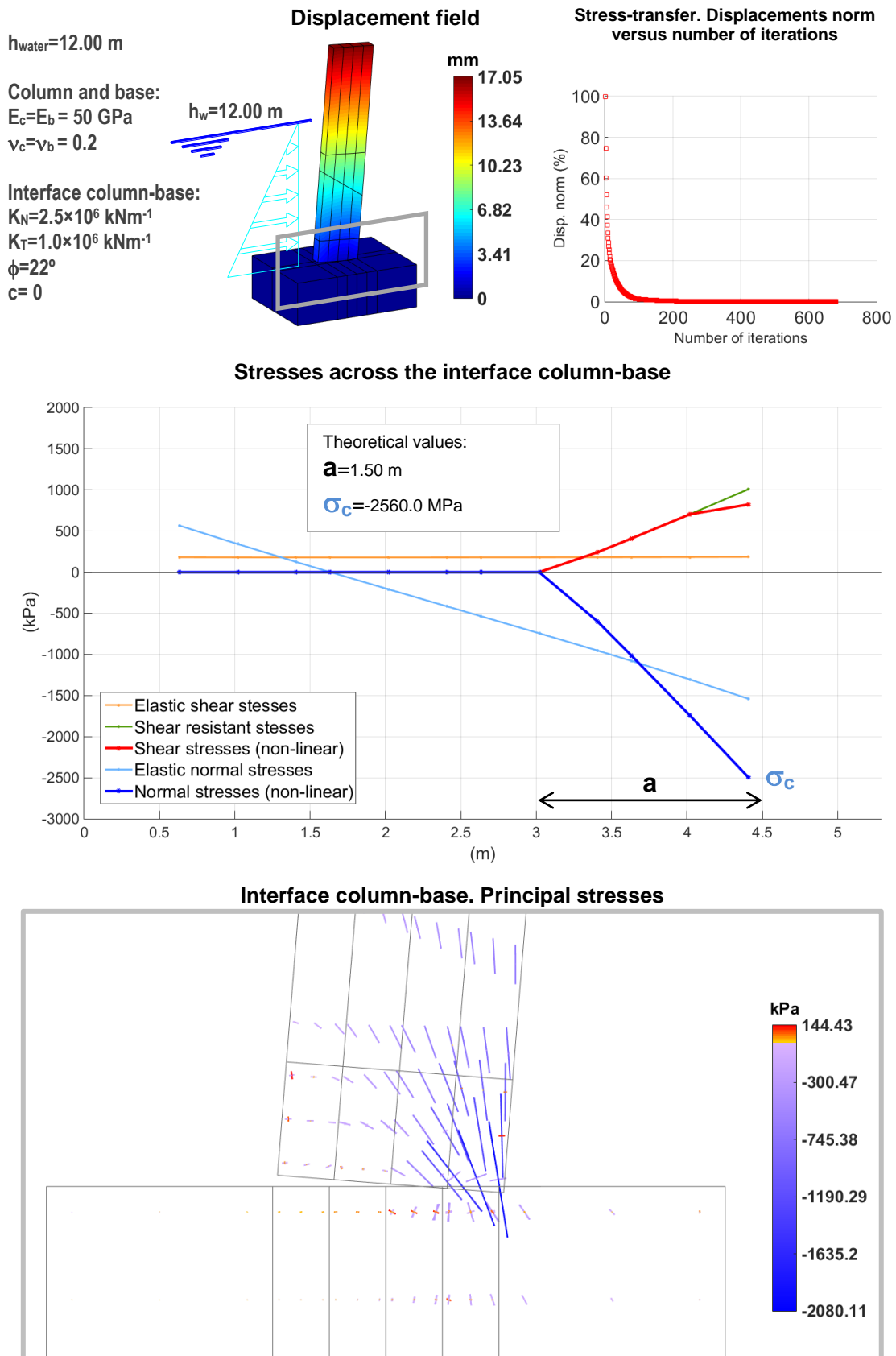


Figure 5.13 – Column-base structural behavior for $\phi=22^\circ$. On top left, dam’s displacement field; on top right, “stress-transfer” convergence, on the middle, elastic and non-linear, normal and shear, stresses across the center section of the interface column-base; on the bottom, the dam’s principal stresses throughout the interface column-base

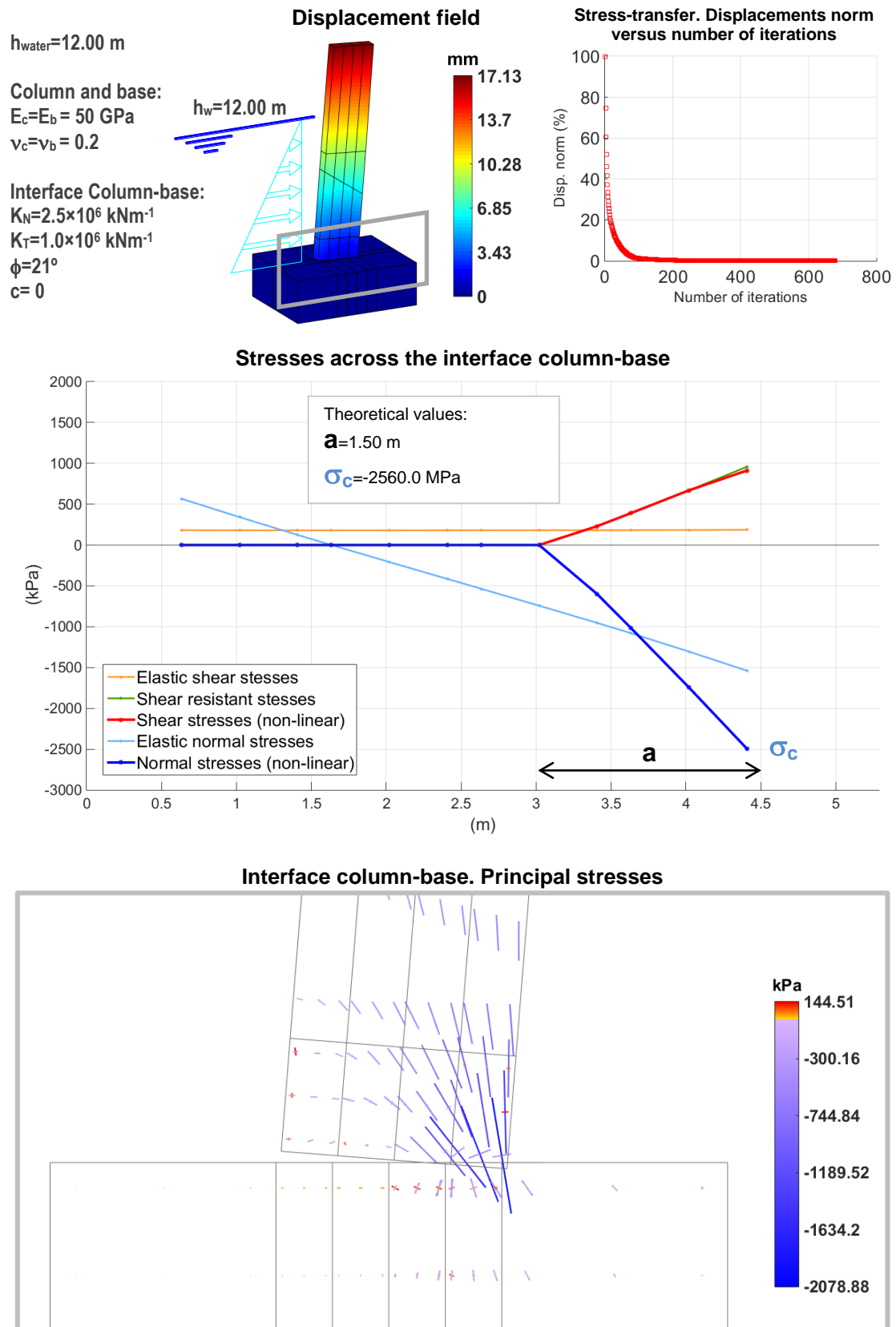


Figure 5.14 – Column-base structural behavior for $\phi=21^\circ$. On top left, dam’s displacement field; on top right, “stress-transfer” convergence, on the middle, elastic and non-linear, normal and shear, stresses across the center section of the interface column-base; on the bottom, the dam’s principal stresses throughout the interface column-base

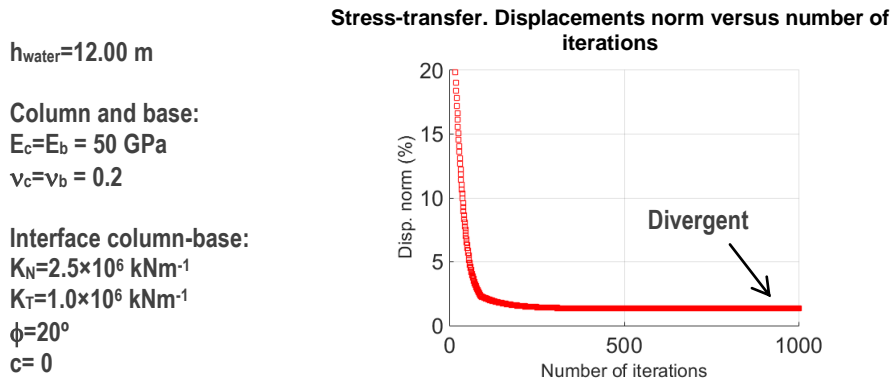


Figure 5.15 – Stress-transfer divergence for $\phi=20^\circ$

From figures 5.8 to 5.14, one can verify, as expected, that the non-linear distribution of the normal stresses (numerically computed) is the same for the different values of the friction angle ϕ (compressions along the length $a=1.5 \text{ m}$, with maximum value of $\sigma_c \approx 2560 \text{ MPa}$). As the friction angle decreases (from 35° to 20° , in this study) there is a decrease in the resistant shear stress distribution (along the length a), that means there is a decrease in the resistant shear stress capacity. In order to have no sliding, the resultant acting shear force should be lower than the resistant shear force correspondent to the resistant shear stress capacity: this equilibrium condition is numerically attained for values of the friction angle ϕ higher than 20° . So, with **DamSlide3D**, it was found, numerically, that sliding along the horizontal base joint only occurs for $\phi \leq 20^\circ$ (in Figure 5.15 is shown, graphically, the iterative stress-transfer divergence in terms of the used displacements norm).

5.3.3 Analysis of the base joint behavior considering hydrostatic pressure.

Parametric study on the influence of water height (constant friction angle $\phi=30^\circ$)

In this sub-section the joint behavior of the horizontal base joint is studied for different values of water height (h_w), considering a constant value for the friction angle $\phi = 30^\circ$. The numerical results are presented in Figure 5.9 (for $h_w = 12 \text{ m}$) and in Figure 5.16 to Figure 5.19, for, respectively, $h_w = 12.25$, 12.30 , 12.35 and 12.40 m . The analytical values of σ_c and a (eq.49) are compared with the correspondent numerical values from **DamSlide3D**.

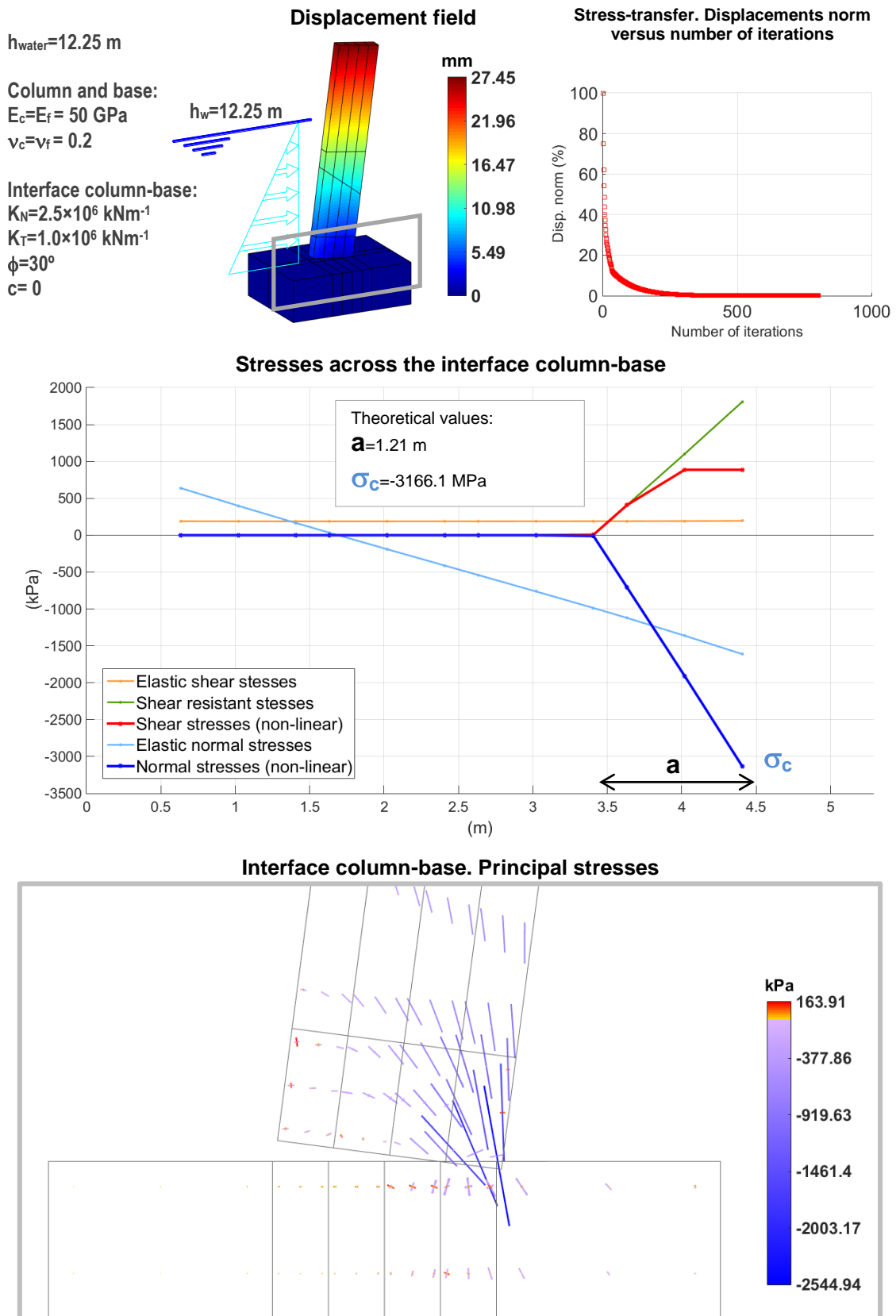


Figure 5.16 – Column-base structural behavior for $h_{water}= 12.25\text{ m}$. On top left, dam’s displacement field; on top right, “stress-transfer” convergence, on the middle, elastic and non-linear, normal and shear, stresses across the center section of the interface column-base; on the bottom, the dam’s principal stresses throughout the interface column-base

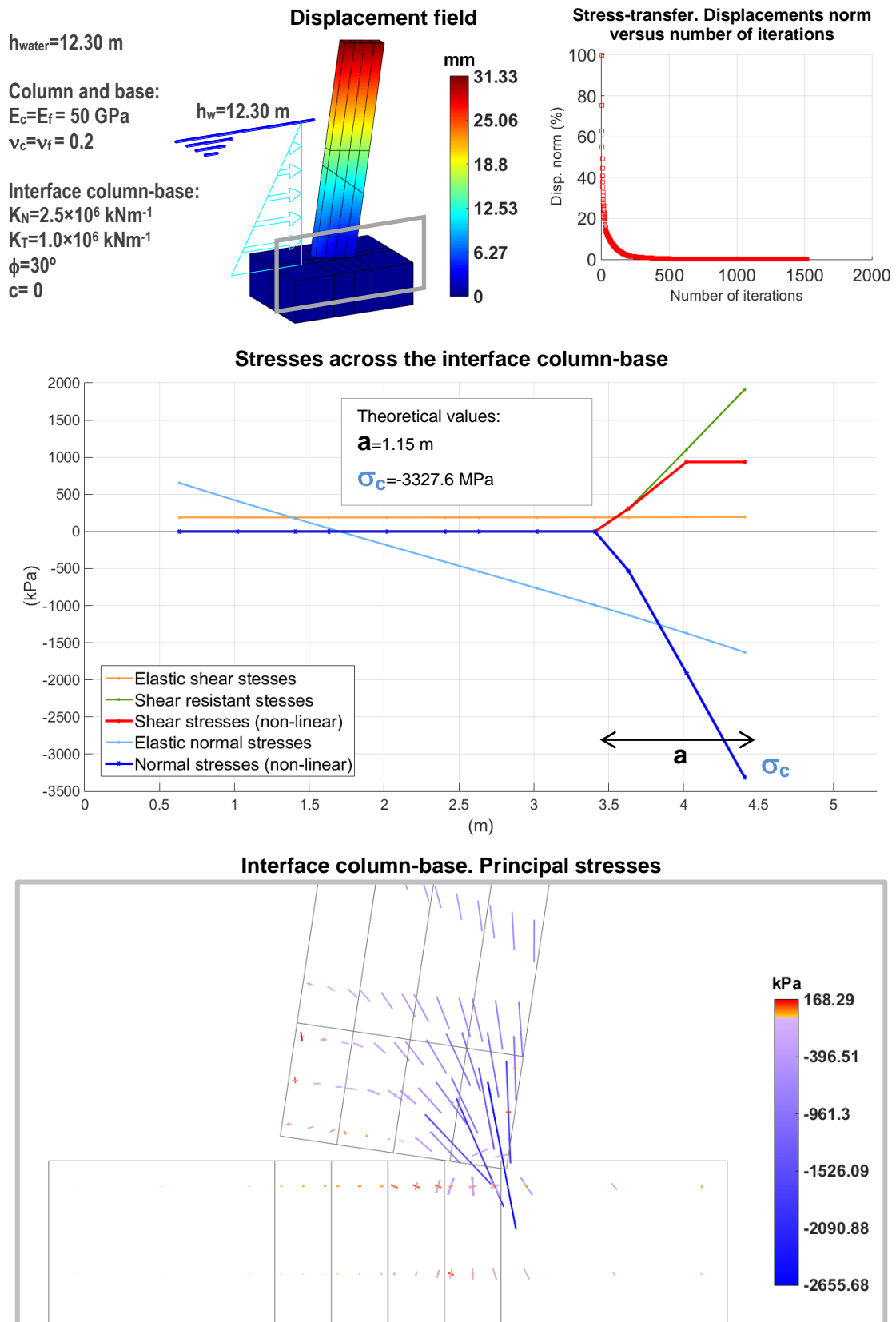


Figure 5.17 – Column-base structural behavior for $h_{water}=12.30\text{ m}$. On top left, dam’s displacement field; on top right, “stress-transfer” convergence, on the middle, elastic and non-linear, normal and shear, stresses across the center section of the interface column-base; on the bottom, the dam’s principal stresses throughout the interface column-base

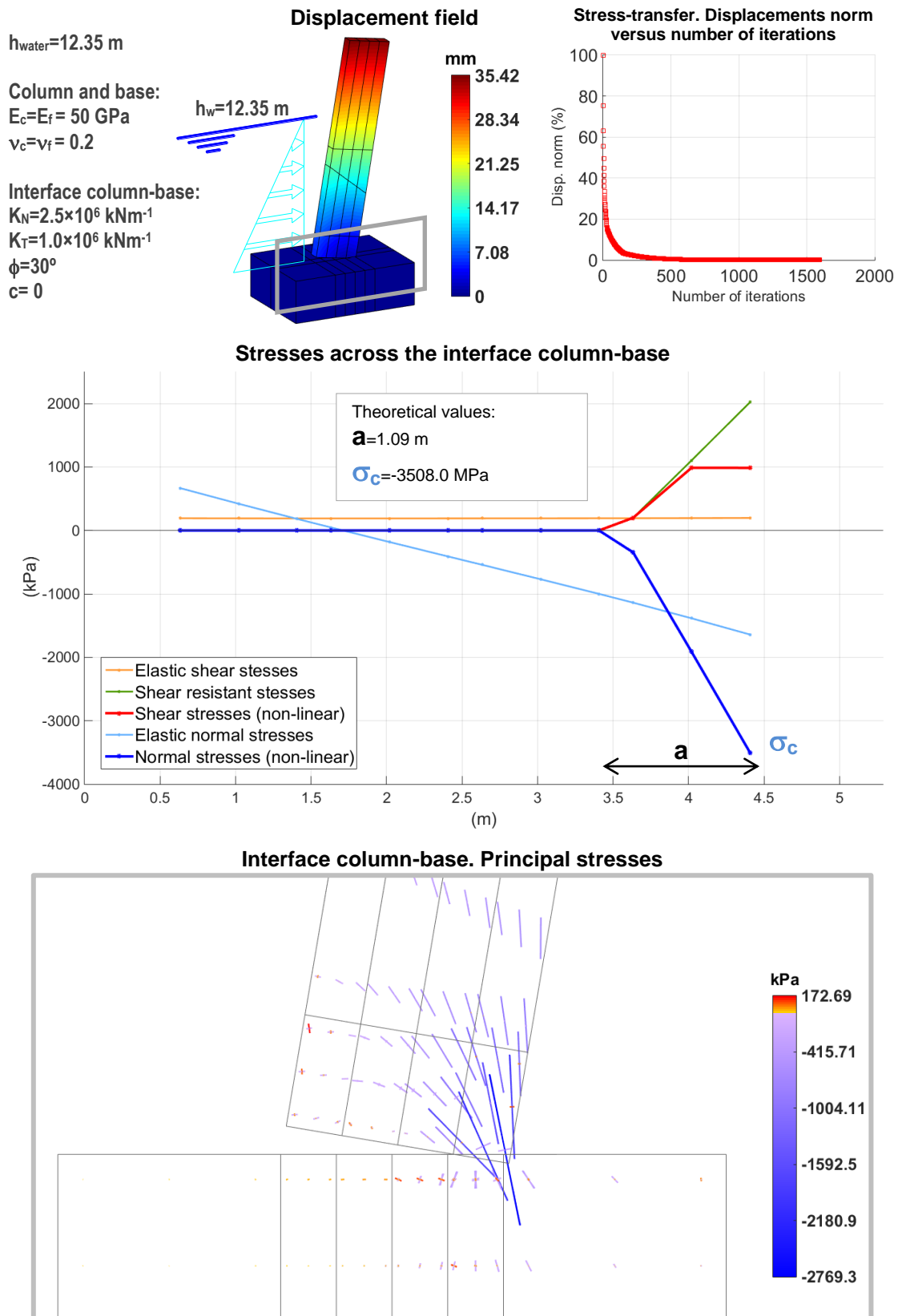


Figure 5.18 – Column-base structural behavior for $h_{water}=12.35\text{ m}$. On top left, dam’s displacement field; on top right, “stress-transfer” convergence, on the middle, elastic and non-linear, normal and shear, stresses across the center section of the interface column-base; on the bottom, the dam’s principal stresses throughout the interface column-base

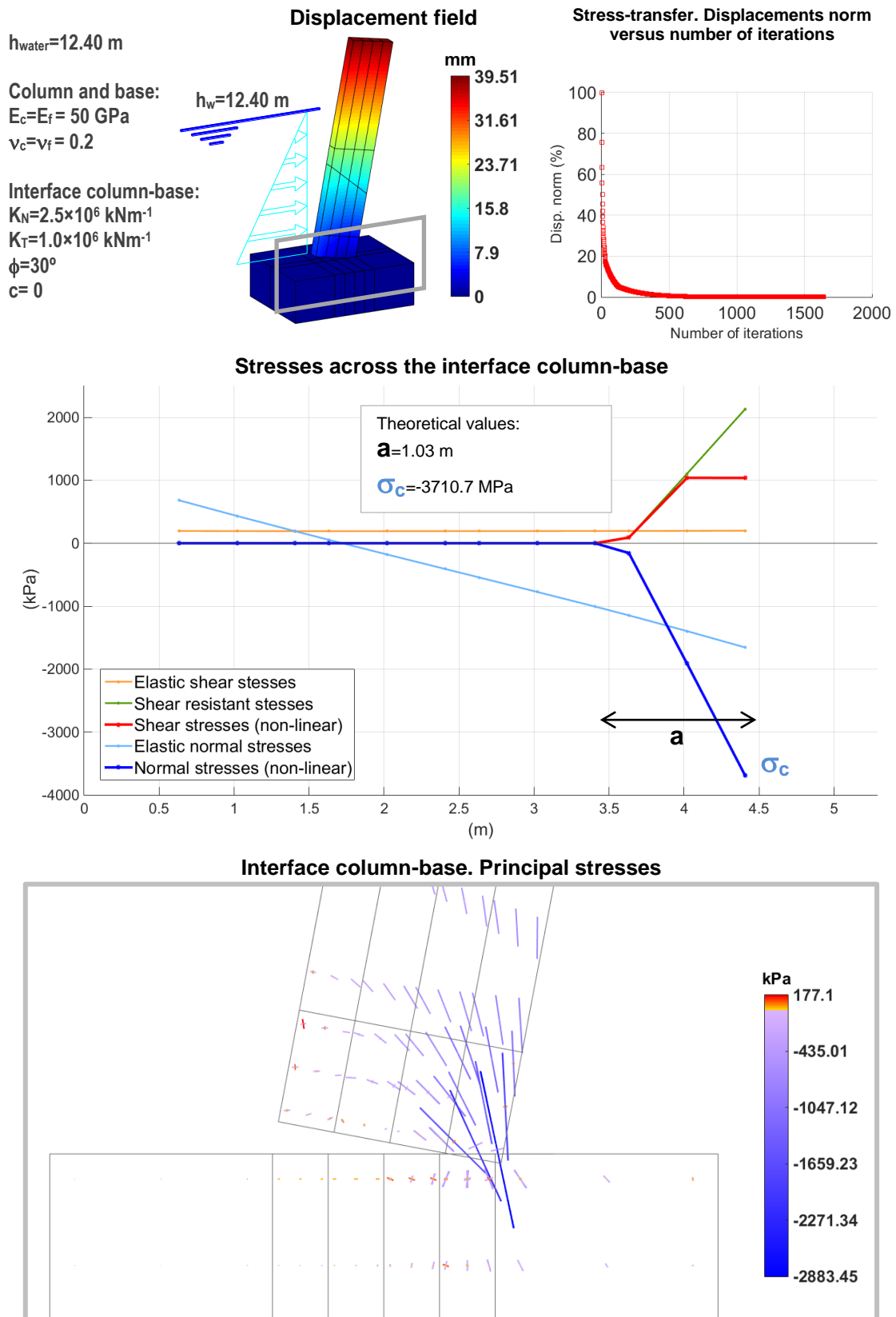


Figure 5.19 – Column-base structural behavior for $h_{water}=12.40\text{ m}$. On top left, dam’s displacement field; on top right, “stress-transfer” convergence, on the middle, elastic and non-linear, normal and shear, stresses across the center section of the interface column-base; on the bottom, the dam’s principal stresses throughout the interface column-base

$h_{\text{water}}=12.45$ m

Column and base:

$E_c=E_b = 50$ GPa

$\nu_c=\nu_b = 0.2$

Interface column-base:

$K_N=2.5 \times 10^6$ kNm⁻¹

$K_T=1.0 \times 10^6$ kNm⁻¹

$\phi=30^\circ$

$c=0$

Stress-transfer. Displacements norm versus number of iterations

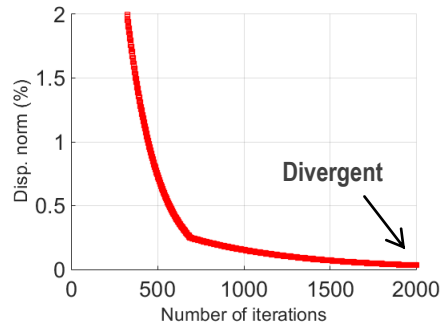


Figure 5.20 – Stress-transfer divergence for $h_{\text{water}}=12.45$ m

For this scenario of water level increase, one can verify, from figure 5.8 and figures 5.16 to 5.19, that, as expected, the non-linear distribution of the normal and shear stresses (numerically computed) increase with water level increase. The maximum value of σ_c increases from 2560 MPa for $h_w=12$ m, until 4000 MPa for $h_w=12.40$ m. With **DamSlide3D**, it was found, numerically, that sliding along the horizontal base joint only occurs for $h_w \geq 12.45$ m (in 5.19 is shown, graphically, the iterative stress-transfer divergence in terms of the used displacements norm).

6 | Case Study: Gravity Dam

6.1 Dam presentation

The case study presented in this work is a gravity dam (Figure 6.1) located in the Vouga river, that was built for energy production, flood control, and water supply for consumption and irrigation.

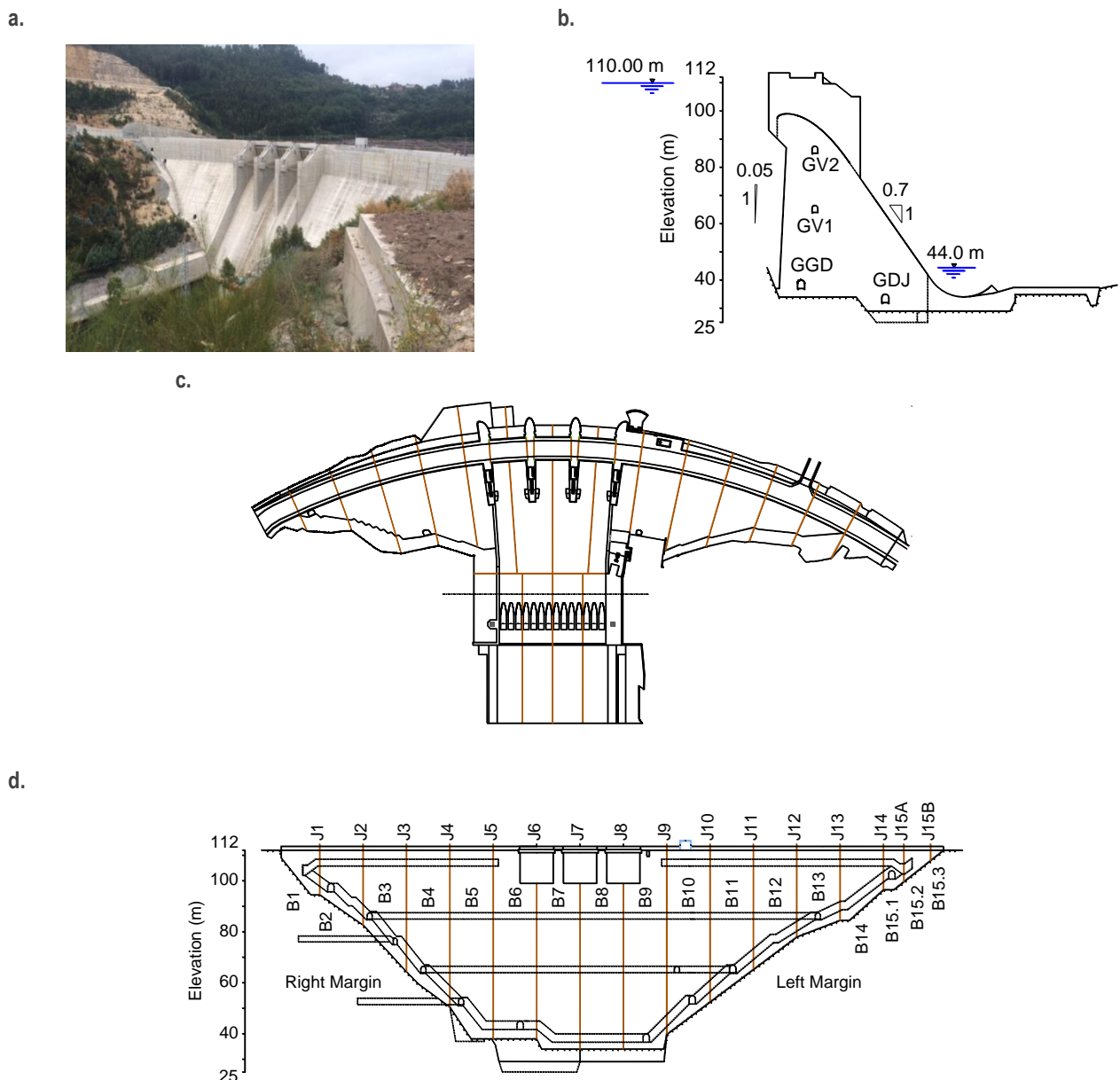


Figure 6.1 – Gravity dam. (a.) Downstream view (photo). (b.) Cross section (block 7, B7). (c.) The site plan. (d.) Downstream view

The dam studied is a gravity concrete dam (Figure 6.1), with a small curvature in plan, founded in a rock massif mainly composed by granite. The structure has a maximum height above foundation of 83.0 m. The crest is 9.0 m thick with its axis following an arc of a circle with 240 m radius which extends itself along approximately 264 m.

The structure is composed by 17 blocks, separated by contraction joints defined by vertical planes perpendicular to the dam reference surface. The cross section is defined by a triangle whose top vertice is 4.5 m upstream of the crest axis elevation, furthermore, the upstream and downstream faces are inclined 0.05 h:v and 0.70 h:v, respectively. For the crest, one can overlap a rectangle with 9 m of width.

6.2 Dam sliding scenario. Analysis of dam-foundation interface non-linear behavior

In order to study the dam sliding scenario along the dam-foundation interface, using **DamSlide3D**, it was developed a 3DFEM model, only considering the dam central block. In Figure 6.2 is presented the adopted 3D finite element discretization, using cubic “serendipity” elements of 20 nodes, and the correspondent joint elements of 16 nodes at the dam-foundation interface.

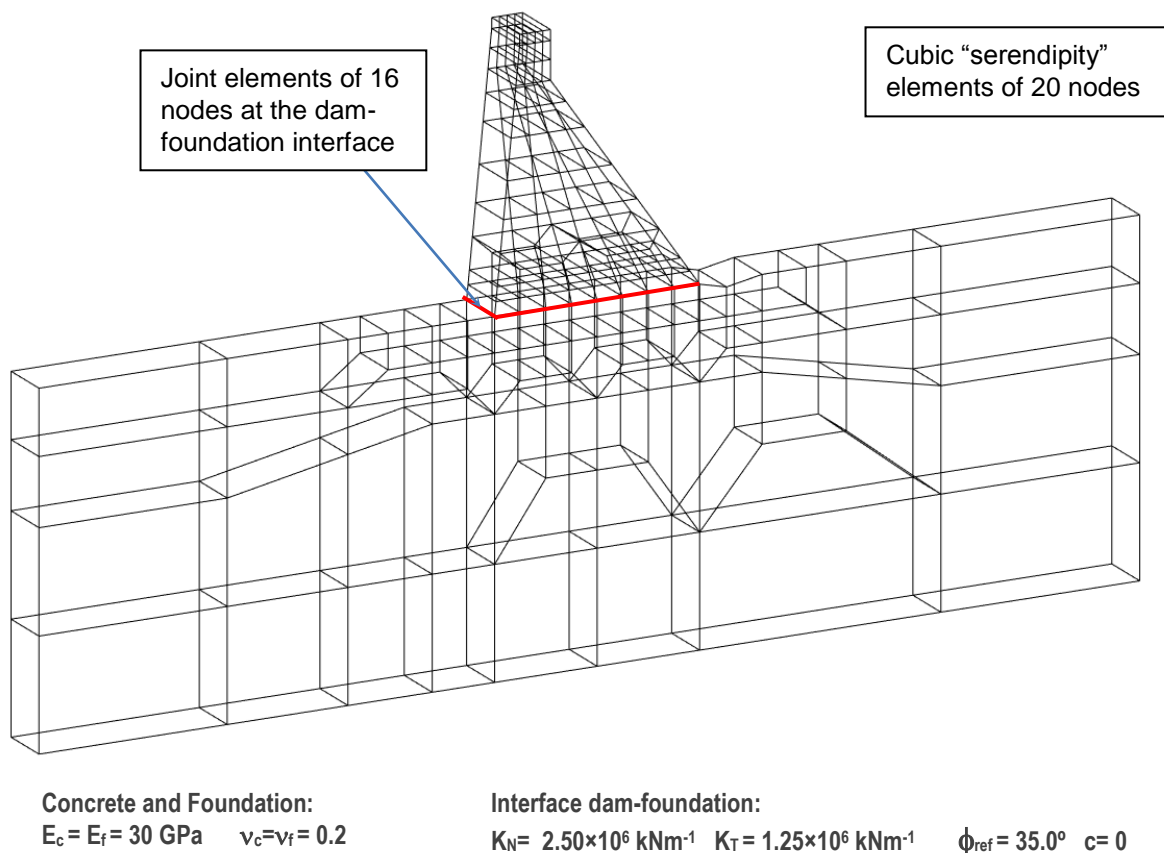


Figure 6.2 – Finite element mesh adopted to study the dam sliding along the dam-foundation interface

The dam is subjected to the usual load combination SW+HP (full reservoir, $h_w = 76$ m). The cohesion at the interface dam-foundation is assumed, conservatively, to be null ($c = 0$). The reference value of the interface friction angle is $\phi = 35^\circ$.

6.2.1 Parametric study on the influence of friction angle (full reservoir)

In this sub-section the joint behavior at the interface dam-foundation is studied for different values of the friction angle: the numerical results are presented from Figure 6.3 to Figure 6.7, being, respectively, for $\phi = 35^\circ, 30^\circ, 27^\circ, 26.5^\circ, 26^\circ$.

From Figure 6.3 to Figure 6.7, one can verify, as expected, that as the friction angle decreases (from 35° to 26°) there is a decrease in the resistant shear stress distribution, which means there is a decrease in the resistant shear stress capacity at the dam base. In order to have no sliding, the resultant acting shear force should be lower than the resistant shear force correspondent to the resistant shear stress capacity: this equilibrium condition is numerically attained for values of the friction angle ϕ higher than 26° . So, with **DamSlide3D**, it was found, numerically, that sliding along the dam-foundation base joint only occurs for $\phi \leq 26^\circ$ (in Figure 6.8 is shown, graphically, the iterative stress-transfer divergence in terms of the displacements norm).

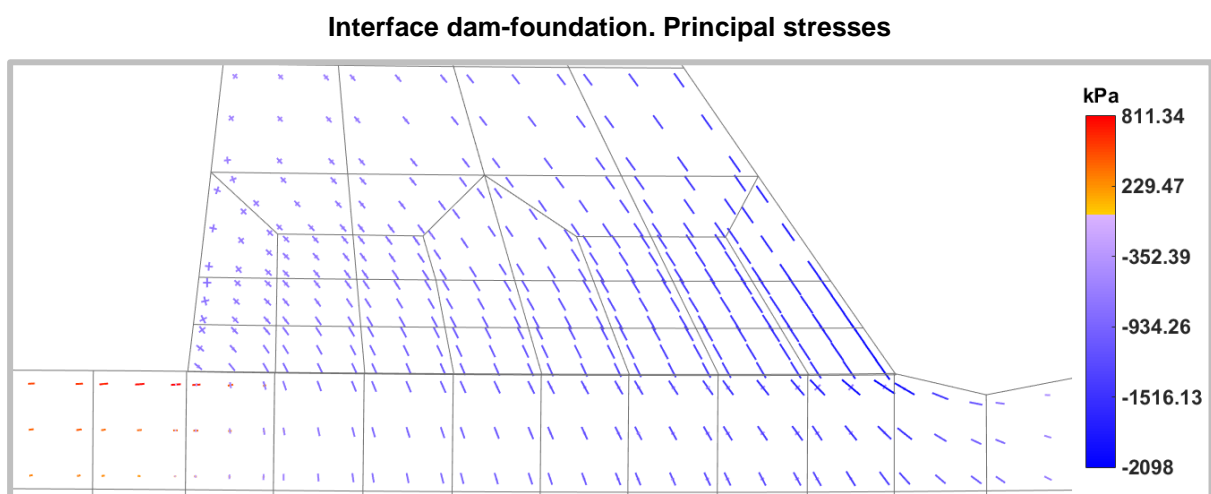
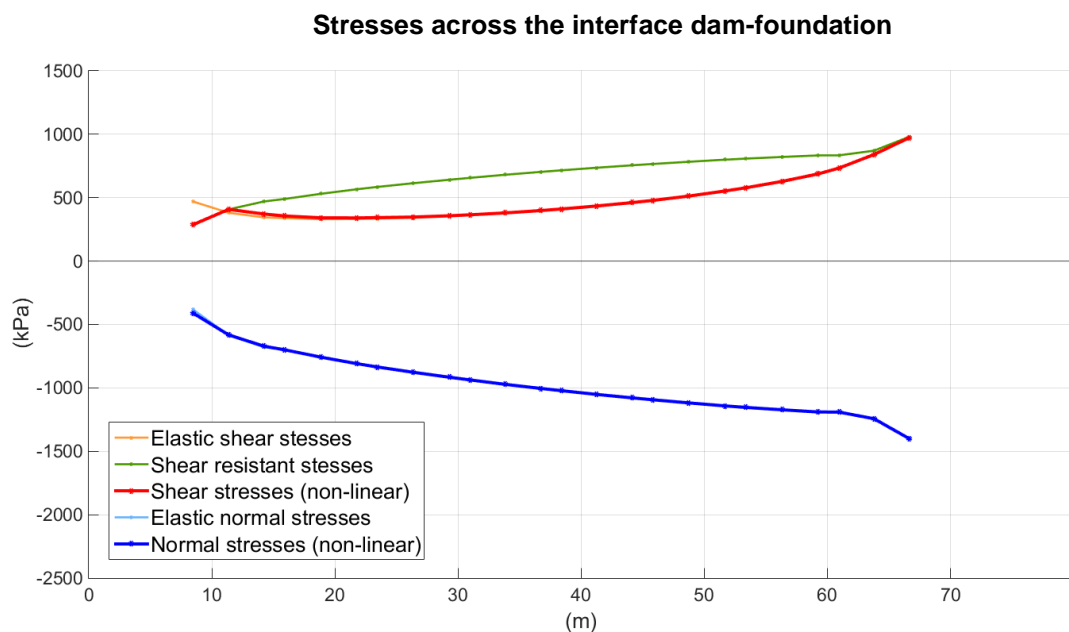
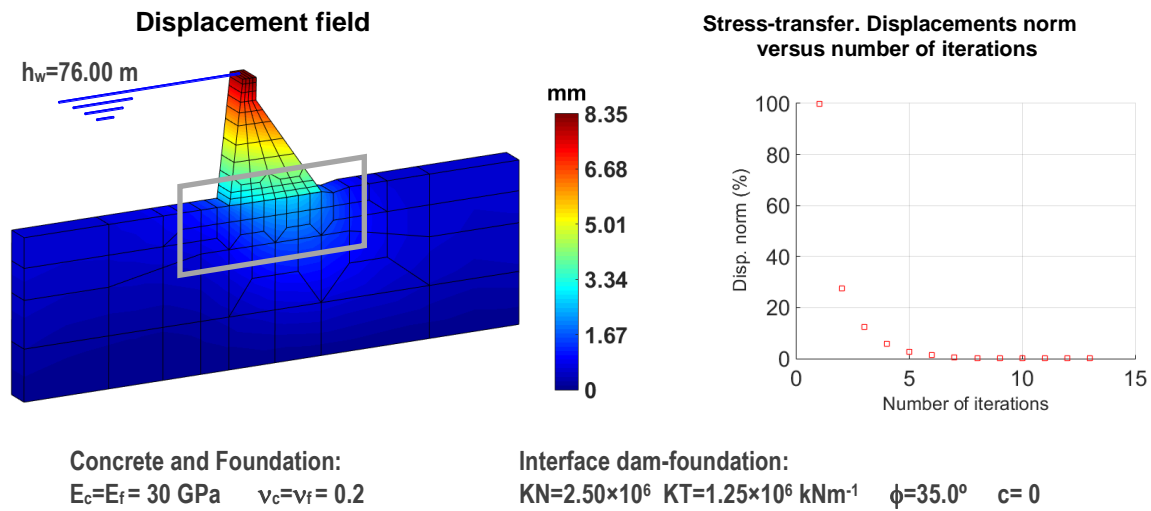
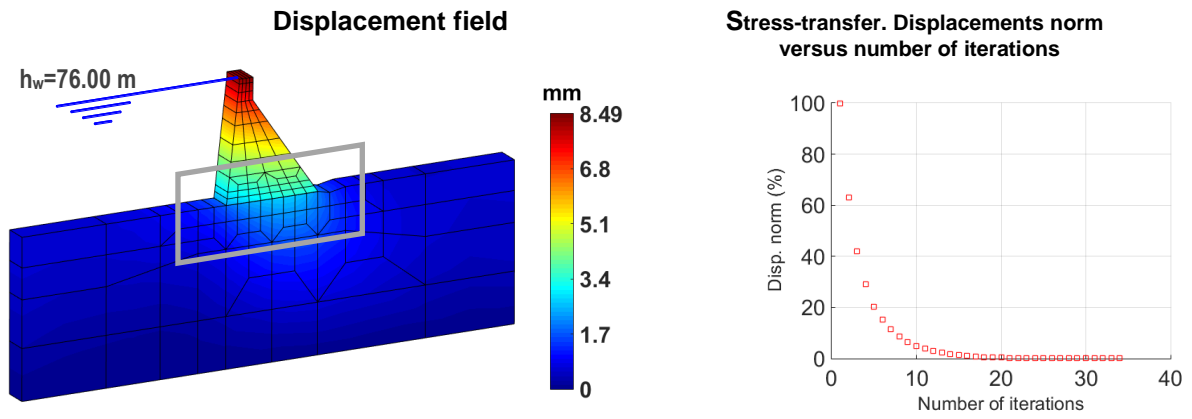


Figure 6.3 – Dam structural behavior for $\phi=35^\circ$. On top left, displacement field; on top right, stress-transfer convergence, in the middle, stresses across the center section of the interface dam-foundation; on the bottom, the dam's principal stresses throughout the interface dam-foundation



Concrete and Foundation:
 $E_c = E_f = 30 \text{ GPa}$ $\nu_c = \nu_f = 0.2$

Interface dam-foundation:
 $K_N = 2.50 \times 10^6$ $K_T = 1.25 \times 10^6 \text{ kNm}^{-1}$ $\phi = 30.0^\circ$ $c = 0$

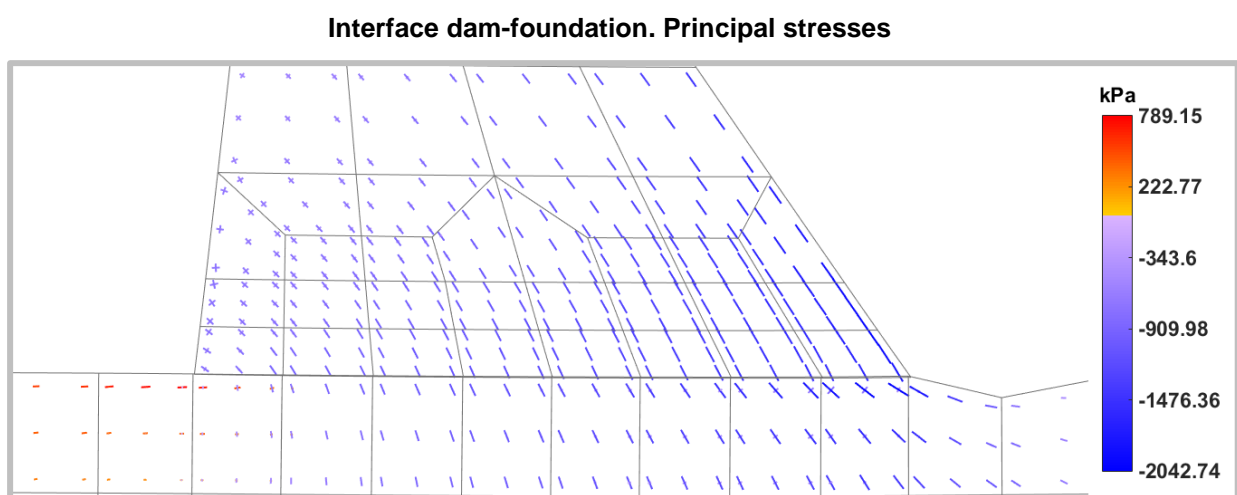
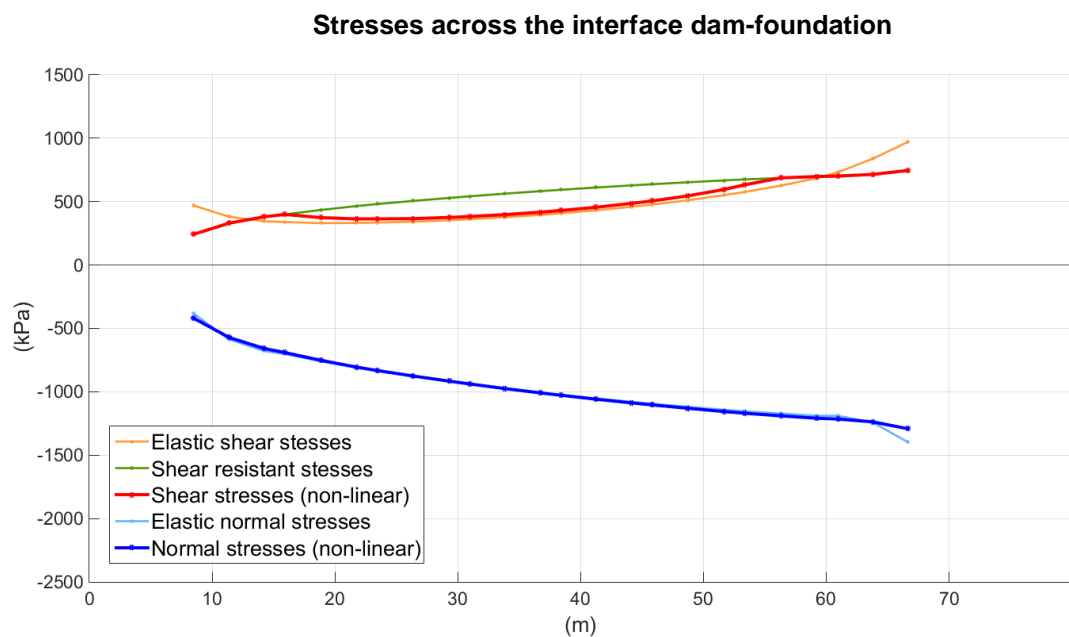


Figure 6.4 – Dam structural behavior for $\phi = 30^\circ$. On top left, displacement field; on top right, stress-transfer convergence, in the middle, stresses across the center section of the interface dam-foundation; on the bottom, the dam's principal stresses throughout the interface dam-foundation

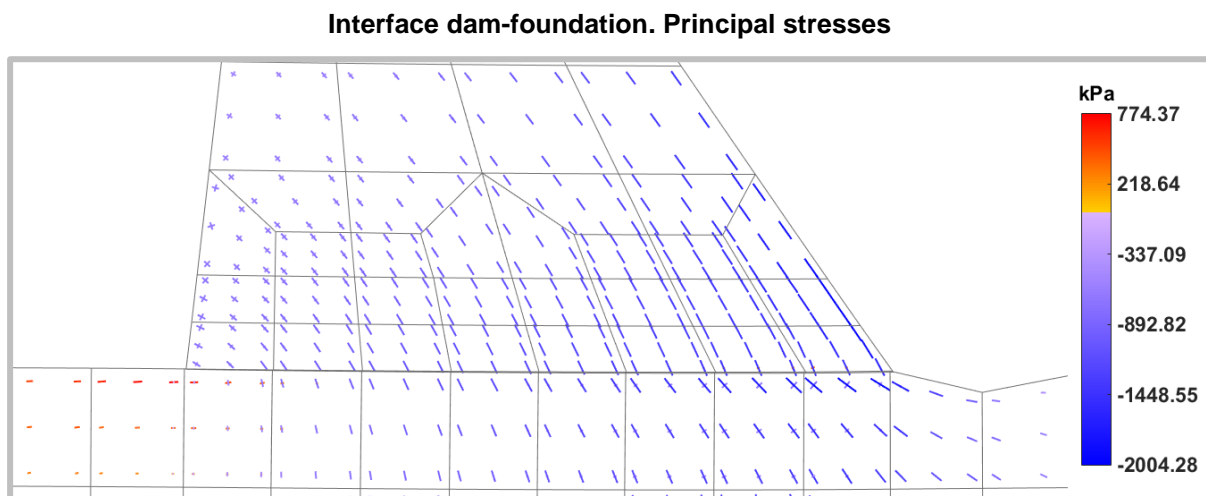
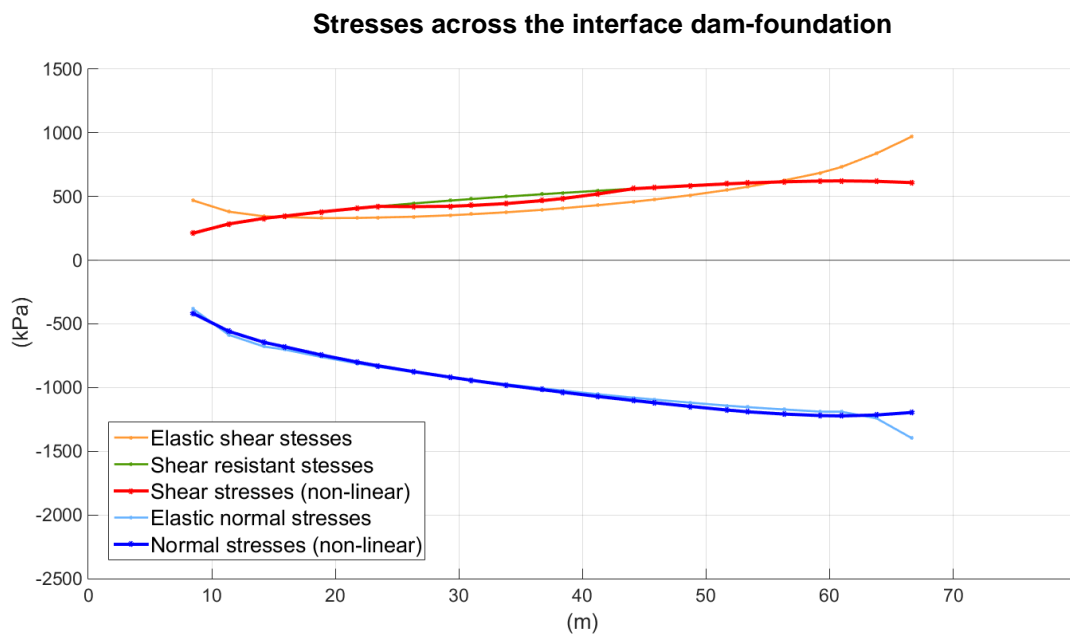
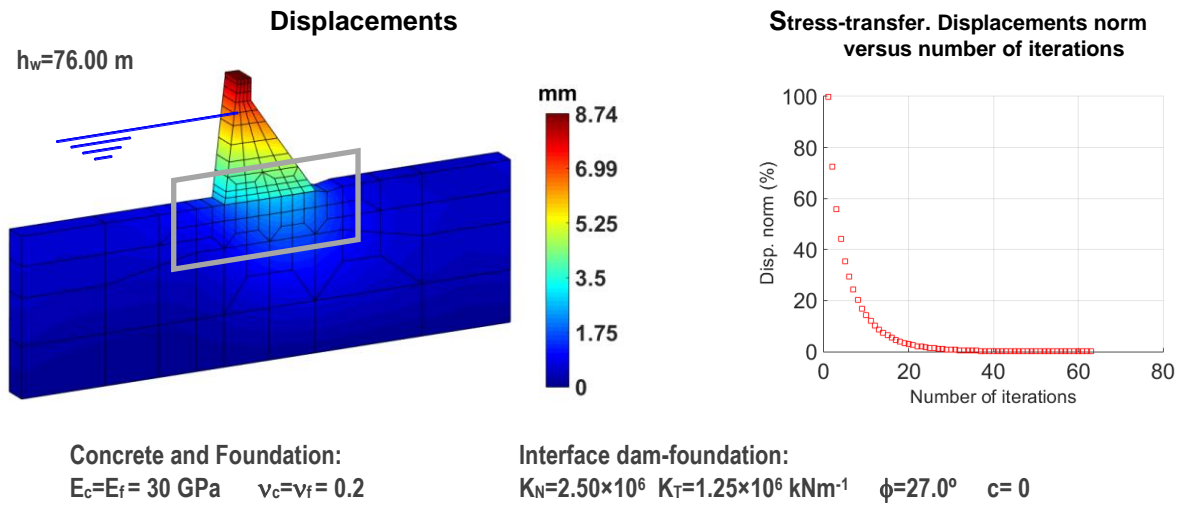


Figure 6.5 – Dam structural behavior for $\phi=27^\circ$. On top left, displacement field; on top right, stress-transfer convergence, in the middle, stresses across the center section of the interface dam-foundation; on the bottom, the dam's principal stresses throughout the interface dam-foundation

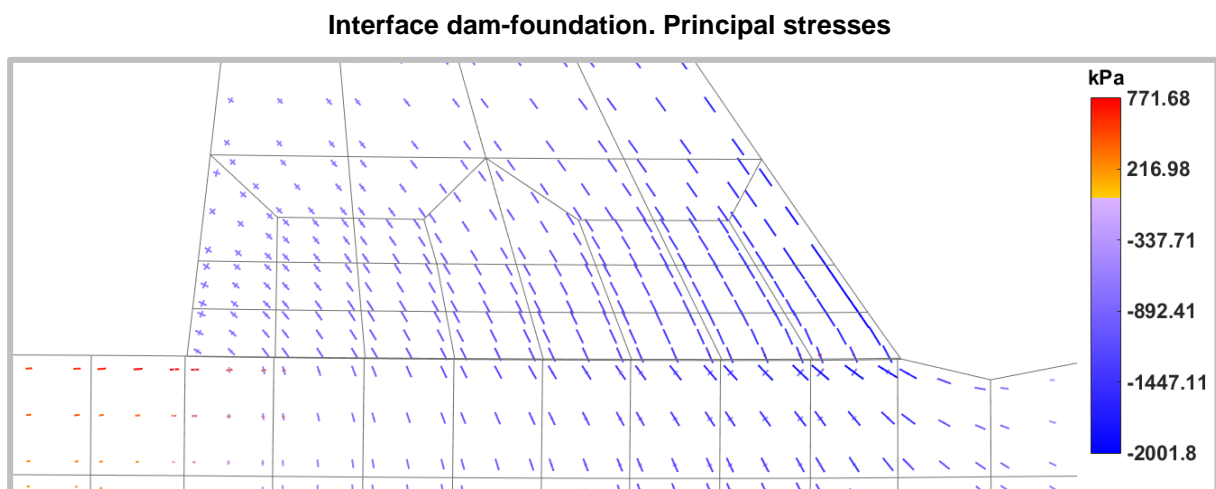
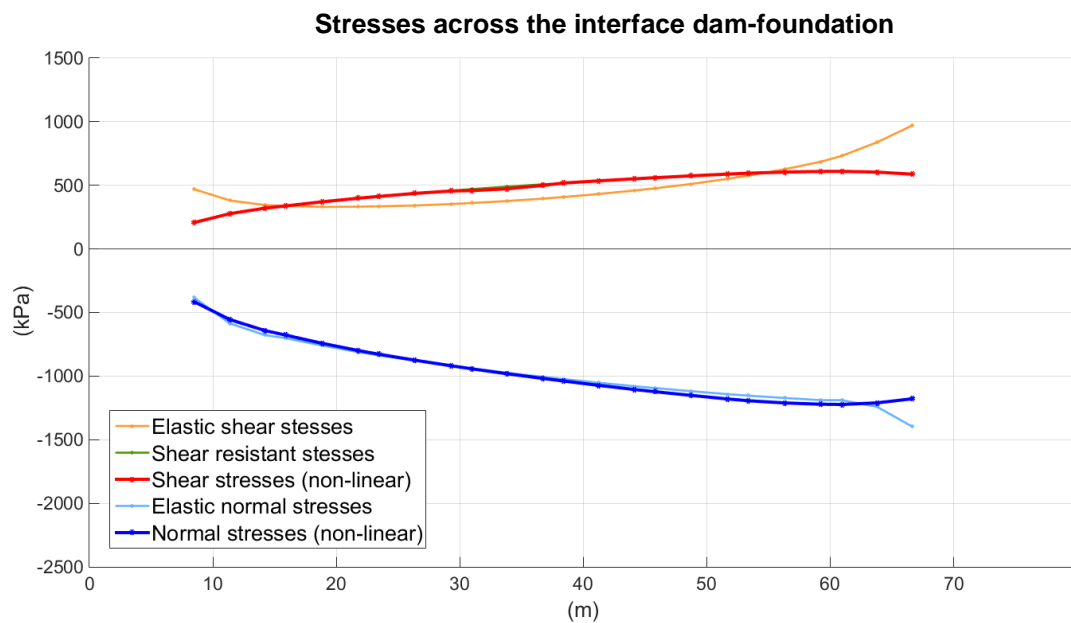
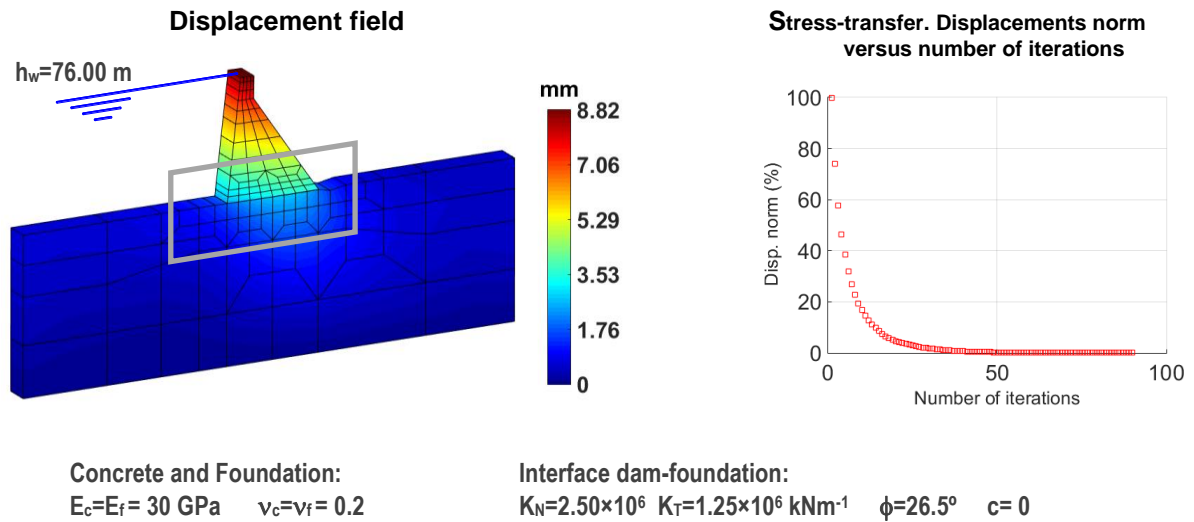


Figure 6.6 – Dam structural behavior for $\phi=26.5^\circ$. On top left, displacement field; on top right, stress-transfer convergence, in the middle, stresses across the center section of the interface dam-foundation; on the bottom, the dam's principal stresses throughout the interface dam-foundation

$h_{\text{water}}=76.00 \text{ m}$

Concrete and foundation:

$E_c=E_f = 30 \text{ GPa}$

$\nu_c=\nu_f = 0.2$

Interface column-base:

$K_N=2.50 \times 10^6 \text{ kNm}^{-1}$

$K_T=1.25 \times 10^6 \text{ kNm}^{-1}$

$\phi=26^\circ$

$c=0$

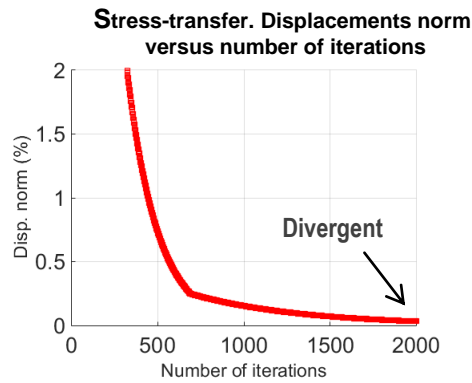


Figure 6.7 – Stress-transfer convergence for $\phi=26.0^\circ$

6.2.2 Parametric study on the influence of water level (friction angle $\phi=30^\circ$)

In this sub-section the joint behavior of the dam-foundation interface is studied for different values of water height (h_w), simulating a overtopping scenario. It is assumed a constant value for the friction angle $\phi = 30^\circ$. The numerical results are presented in Figure 6.4 (for $h_w = 76 \text{ m}$) and in Figure 6.8 to Figure 6.13, for, respectively, $h_w = 77.0, 78.0, 79.0, 80.0, 81.0$ and 82.0 m .

For this scenario of water level increase (overtopping), one can verify, that, as expected, the non-linear distribution of the normal and shear stresses (numerically computed) increase with water level increase. The maximum value of compression normal stresses increases from $\sim 1300 \text{ MPa}$ for $h_w=76 \text{ m}$, until $\sim 1500 \text{ MPa}$ for $h_w=82.0 \text{ m}$. The maximum value of shear stresses increases from $\sim 750 \text{ MPa}$ for $h_w=76 \text{ m}$, until $\sim 900 \text{ MPa}$ for $h_w=82.0 \text{ m}$.

With **DamSlide3D**, it was found, numerically, that sliding along the dam-foundation joint only occurs for $h_w \geq 83 \text{ m}$ (in Figure 6.14 is shown, graphically, the iterative stress-transfer divergence in terms of the used displacements norm).

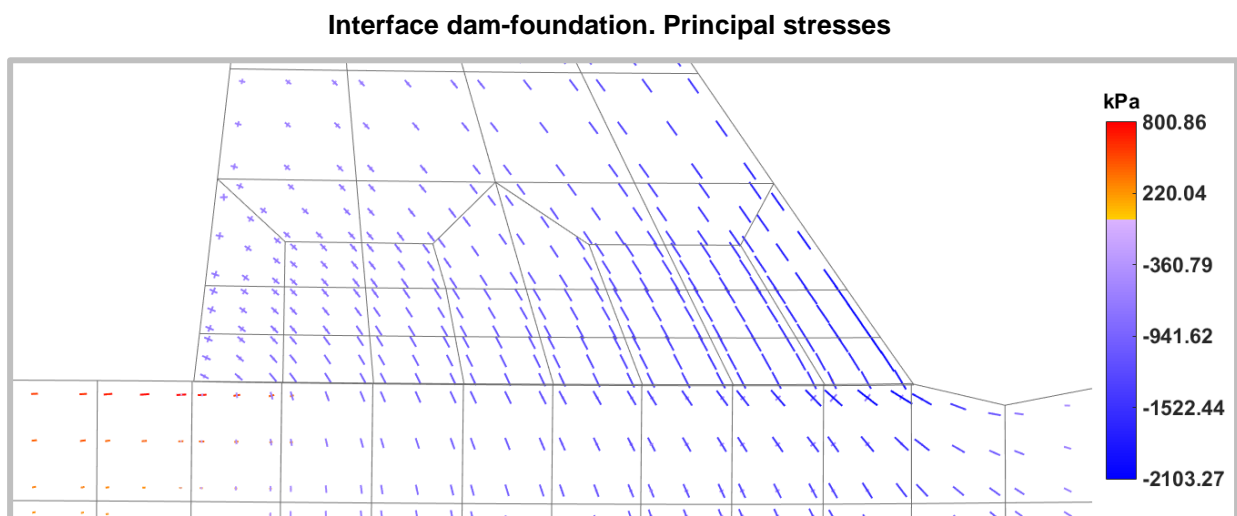
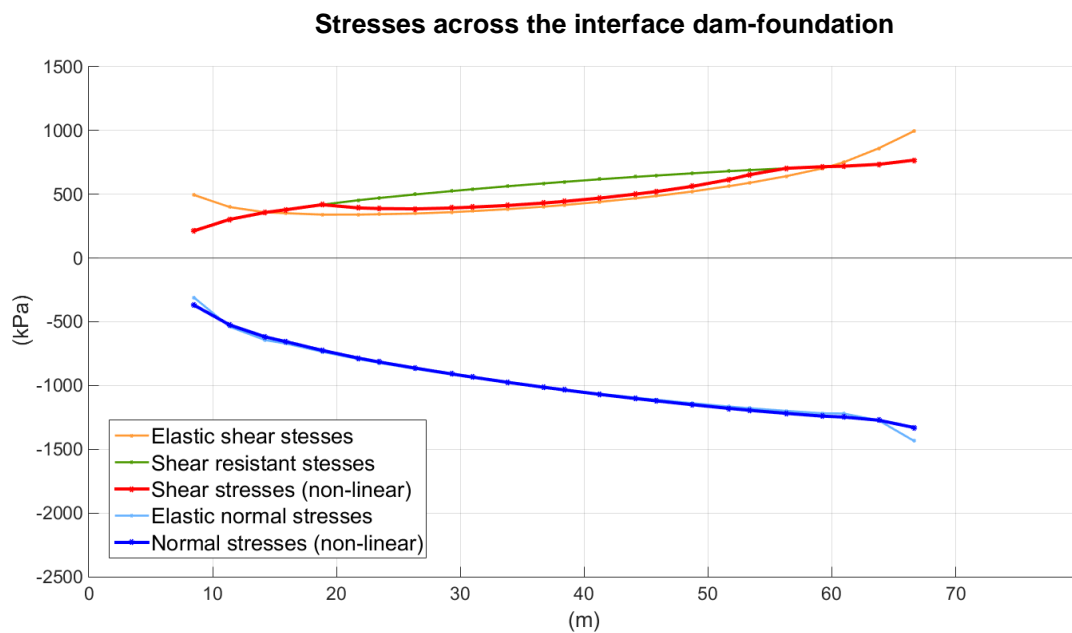
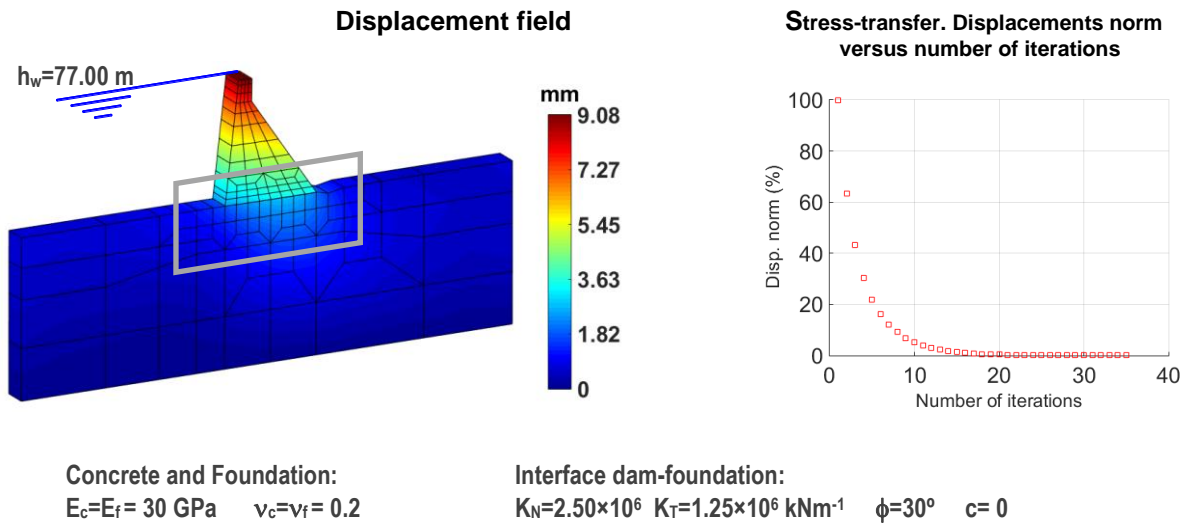


Figure 6.8 – Dam structural behavior for $h_{\text{water}} = 77 \text{ m}$. On top left, displacement field; on top right, stress-transfer convergence, in the middle, stresses across the center section of the interface dam-foundation; on the bottom, the dam's principal stresses throughout the interface dam-foundation

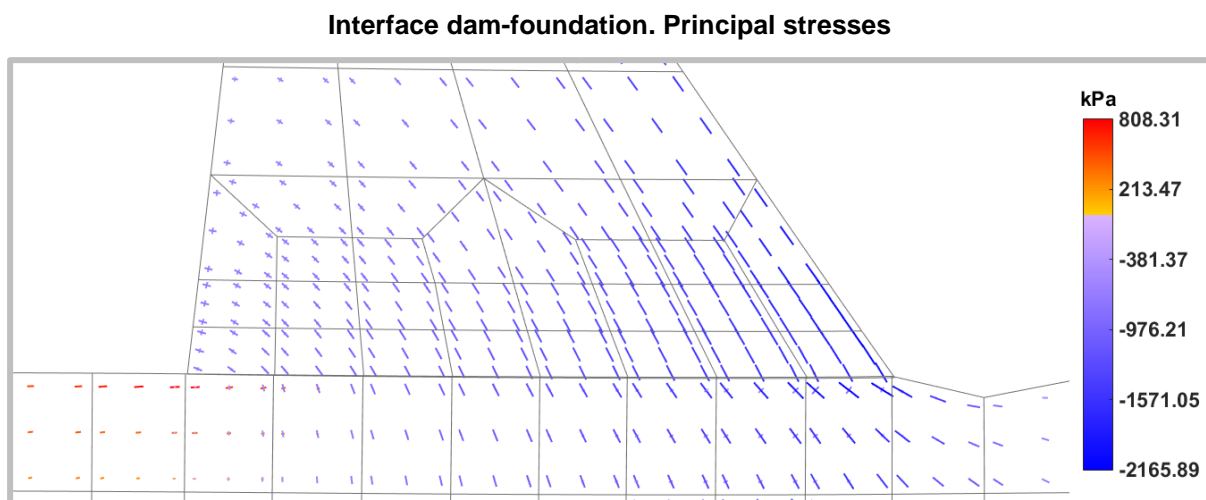
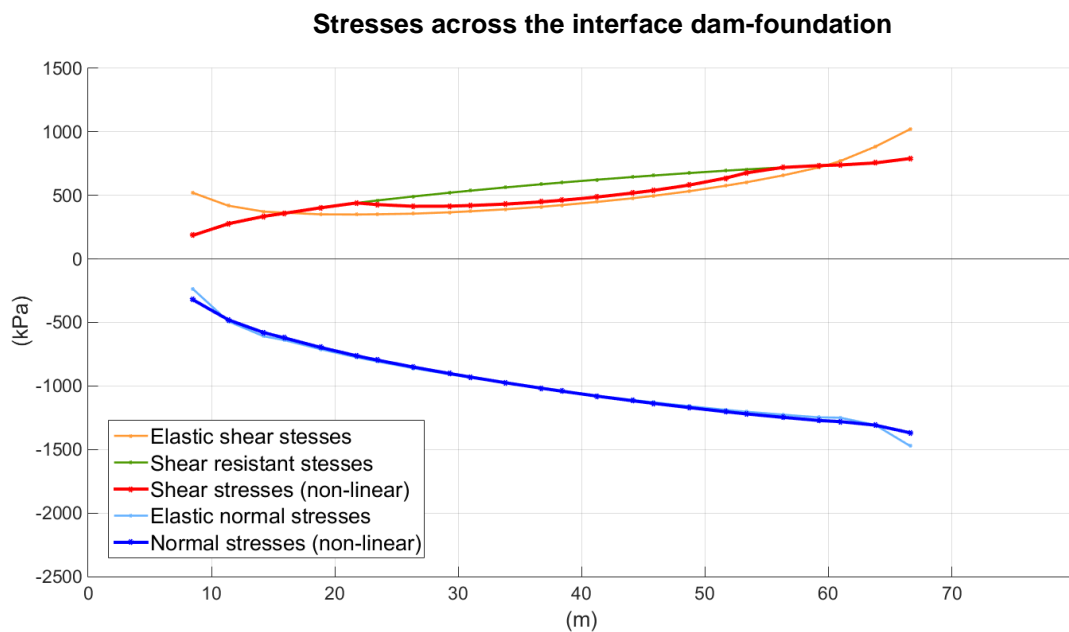
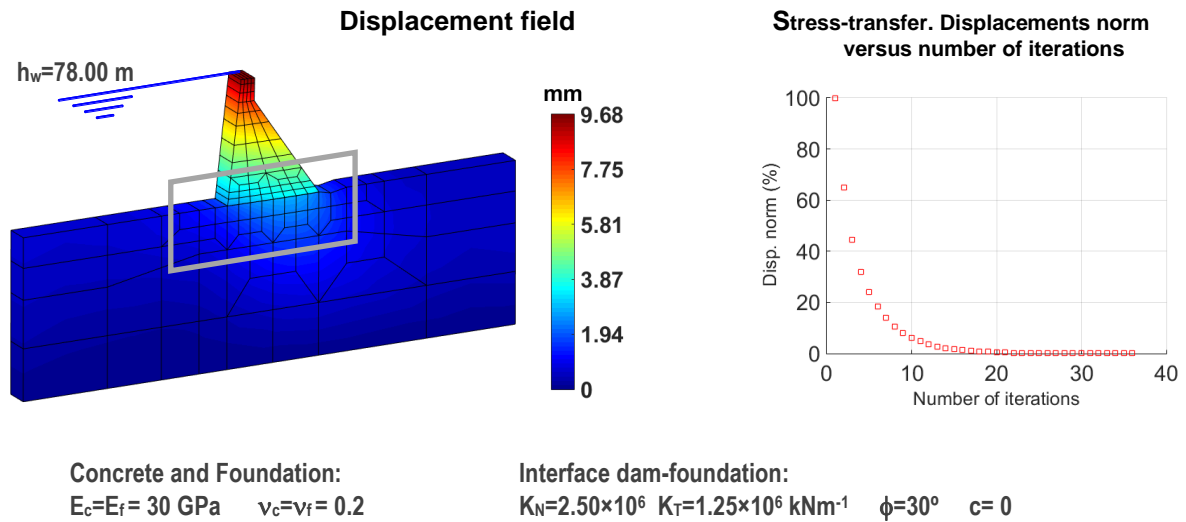
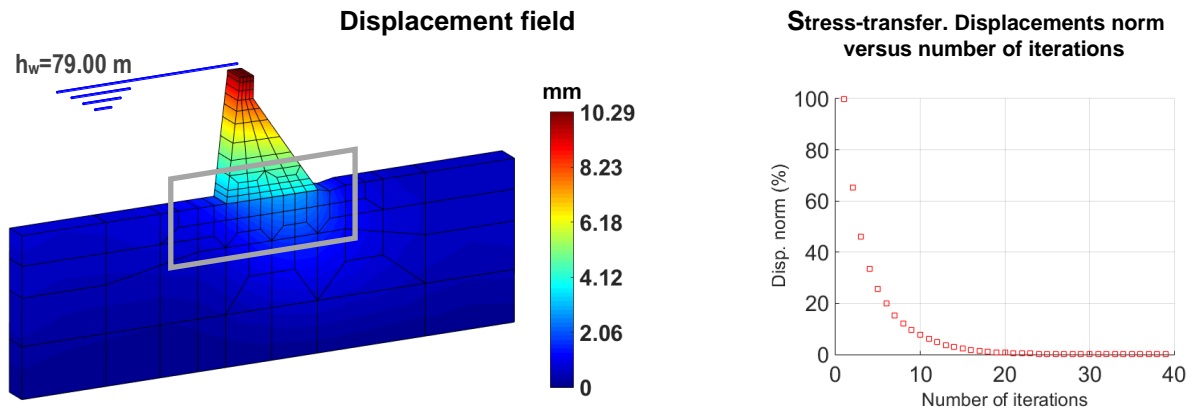


Figure 6.9 – Dam structural behavior for $h_{\text{water}} = 78 \text{ m}$. On top left, displacement field; on top right, stress-transfer convergence, in the middle, stresses across the center section of the interface dam-foundation; on the bottom, the dam's principal stresses throughout the interface dam-foundation



Concrete and Foundation:
 $E_c=E_f= 30$ GPa $\nu_c=\nu_f= 0.2$

Interface dam-foundation:
 $K_N=2.50 \times 10^6$ $K_T=1.25 \times 10^6$ kNm⁻¹ $\phi=30^\circ$ $c=0$

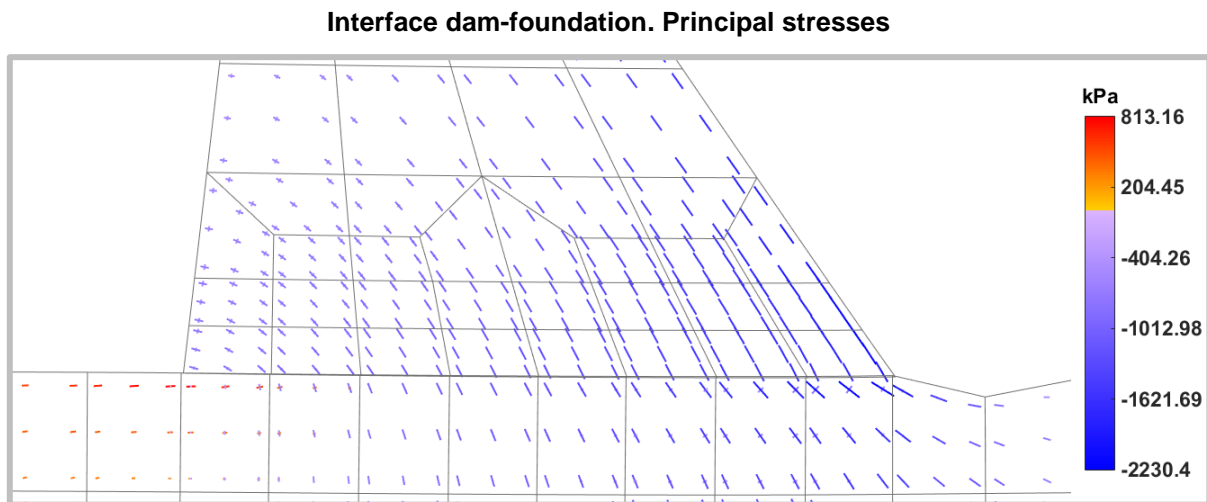
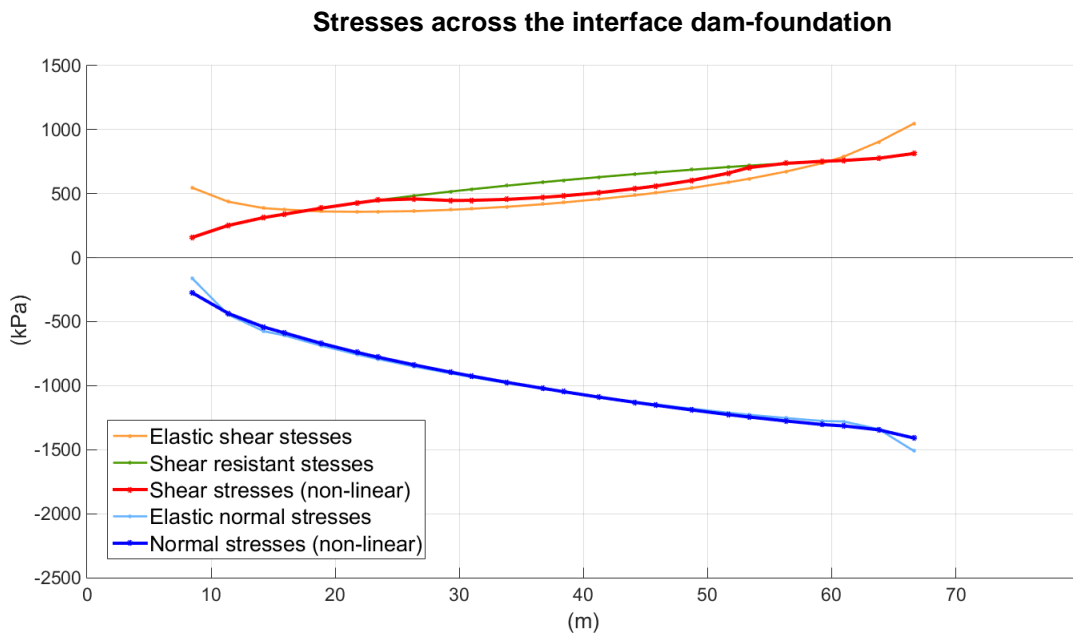


Figure 6.10 – Dam structural behavior for $h_{water}=79$ m. On top left, displacement field; on top right, stress-transfer convergence, in the middle, stresses across the center section of the interface dam-foundation; on the bottom, the dam's principal stresses throughout the interface dam-foundation

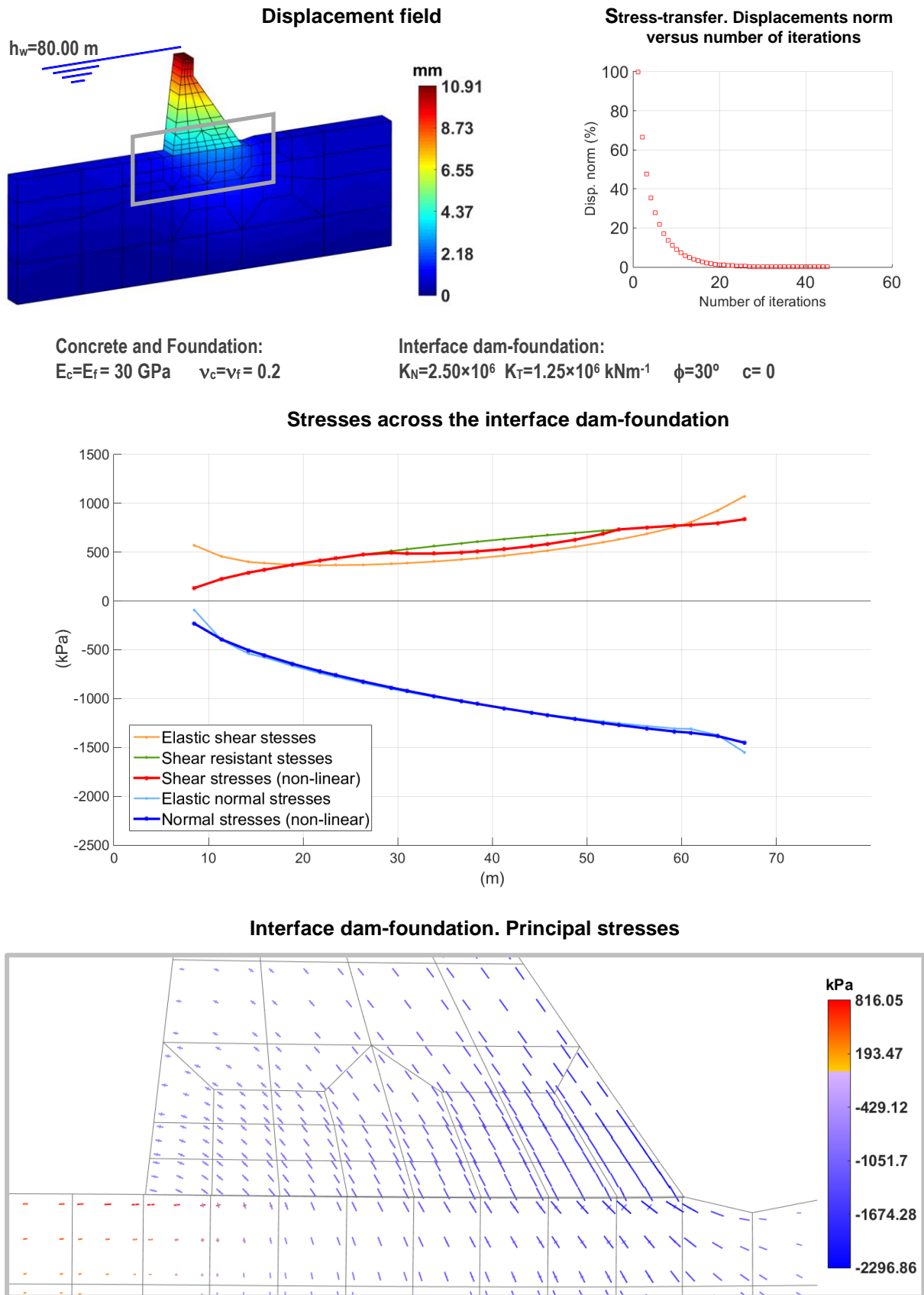
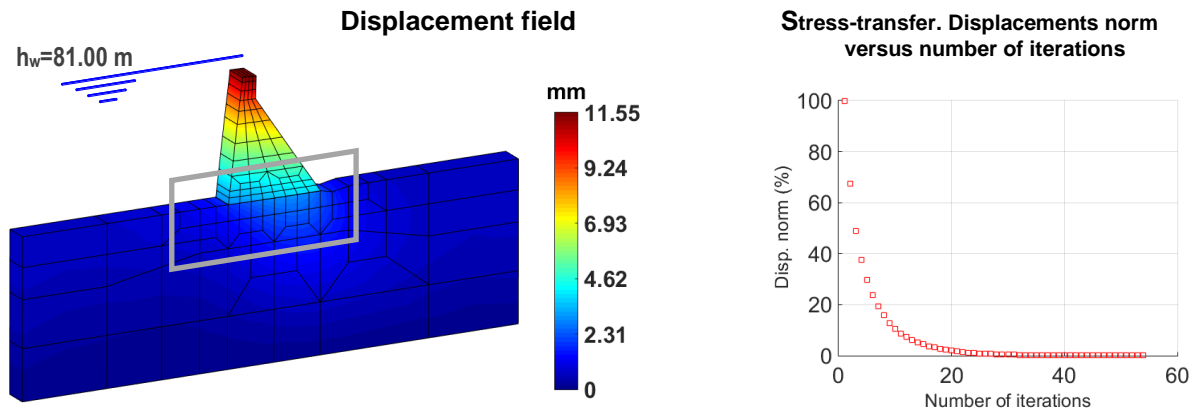


Figure 6.11 – Dam structural behavior for $h_{\text{water}}=80 \text{ m}$. On top left, displacement field; on top right, stress-transfer convergence, in the middle, stresses across the center section of the interface dam-foundation; on the bottom, the dam's principal stresses throughout the interface dam-foundation



Concrete and Foundation:
 $E_c=E_f= 30\text{ GPa}$ $\nu_c=\nu_f= 0.2$

Interface dam-foundation:
 $K_N=2.50 \times 10^6$ $K_T=1.25 \times 10^6\text{ kNm}^{-1}$ $\phi=30^\circ$ $c=0$

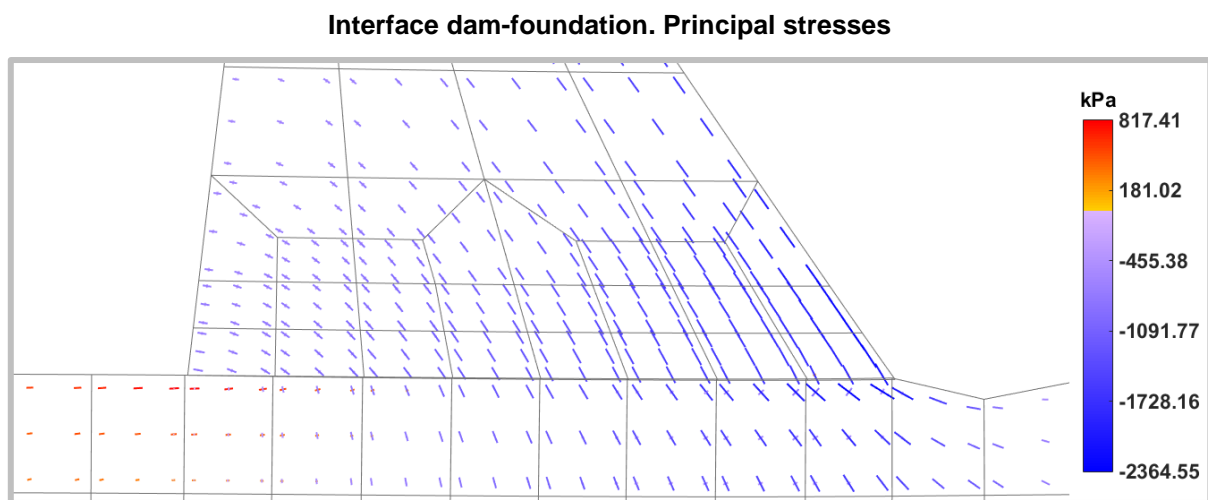
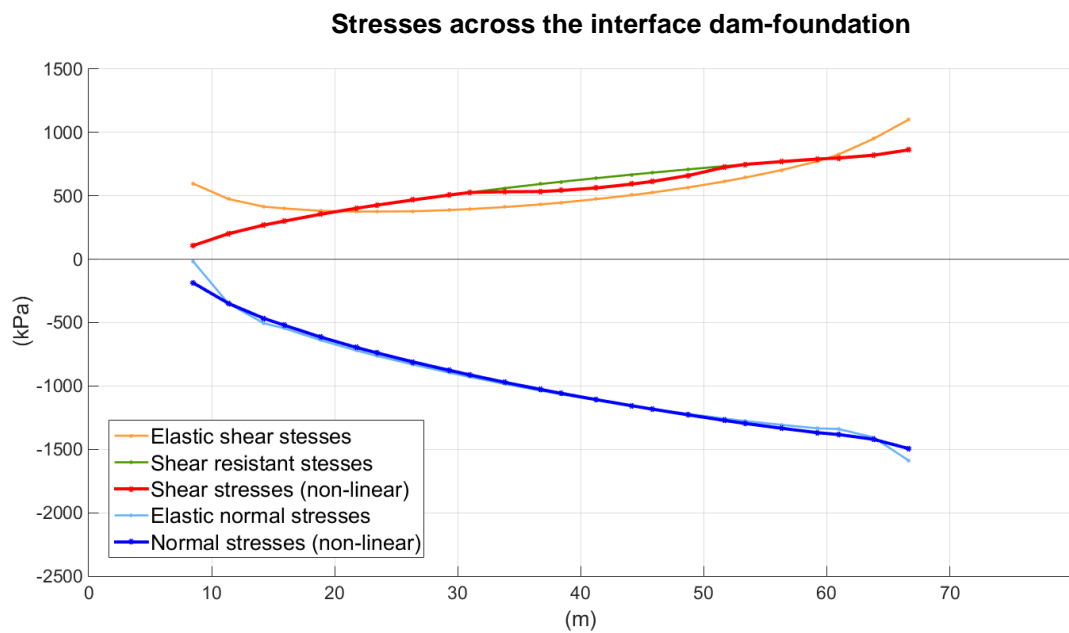
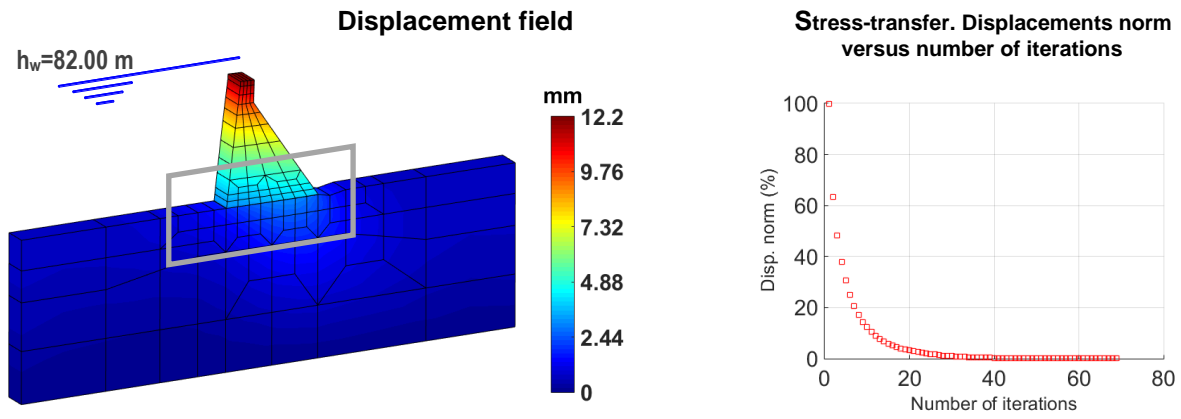


Figure 6.12 – Dam structural behavior for $h_{water}=81\text{ m}$. On top left, displacement field; on top right, stress-transfer convergence, in the middle, stresses across the center section of the interface dam-foundation; on the bottom, the dam's principal stresses throughout the interface dam-foundation



Concrete and Foundation:
 $E_c=E_f=30$ GPa $\nu_c=\nu_f=0.2$

Interface dam-foundation:
 $K_N=2.50 \times 10^6$ $K_T=1.25 \times 10^6$ kNm⁻¹ $\phi=30^\circ$ $c=0$

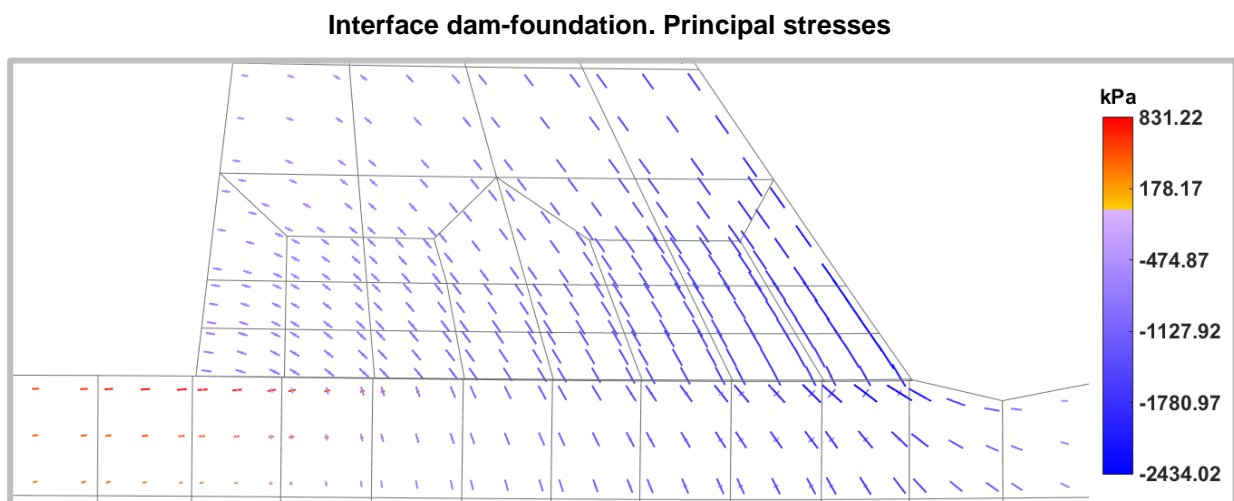
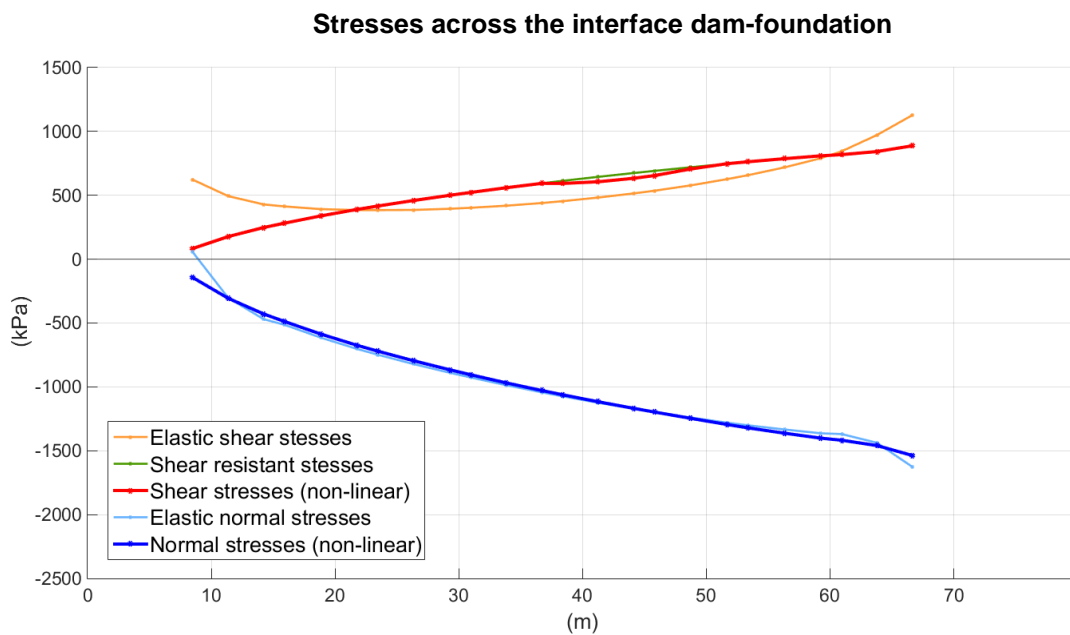


Figure 6.13 – Dam structural behavior for $h_{water}=82$ m. On top left, displacement field; on top right, stress-transfer convergence, in the middle, stresses across the center section of the interface dam-foundation; on the bottom, the dam's principal stresses throughout the interface dam-foundation

$h_{\text{water}}=83.00$ m

Concrete and foundation:

$E_c=E_f = 30$ GPa

$\nu_c=\nu_f = 0.2$

Interface column-base:

$K_N=2.50 \times 10^6$ kNm⁻¹

$K_T=1.25 \times 10^6$ kNm⁻¹

$\phi=30^\circ$

$c=0$

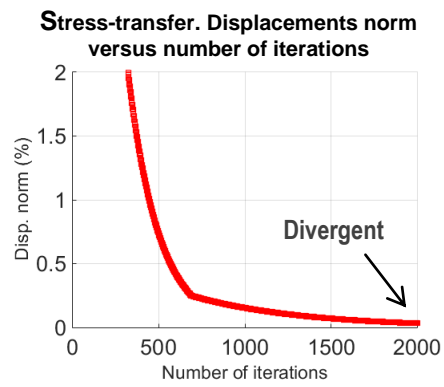


Figure 6.14 – Stress-transfer divergence for $h_{\text{water}}=83.00$ m

7 | Conclusions

The main objective of this work was the development and presentation of a three-dimensional finite element program, **DamSlide3D**, to study the behavior of gravity dams considering scenarios of sliding in the dam-foundation interface. The **DamSlide3D**, developed using MATLAB, includes cube-type finite elements with 20 nodal points ("serendipity") and the correspondent interface finite elements with 16 nodal points (joint elements).

Initially, it were presented the fundamental equations of the solids mechanics, referring to the main simplified hypotheses considered in the computationally implemented formulation, which is presented mathematically as a problem of boundary values using a displacement formulation. For the structure body and for the foundation, the hypothesis of isotropic materials with linear elastic behavior was assumed and for the interfaces the hypothesis of non-linear behavior was considered (Mohr-Coulomb criterion).

For **DamSlide3D** input data is provided in an excel file and includes structure geometry data, material properties, support conditions and load parameters. As output, the program graphically displays the stress field (principal stresses) and the displacement field (deformed structure).

The program was verified using three numerical tests with known theoretical solutions. In these tests a simple structure was used, composed by a column discretized in 3DFE, on a base, also discretized in 3DFE. At the contact surface between the column and the base (horizontal surface) it was considered an interface discretized using joint finite elements. A plane surface plane that crosses the column with a given slope is also considered, discretized using the same type of joint finite elements. In the first test, the field of elastic stresses at the base, due to dead weight (DW) and hydrostatic pressure (HP), was compared with the theoretical results. In the second test the nonlinear column response was studied for different values of the friction angle at the inclined interface (in this test the structure is only submitted to DW). In the third test, for the main DW + HP loads, the stability of the column is initially studied for a variation of ϕ , and later for a variation of the water level. In these three numerical tests the results were always consistent with the theoretical solutions.

Finally, as an example of application, a gravity dam structural behavior was analyzed considering the non-linear behavior in the dam-foundation interface. The dam was subjected to self-weight and hydrostatic pressure. A parametric study was developed in order to study the dam stability for different values of water level (h_w) and for different values of ϕ .

As a perspective for future studies, considering the results obtained with the use of the 20 nodes "serendipity" quadratic master element, it would be interesting to compare these results with the ones considering a different master element, this time, a 27 nodes Lagrangian quadratic element. Therefore, it would be interesting to verify if the extra calculus effort is offset by the outputs quality gain. Additionally, since the program outputs prove to be satisfactory, it would be interesting to model the behavior of he studied gravity dam, considering a complete 3D dam FE model. Also, it would be interesting to apply a different iteration process (convergence) on the program, for example the

Newton-Raphson method (which implies that, at each iteration, the stiffness matrix is recalculated) and compare the results of both methods (Newton-Raphson and stress-transfer). Finally, it would also be interesting to expand the domain of the non-linear application, from the joint elements to the dam body (solid elements) using, e.g., a damage model.

Lisbon, LNEC, April 2019

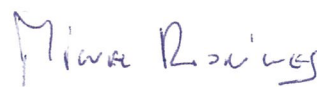
APPROVED

AUTHORS

Head of Modelling and Rock
Mechanics Unit



Luís Nolasco Lamas



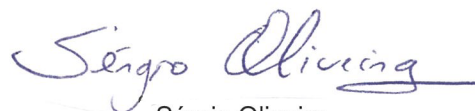
Miguel Rodrigues

Doctoral Research Fellow

Head of Concrete Dams Department



António Lopes Batista



Sérgio Oliveira

Assistant Researcher

Bibliographic References

- DAES-UCB, 2017 – **Introduction to Finite Element Method. Part II: Mathematical Formulation of Finite Elements. FEM Convergence Requirements.** University of Colorado at Boulder. Retrieved January 25, 2017, from <http://www.colorado.edu/engineering/cas/courses.d/IFEM.d/IFEM.Ch19.d/IFEM.Ch19.pdf>
- DES-UA, 2008 – **Solid Mechanics Lecture Notes. Engineering Solid Mechanics. Differential Equations of Solid Mechanics. The Equations of Motion.** Department of Engineering Science, University of Auckland. Retrieved January 5, 2017, from http://homepages.engineering.auckland.ac.nz/~pkel015/SolidMechanicsBooks/Part_II/01_DifferentialEquilibriumAndCompatibility/DifferentialEquations_01_Eqns_of_Motion.pdf
- DES-UA, 2008 – **Solid Mechanics Lecture Notes. Engineering Solid Mechanics. Differential Equations of Solid Mechanics. The Strain-Displacement Relation.** Department of Engineering Science, University of Auckland. Retrieved January 4, 2017, from http://homepages.engineering.auckland.ac.nz/~pkel015/SolidMechanicsBooks/Part_II/01_DifferentialEquilibriumAndCompatibility/DifferentialEquations_02_Strain_Disp_Eqns.pdf
- DES-UA, 2015 – **Solid Mechanics Lecture Notes. An Introduction to Solid Mechanics. Linear Elasticity. The Linear Elasticity Model.** Department of Engineering Science, University of Auckland. Retrieved January 4, 2017, from http://homepages.engineering.auckland.ac.nz/~pkel015/SolidMechanicsBooks/Part_I/Book_SM_Part_I/06_LinearElasticity/06_Linear_Elasticity_01_Elastic_Model.pdf
- DoITPoMS, 2000 – **Tensors in Materials Science.** Dissemination of IT for the Promotion of Materials Science. University of Cambridge. Retrieved March 23, 2017, from <https://www.doitpoms.ac.uk/tlplib/tensors/index.php>
- FREITAS, J. A. T., 2009 – **Introdução ao Método dos Elementos Finitos: Elasticidade Plana e Tridimensional.** Análise de Estruturas II. Instituto Superior Técnico. Lisbon.
- GENÉSIO, M. L. V. P., 1993 – **Simulação do comportamento de juntas de barragens.** Tese de mestrado. FEUP. Oporto.
- OLIVEIRA, E. R. A., 1961 – **Automatização do Cálculo de Estruturas.** Memória n.º 220. LNEC. Lisbon.
- OLIVEIRA, E. R. A., 1968 – **Theoretical Foundations of the Finite Element Method.** Int. J. Solids Struct., Vol. 4, pp. 929-952. LNEC. Lisbon
- OLIVEIRA, S., 1991 – **Elementos finitos parabólicos para análise estática e dinâmica de equilíbrios tridimensionais.** LNEC. Lisbon.
- OLIVEIRA, S., 2000 – **Modelos para análise do comportamento de barragens de betão considerando a fissuração e os efeitos do tempo. Formulações de dano.** Tese de doutoramento. FEUP. LNEC. Lisbon.

- OLIVEIRA, S., 2016 – **Documentação da Unidade Curricular de Modelação de Estruturas com Elementos Finitos**. Curso de Mestrado em Engenharia Civil. Instituto Superior de Engenharia de Lisboa. Lisbon.
- OLIVEIRA, S.; SILVESTRE, A.; CÂMARA, R., 2014 – **Barragem de Ribeiradio. Obra Construída. Verificação de Segurança Estrutural para Ações Estáticas e Dinâmicas. Cenários Correntes e de Rotura**. LNEC - Proc. 0402/121/18081. Relatório 419/2014 – DBB/NMMR. Lisbon.
- PEDRO, J. O., 1977 – **Dimensionamento de barragens abóbada pelo método dos elementos finitos**. Memória n.º 479. Tese para especialista. LNEC. Lisbon.
- ZIENKIEWICZ, O. C., 1961 – **Aplicação das Técnicas de Diferenças Finitas ao Estudo das Barragens e das Cascas**. Memória n.º 161. LNEC. Lisbon.
- ZIENKIEWICZ, O. C.; TAYLOR, R. L.; ZHU, J. Z., 2005 – **The Finite Element Method: Its Basis and Fundamentals**. 6th Edition. Elsevier Butterworth-Heinemann. Burlington, England.

